Hochschule für Angewandte Wissenschaften Hamburg
Hamburg University of Applied Sciences

Bachelorthesis

Janak Singh Bhat

Development and Implementation of a Concept for Optimizing a Piezoelectric System on a Machine Tool Lathe

Fakultät Technik und Informatik
Department Maschinenbau und Produktion

Faculty of Engineering and Computer Science
Department of Mechanical Engineering and Production Management

Janak Singh Bhat

Development and Implementation of a Concept for Optimizing a Piezoelectric System on a Machine Tool Lathe

Bachelorarbeit eingereicht im Rahmen der Bachelorprüfung

im Studiengang Maschinenbau und Produktion
am Department Maschinenbau und Produktion
der Fakultät Technik und Informatik
der Hochschule für Angewandte Wissenschaften Hamburg

Erstprüfer: Prof. Dr.-Ing. Christian Müller
Zweitprüfer: Prof. Dr.-Ing. Stefan Wiesemann

Abgabedatum: 06.04.2023

Zusammenfassung

Janak Singh Bhat

Thema der Bachelorthesis

Entwicklung und Umsetzung eines Konzepts zur Optimierung eines piezoelektrischen Systems an einer Drehmaschine

Stichworte

Piezoelektrischer Sensor, Aktuator, Spanbildung, Vibration, Schneidprozess

Kurzzusammenfassung

In dieser Bachelorarbeit liegt der Fokus auf der Untersuchung, wie ein Piezo-System, bestehend aus einem Sensor und Aktuator, die Schneidprozesse in einer Drehmaschine verbessern kann. Es werden verschiedene bestehende Methoden bewertet und am Ende eine Empfehlung vorgelegt, wie die Ergebnisse der Studie praktisch auf der Drehmaschine an der HAW Hamburg umgesetzt werden können.

Janak Singh Bhat

Title of the paper

Development and Implementation of a Concept for Optimizing a Piezoelectric System on a Machine Tool Lathe

Keywords

piezoelectric sensor, actuator, chips formation, vibration, cutting process

Abstract

In this Bachelor thesis the study is focused on how and in what way a piezo system, consisting of both a sensor and actuator, can improve cutting processes in a lathe. Different types of existing methods are evaluated and, at the end, a recommendation is to be submitted how the findings of the thesis’ studies can practically be used on lathe at the UAS Hamburg (HAW).

CONTENTS

LIST OF FIGURES

LIST OF TABLES

ABSTRACT

This Bachelor thesis explores the use of piezoelectric technology to improve cutting processes in a lathe for quality assurance purposes. The study evaluates different methods for optimizing piezoelectric systems that can measure force, pressure, acceleration, and torque, as well as work as actuators to actively influence process behavior. The goal is to provide recommendations on how the findings of the study can be practically applied on a lathe at the UAS Hamburg. The study shows that piezoelectric technology can improve process reliability and productivity, leading to zero-defect production. It also highlights the need for integrating piezoelectric sensors into monitoring systems to verify the quality of manufactured products. The thesis concludes with a recommendation on the best method for optimizing piezoelectric systems in cutting processes.

The thesis is divided into six chapters. This thesis covers several topics, including piezoelectricity, the construction of a lathe machine, and various lathe operations such as turning, facing, and grooving. The document also describes different types of piezoelectric materials and their working principles, as well as methods for simulating and characterizing piezoelectric sensors and actuators. Chapter 5 includes experimental verifications, such as the design of a piezoelectric actuator for turning and the analysis of a piezoelectric film-embedded smart cutting tool. The final chapter includes general conclusions concerning obtained research results and achievements, as well as possible future works.

NOTATIONS

A	Ampere
C_{PZT}	Capacitance of piezoelectric sensor (Farad)
Cr	Capacitance of charge amplifier (Farad)
d, e, g, h	Piezoelectric constants
D_i	Electric displacement tensor
E, E*	Young modulus, reduced Young modulus
E_c	Coercive field intensity
E_k	Electric field tensor
g_{33}	Piezoelectric voltage constant (Vm/N)
h	Height (thickness) of ceramic element (m)
Hz	Hertz
k	Electromechanical coupling coefficient
Pa	Pascal
P(E)	Electric polarization
Q	Generated charge (C)
S_{ij}	Strain tensor
s_{ijkl}, c_{ijkl}	Compliance and stiffness tensors
S_{out}	Resulting deformation
S(E)	Mechanical strain
T	Stress on element (Pa)
T_{in}	Mechanical Stress
T_{kl}	Stress tensor
u, w	Displacement components
V	Volt
ε_{ij}, β_{ij}	Permeability and impermeability tensors
φ	Electric potential
$[C^E]$	Stiffness matrix evaluated at constant electric field
$\{D\}$	Electric displacement vector
$\{E\}$	Electric field vector
$[e]$	Piezoelectric matrix relating stress/electric field

$\boldsymbol{[e]^t}$	Piezoelectric matrix relating stress/electric field (transposed)
$\boldsymbol{\{S\}}$	Strain vector
$\boldsymbol{\{T\}}$	Stress vector
$\underline{\boldsymbol{Z}}_T\boldsymbol{(f)}$	Electrical impedance
$[\boldsymbol{\varepsilon}^S]$	Dielectric matrix evaluated at constant strain

1 INTRODUCTION

The term "piezo" originates from the Greek word "piezein", meaning to press or squeeze. Piezoelectricity is a property of certain crystalline materials that enables them to convert mechanical strain into an electrical voltage, or vice versa. When a piezoelectric material is subjected to mechanical stress, it generates an electrical voltage across it. Conversely, when an electric voltage is applied to a piezoelectric material, it causes it to deform as shown in Figure 1. Piezoelectric materials find diverse applications in our daily lives, such as in lighters where pressing the button releases a large amount of charge from the crystal, igniting the gas. In modern times, the significance of piezoelectricity is increasing rapidly, and it has found applications in various industries, including conventional machining, active and passive vibration control, and ultrasonic-assisted machining [1].

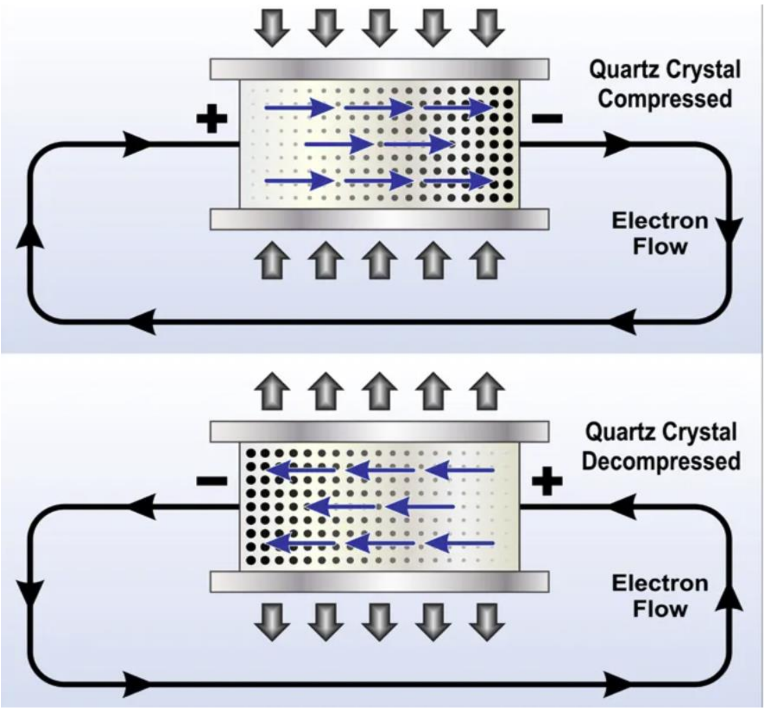

Figure 1 Piezoelectric Effect [2]

In the context of manufacturing processes, such as turning, achieving a high-quality surface finish of the turned parts is a significant challenge. This quality is primarily affected by the vibrations and dynamic interactions that occur between the part and the cutting tool. The vibrations and interactions are influenced by various factors such as the cut depth, feed rate, material properties, spindle speed, etc., which vary under different conditions. One effective solution to this problem is to use a piezoelectric actuator to dampen the vibrations. Numerous studies have demonstrated that using piezoelectric actuators can significantly improve the cutting process and lead to a better surface finish [3].

2 ASSIGNMENTS

Production processes nowadays must be constantly monitored for quality assurance purposes. For this reason, the measuring signals can either be evaluated by a PLC or condensed directly on-site to provide informative parameters. Piezoelectric technology causes a remarkable increase in process reliability within a company’s production and delivers sustained improvement in productivity which leads to zero defect production in joining, assembly and testing. It optimizes and controls processes of production by measuring force, pressure, acceleration, and torque. The data from piezoelectric sensors are visualized, evaluated, and documented in suitable monitoring systems. This has to be integrated into production so the quality of the manufactured products can be verified. Nowadays, also such applications in cutting processes are even known. Besides measuring piezoelectric systems can also work as actuators to influence process behavior actively, e.g., to reduce vibrations in tool holders. These systems are often not completely on an industrial application level since the mechanisms and the mechanics of cutting are not completely understood. Many research aims to apply innovative solutions to obtain high machining performance and quality of products is studied. Therefore, different existing methods for optimizing piezoelectric systems are to be reviewed and evaluated.

In this Bachelor thesis the study is focused on how and in what way a piezo system, consisting of both a sensor and actuator, can improve cutting processes in a lathe. Different types of existing methods are evaluated and, at the end, a recommendation is to be submitted how the findings of the thesis studies can practically be used on lathe at the UAS Hamburg (HAW).

Focal Points:

- Review the status of available research work
- Focus on the state of the technology, existing solutions on the market, if available
- Study in influence on chip formation
- Develop a proposal for an experimental set-up in the IPT laboratory on a lathe at the UAS Hamburg (HAW)

3 PIEZOELECTRICITY

Piezoelectricity refers to the property of certain crystal materials to convert strain into voltage or voltage into strain. These materials are commonly used in piezoelectric sensors that are employed in measuring force, pressure, and vibration in various industrial applications. In manufacturing, piezoelectric sensors have been found to be highly effective, especially in sectors such as production and automobile, where the goal is to ensure zero-defect production. These sensors typically contain piezoelectric materials [4].

3.1 Piezoelectric Materials and its working principle

Piezoelectric materials are found everywhere in our daily lives, but their workings are often not widely understood by the general public. These materials find applications in a wide range of fields such as mobile phones, electronics, medical technology, and industry. This lesson aims to describe the fundamental working principles of piezoelectric materials. Piezoelectric materials comprise positively and negatively charged particles, which are grouped at a central point. When pressure is applied to the crystal, it deforms and undergoes electronic redistribution, leading to a separation of positive and negative charges, which results in a potential difference between the two faces of the crystal. The resulting voltage and power are directly proportional to the applied pressure. In machine tool Lathe, piezoelectric materials reduce vibrations. The unique property of piezoelectric materials is their ability to exhibit direct and inverse piezoelectric effects as illustrated in Figure 2. The direct piezoelectric effect occurs when the piezoelectric material is deformed, resulting in the production of a voltage. Conversely, the inverse piezoelectric effect occurs when a voltage is applied to the piezoelectric material, causing it to deform. Materials that exhibit the piezoelectric effect can be classified into three groups, namely natural and synthetic crystals, polarized piezoelectric ceramics, and certain polymer films. The change in position of atoms in these materials due to applied pressure results in the formation of dipole moments and ultimately leads to polarization. Ferroelectric ceramics such as barium titanate ($BaTiO_3$) and lead zirconate titanate (PZT) are widely used in engineering due to their low production costs and excellent piezoelectric and dielectric properties. Piezoelectric ceramics can be classified into two groups based on their stability: "Hard" and "Soft". "Hard" piezoelectric materials have stable properties with respect to temperature, electric field, and stress and are commonly used in applications requiring high power actuation or projection. In contrast, "Soft" piezoelectric materials have properties that have been enhanced for sensing, actuation, or both at the expense of temperature, electric field, and stress stability.

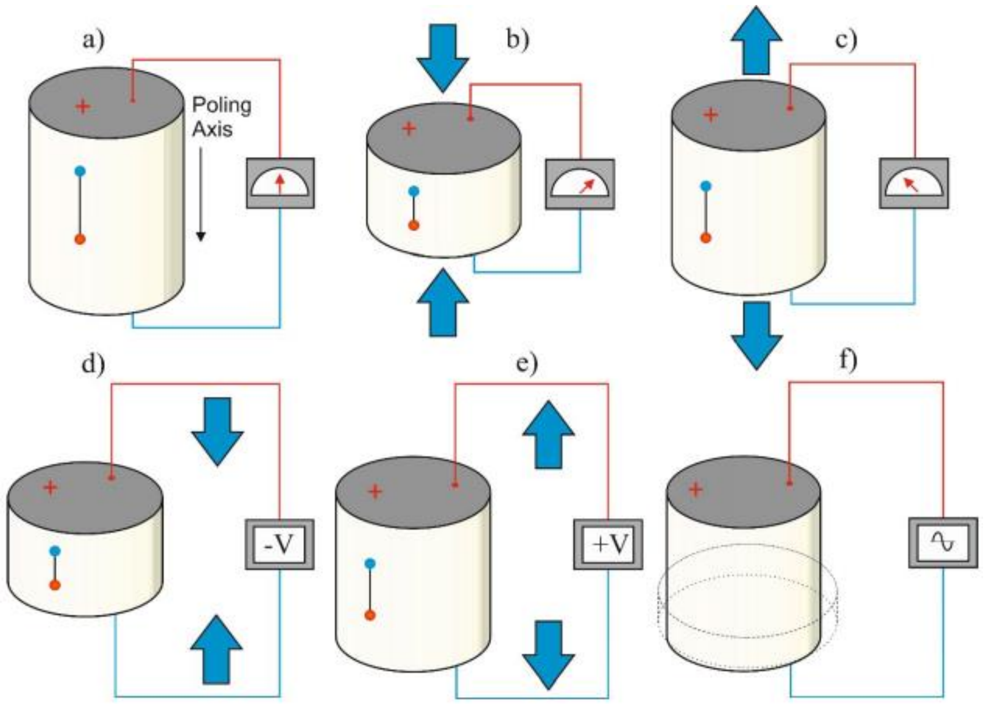

Figure 2 Illustrations of piezoelectric effects: direct piezoelectric effect a), b), c) and reverse piezoelectric effect d), e), f) [5]

Out of the 32 crystal classes that exist, only 20 of them exhibit piezoelectric properties. Among these, only ten are polar, meaning they show polarization without external pressure, while the rest are unipolar, as polarization is directly dependent on mechanical stress. Figure 3 depicts a molecular model of piezoelectric materials and illustrates how electric charge is generated in these materials when external stress is applied. In Figure 3a, negative and positive charges cancel each other out, resulting in a neutral molecule. When mechanical pressure or load is applied, it causes deformation, which separates positive and negative gravity centers. The poles inside the circle neutralize, and charges are distributed on the surface, resulting in polarization and the ability to convert mechanical energy into electrical energy.

There are different methods to manufacture PZT (Lead Zirconate Titanate) one of which is the solid-state reaction technique. In this method, various types of oxides are mixed in the required amounts and allowed to undergo a solid-state reaction through a calcination process. The oxides are continuously heated for 2 to 3 hours at a temperature of approximately 650°C. The resulting product is then heated again at 850°C, after which particle sizes are produced through milling. These particles are then shaped into desired forms, mostly discs, cylinders, or plates for use in transducers and actuators. The powder is mixed with a polymer binder using techniques such as uniaxial pressing and isostatic pressing. In uniaxial pressing, the powder is pressed along a single axis, resulting in the formation of a compacted powder. In contrast, isostatic pressing applies uniform pressure from all sides [5].

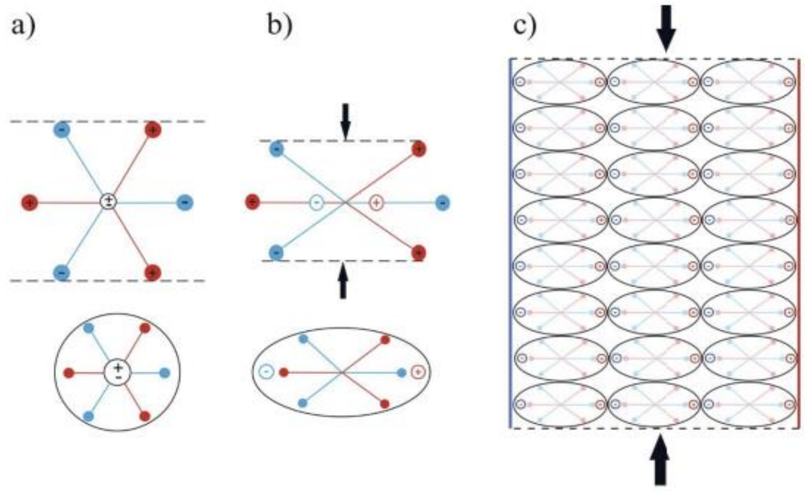

.

Figure 3 Model of piezoelectric material: a) an electrically neutral molecule appears b) generating little dipoles c) the material polarized [5]

3.2 Constitutive equations

This section of the thesis will cover the constitutive equations for linear piezoelectricity, presented in both tensor and matrix forms.

3.2.1 Global relations

When formulating the equation for the direct effect of electrical and mechanical stress, it is important to consider the changes in strain and electrical displacement in three orthogonal directions due to cross-coupling effects. To do so, tensor notations should be used to simultaneously describe the state of strain and stress with S_{ij} and T_{kl}, respectively. The stress sensor is correlated to the strain sensor through the fourth rank tensors of compliance s_{ijkl} and stiffness c_{ijkl}. The correlation between the electric field (Ek) and electric displacement (Di) is represented by the symbol ε_{ik}, which is known as permittivity. Therefore, the piezoelectric equations can be expressed as follows:

$$S_{ij} = s_i{}^{\mathrm{E}}{}_{jkl}\mathrm{T}_{\mathrm{kl}} + d_{ijk}E_k \quad (1.1)$$

$$Di = d_{ijk}T_{jk} + \varepsilon_i{}^{\mathrm{T}}{}_j E_{\mathrm{j}} \quad (1.2)$$

In equation 1.2 d_{ijk} represents piezoelectric constant. In the above equations E and T represent under constant stress and electric field respectively will be dielectric constant and the electric constant measured. In each of the first rank tensor there is three components which is followed by second rank tensor with 9 and third rank tensor with 27 components and so on. The number of components can be determined by 3^n rule. One important fact about them is that not all of them are independent. They depend mainly on orientation of the material. The number of independent components can be reduced by crystal symmetry and the choice of reference axes. In below Figure 4 the reference axes are shown [5].

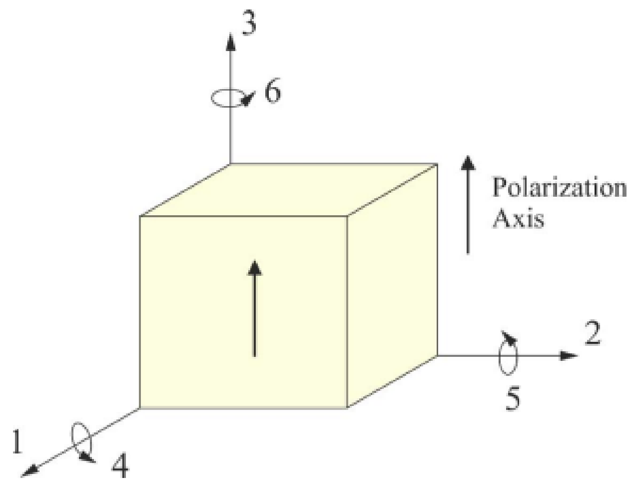

Figure 4 Reference axes [5]

3.2.2 Matrix notation

The above mentioned notation will be simplified here, where a 3- subscript tensor notation is replaced by a 2-subscript matrix notation and a 2-subscript tensor notation is replaced by a 1-subscript matrix notation.

Table 1 Matrix Notation [5]

ij or kl	p or q
11	1
22	2
33	3
23 or 32	4
13 or 31	5
12 or 21	6

$$c_{ijk} = c_{pq} \tag{1.3}$$

$$e_{ikl} = e_{iq} \tag{1.4}$$

$$T_{ij} = T_p \tag{1.5}$$

$$Sij = Sp \text{ when } i = j \tag{1.6}$$

$$2Sij = Sp \text{ when } i \neq j \tag{1.7}$$

With the help of notations as mentioned in table (Figure 5) can be returned as follows in matrix form:

$$\{S\} = [s]\{T\} + [d]\{E\} \tag{1.8}$$

$$\{D\} = [d]^T \{T\} + [\varepsilon]\{E\} \tag{1.9}$$

While comparing 1.2 and 1.9, in 1.9 there are other subscripts removed remaining just T which means transposed. It is assumed that the coordinate system coincides with the orthotropy axes of the material and that the direction of polarization coincides with direction 3 which results in (1.8) and (1.9) explicit forms as shown below in equation1.10 and 1.11 [5].

$$\begin{Bmatrix} S_{11} \\ S_{22} \\ S_{33} \\ 2S_{23} \\ 2S_{31} \\ 2S_{12} \end{Bmatrix} = \begin{bmatrix} s_{11} & s_{12} & s_{13} & 0 & 0 & 0 \\ s_{12} & s_{22} & s_{23} & 0 & 0 & 0 \\ s_{13} & s_{23} & s_{33} & 0 & 0 & 0 \\ 0 & 0 & 0 & s_{44} & 0 & 0 \\ 0 & 0 & 0 & 0 & s_{55} & 0 \\ 0 & 0 & 0 & 0 & 0 & s_{66} \end{bmatrix} \begin{Bmatrix} T_{11} \\ T_{22} \\ T_{33} \\ T_{23} \\ T_{31} \\ T_{12} \end{Bmatrix} + \begin{bmatrix} 0 & 0 & d_{31} \\ 0 & 0 & d_{32} \\ 0 & 0 & d_{33} \\ 0 & d_{24} & 0 \\ d_{15} & 0 & 0 \\ 0 & 0 & 0 \end{bmatrix} \begin{Bmatrix} E_1 \\ E_2 \\ E_3 \end{Bmatrix} \tag{1.10}$$

$$\begin{Bmatrix} D_1 \\ D_2 \\ D_3 \end{Bmatrix} = \begin{bmatrix} 0 & 0 & 0 & 0 & d_{15} & 0 \\ 0 & 0 & 0 & d_{24} & 0 & 0 \\ d_{31} & d_{32} & d_{33} & 0 & 0 & 0 \end{bmatrix} \begin{Bmatrix} T_{11} \\ T_{22} \\ T_{33} \\ T_{23} \\ T_{31} \\ T_{12} \end{Bmatrix} + \begin{bmatrix} \varepsilon_{11} & 0 & 0 \\ 0 & \varepsilon_{22} & 0 \\ 0 & 0 & \varepsilon_{33} \end{bmatrix} \begin{Bmatrix} E_1 \\ E_2 \\ E_3 \end{Bmatrix} \tag{1.11}$$

3.2.3 Coupling modes

The electro-elastic coupling in piezoelectric materials operates in three distinct modes, namely longitudinal mode (33), transverse mode (31), and shear mode (15), as shown in Table 2 for a rectangular bar. In the first configuration, the bar is polarized along its length, and as the potential difference is perpendicular to the polarization axis (Ox_3), there is a change in length in the same direction, which is commonly referred to as the converse piezoelectric effect. In the second case, the bar can be polarized in the thickness direction, which is influenced by the external field in the same direction.

Table 2 Basic coupling modes of piezoelectric material [5]

Constitutive equations	Illustration of the mode
Longitudinal mode $\begin{cases} S_3 = s_{33}^E \cdot T_3 + d_{33} \cdot E_3 \\ D_3 = d_{33} \cdot T_3 + \epsilon_{33}^T \cdot E_3 \end{cases}$	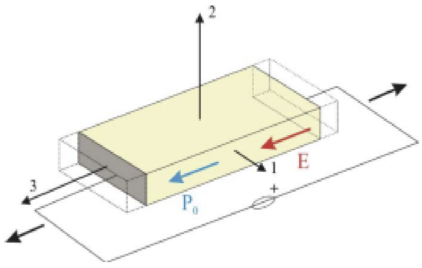 Longitudinal mode of operation: extension along ox3 axis; $d_{33}>0$; S_3 and E_3 of the same sign; electrode surface represented by grey color
Transversal mode $\begin{cases} S_3 = s_{11}^E \cdot T_1 + d_{31} \cdot E_3 \\ D_3 = d_{33} \cdot T_3 + \epsilon_{33}^T \cdot E_3 \end{cases}$	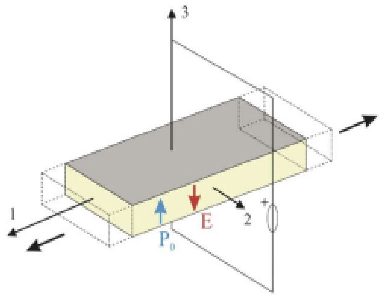 Transversal mode of operation: extension along ox1; $d_{31}<0$; S_1 and E_3 of opposite sign
Shear mode $\begin{cases} S_5 = s_{44}^E \cdot T_5 + d_{15} \cdot E_1 \\ D_1 = d_{15} \cdot T_5 + \epsilon_{11}^T \cdot E_1 \end{cases}$	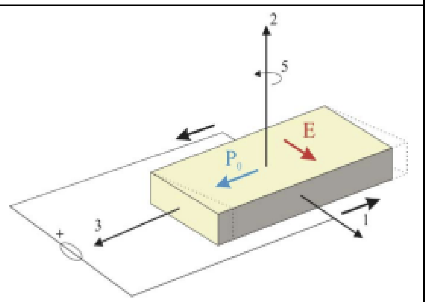 Shear around ox2 axis; $d_{15}>0$; S_5 and E_1 of the same sign

We can observe that in the second case, there is a change in length perpendicular to the direction of polarization, which is a direct result of transverse coupling. In the third case, the electric field is perpendicular to the direction of polarization, which results in deformation and is commonly known as the shear mode. With these three modes, a wide variety of configurations can be produced based on the geometry and polarization type, resulting in the production of various types of piezoelectric transducers that are widely used in manufacturing and other industries [5].

3.3 Overview of applications of piezoelectric materials

There are typically four types of piezoelectric devices: sensors, generators, actuators, and transducers. In sensors and generators, the direct piezoelectric effect is utilized, which means that mechanical energy is converted into electrical energy and measured as charge or voltage. Actuators work on the principle of the indirect piezoelectric effect, where electrical energy is converted into mechanical energy. Transducers combine both effects in a single device. Table 3 summarizes the different effects and their applications.

Table 3 Applications of piezoelectric materials [6]

Design/effect direction	Direct piezoeffect		Indirect piezoeffect	Both effects
	Sensor	Generator	Actuator	Transducer
Bulk material (d33-effect)	Accelerometers Knock Sensors Pressure/ForceSensors	High voltage spark igniters	-	Ultrasonic sonar devices Distance meters Ultrasonic materials charcterisation
Multilayer (d33-effect)	-	Energy Harvesting	Active vibration Reduction Nano-Positioning High -Force-actuation	-
Patch(monolithic) (d31-effect)	Dynamic strain sensor	Energy Harvesting	Active vibration Reduction	-
Patch(fibre composites) (d31 and d33 effect)	Dynamic strain sensor	Energy Harvesting	Active vibration Reduction	-
Bi-/trimorph (d31+bimorp effect)	-	-	Textile machine fans	-
Special designs	-	Cymbal transucers for energy harvesting	Ultrasonic Motors	Transformers

The most commonly used designs for these devices include multilayer, bimorph, and Moonie structures. This chapter extensively discusses the various piezoelectric effects and their diverse applications, ranging from nanoscience and energy harvesting to force sensing and actuator systems. However, the scope of piezoelectric devices is not limited to these applications but extends to numerous other areas such as piezoelectric cables, ultrasonic sensors, airbag sensors, ceramic filters and resonators, piezoelectric buzzers, and piezoelectric transformers. Although these devices were not specifically mentioned in the table, they follow the same operating principles as most of the devices listed in the table and differ only in their specific design [6].

3.4 Simulation of Piezoelectric Sensor and Actuator Devices

Simulation has emerged as a critical element in engineering that aids in anticipating the performance of a device, thereby preventing the needless expense and time involved in developing prototypes. It facilitates the design, enhancement, and characterization of piezoelectric sensors and actuator devices. As a result, the use of simulations can expedite device design, leading to reduced development costs and faster time-to-market. Simulations also enable the determination of quantities, such as those within a material, that would be expensive or impractical to measure. Several simulation approaches exist for technical devices, including finite difference, finite element, boundary element, and lumped circuit element methods. In this part of thesis, we will focus exclusively on the finite element (FE) method, which is particularly well-suited for numerical simulation of piezoelectric sensors and actuator devices. The FE method has numerous advantages, including numerical efficiency, the ability to discretize complex geometries, and the ability to conduct various types of analysis. However, it also has certain drawbacks, such as the need for significant discretization effort for large computational domains and the requirement for spatial boundaries. Special techniques, such as absorbing boundary conditions, may be needed for open domains required in numerical simulations, such as for the free-field radiation of an ultrasonic transducer. There are numerous commercially available FE software packages (FE solvers) for simulation, including ANSYS, COMSOL Multiphysics, NACS, and PZFlex, which differ in their supported physical fields and field coupling. In this chapter, we will focus on linear FE simulations and study the fundamental aspects of the FE method that are crucial for simulating the behavior of piezoelectric sensors and actuators. The basic steps of the FE method are illustrated in Figure 5. The starting point involves the partial differential equations (PDEs) governing the physical fields associated with the piezoelectric sensor and actuator. These PDEs are the so-called strong formulation, which is then multiplied by a suitable test function, resulting in a variational form. Upon partial integration (i.e., integration by parts) of the product over the entire computational domain, the weak formulation of the PDE is obtained. Finally, Galerkin's method is utilized, where both the quantity of interest and the test function are approximated using finite elements. This approach leads to an algebraic system of equations [7, pp. 83-84].

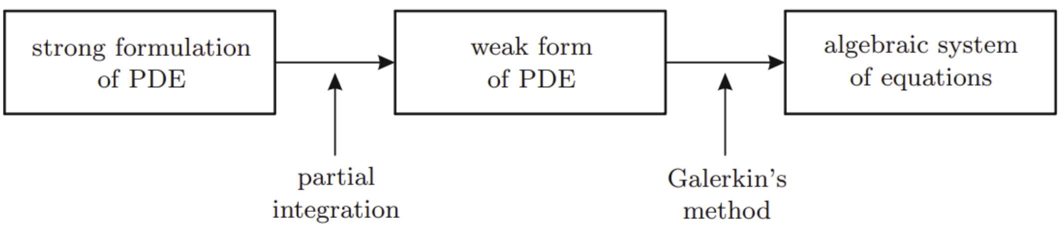

Figure 5 Basic Step of FE Method [7, p. 84]

3.4.1 Finite Element Method for a One-Dimensional Problem

To illustrate the concept of the FE method, a 1-D hyperbolic partial differential equation is examined, which is often encountered in mechanical problems. This type of PDE involves derivatives with respect to both time and space. The first step in the FE method is to formulate the strong form of the PDE, where the expression u (x, t) represents the desired quantity, such as mechanical displacement, that depends on both space x and time t. The constant c is a coefficient, and f(x, t) is a known excitation or source term that varies with space and time.

$$-\frac{\partial^2 u(x,t)}{\partial x^2} + c\frac{\partial^2 u(x,t)}{\partial x^2} = \mathrm{f}\,(\mathrm{x}, \mathrm{t}) \tag{3.1}$$

In addition to equation (3.1), boundary and initial conditions must be specified to solve the hyperbolic PDE uniquely. For the spatial computational domain x ∈ [a, b] and the time interval of interest t ∈ [0, T], appropriate conditions are needed.

boundary conditions: $\mathrm{u}\,(\mathrm{a}, \mathrm{t}) = \mathrm{u}_a$ and $\mathrm{u}\,(\mathrm{b}, \mathrm{t}) = \mathrm{u}_b$

initial conditions: $\mathrm{u}\,(\mathrm{x}, 0) = \mathrm{u}_0(\mathrm{x})$ and $\frac{\partial u(x,t)}{\partial t}|_{t=0} = \dot{\mathrm{u}}_0(\mathrm{x})$

and $\frac{\partial^2 u(x,t)}{\partial^2}|_{t=0} = \ddot{\mathrm{u}}_0(\mathrm{x})$

The terms u_a and u_b are used to describe fixed boundary conditions for the quantity u (x, t) that must be always satisfied, and are commonly known as Dirichlet boundary conditions. When $u_a = 0$, it is referred to as homogeneous Dirichlet boundary conditions, whereas $u_a \neq 0$ is known as inhomogeneous Dirichlet boundary conditions. Additionally, Neumann boundary conditions can be either homogeneous or inhomogeneous and involve specifying the first-order derivative ∂u/∂x with respect to space at the boundary of the spatial computational domain. The initial conditions $u_0(x)$, $\dot{u}_0(x)$, and $\ddot{u}_0(x)$ describe the quantity u (x, t), its first-order derivative, and its second-order derivative, respectively, at time t = 0 within the spatial computational domain x ∈ [a, b]. To create a well-organized representation of partial differential equations in strong form, along with boundary conditions (BC) and initial conditions (IC), utilize a concise scheme is utilized, that is also applied in later steps. Specifically, for the 1-D hyperbolic PDE, this scheme can be expressed as [7, p. 85]:

PDE

$$-\frac{\partial^2 u(x,t)}{\partial x^2} + c\frac{\partial^2 u(x,t)}{\partial x^2} = \mathrm{f}\,(\mathrm{x}, \mathrm{t})$$

$$\mathrm{x} \in [\mathrm{a}, \mathrm{b}];\ [\mathrm{a}, \mathrm{b}] \subset \mathrm{R}$$

$$\mathrm{t} \in [0, \mathrm{T}];\ [0, \mathrm{T}] \subset \mathrm{R}$$

3.4.2 Finite Element Method for a Multi-Dimensional Problem

In practical applications such as numerical simulations for sensors and actuators, dealing with two-dimensional (2-D) and three-dimensional (3-D) problems is often necessary. As a result, the spatial computational domain Ω cannot be divided into line intervals and alternative finite elements in R^2 and R^3 are required. Like 1-D problems, these finite elements must adhere to two important properties: (i) complete coverage of the computational domain and (ii) absence of element intersections. Figure 6 illustrates appropriate finite elements for 2-D (triangular and quadrilateral elements) and 3-D (tetrahedron and hexahedron elements) spaces. These elements are commonly referred to as nodal (Lagrangian) finite elements due to the local support of the ansatz functions on the nodes within the elements. FE simulations fundamentally require ansatz functions that have local support. This implies that each ansatz function must be non-zero only within the finite element under consideration and in its immediate neighbors. Lagrange and Legendre ansatz functions fulfill this requirement and are therefore suitable for the FE method.

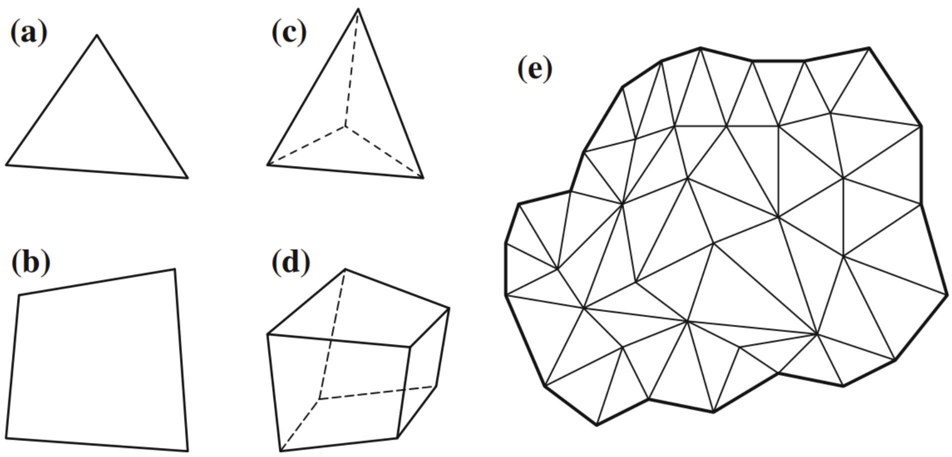

Figure 6 Finite elements to spatially discretize 2-D and 3-D computational domains :a) triangular element for R^2; b) quadrilateral element for R^2; c) tetrahedron element for R^3; d) hexahedron element for R^3; e) spatial discretization (also denoted as mesh or computational grid) of a 2-D computational domain by means of triangles [7, p. 90]

So far, we have only considered the spatial dependence in the FE method. However, physical processes often depend on both space and time. To account for time in the FE procedure, an appropriate time discretization must be employed [7, pp. 89-90].

3.5 Determination of physical and chemical quantities by piezoelectric sensors

Piezoelectric sensors are widely used in process measurement technology as they can determine various physical and chemical quantities. These include force, torque, pressure, acceleration, geometric distance, layer thickness, properties of liquids, concentrations of substances in fluids, fluid flow, cavitation activity, and temperature. Piezoelectric sensors work by measuring the impact of the targeted quantities on mechanical quantities, which in turn influences the electrical sensor characteristic due to the direct piezoelectric effect.

One type of piezoelectric sensor is the quartz crystal microbalance (QCM or QMB), which evaluates the resonance frequency of a specific vibration mode inside a disk-shaped quartz plate. QCM sensors mostly operate in thickness shear mode of piezoelectricity, and when the quartz disk is mechanically loaded by a mass, the frequency shift of the resonance frequency can be used to determine the thickness of a homogeneous material layer on the disk, as well as the material density when the layer thickness is known. In liquids, QCM sensors can determine density and viscosity, and with a sensitive layer, they can also measure substance concentration.

Other piezoelectric sensors are based on the propagation of waves between transducers. By calculating the time-of-flight of these waves, the sound velocity in the propagating medium can be determined when the geometric distance between transmitter and receiver is known. The ratio of emitted and received waves can be used to deduce characteristic parameters like liquid density and viscosity. Some piezoelectric sensors are compact and include both transmitter and receiver, commonly comprising a piezoelectric material or a silicon substrate with an additional piezoelectric film. These sensors differ in the type of waves that propagate inside as shown in Figure 7, such as surface acoustic wave (SAW) sensors, love wave (LW) sensors, flexural plate wave (FPW) sensors, and shear-horizontal acoustic plate mode (SH-APM) sensors. All these sensors are commonly referred to as bulk acoustic wave (BAW) sensors and are based on wave propagation in solids. They are also referred to as micro acoustic resonators depending on their underlying operation principle and geometric size. These sensors can be equipped with a sensitive layer between transmitter and receiver, allowing for biological and chemical analyses [7, pp. 407-409] [8].

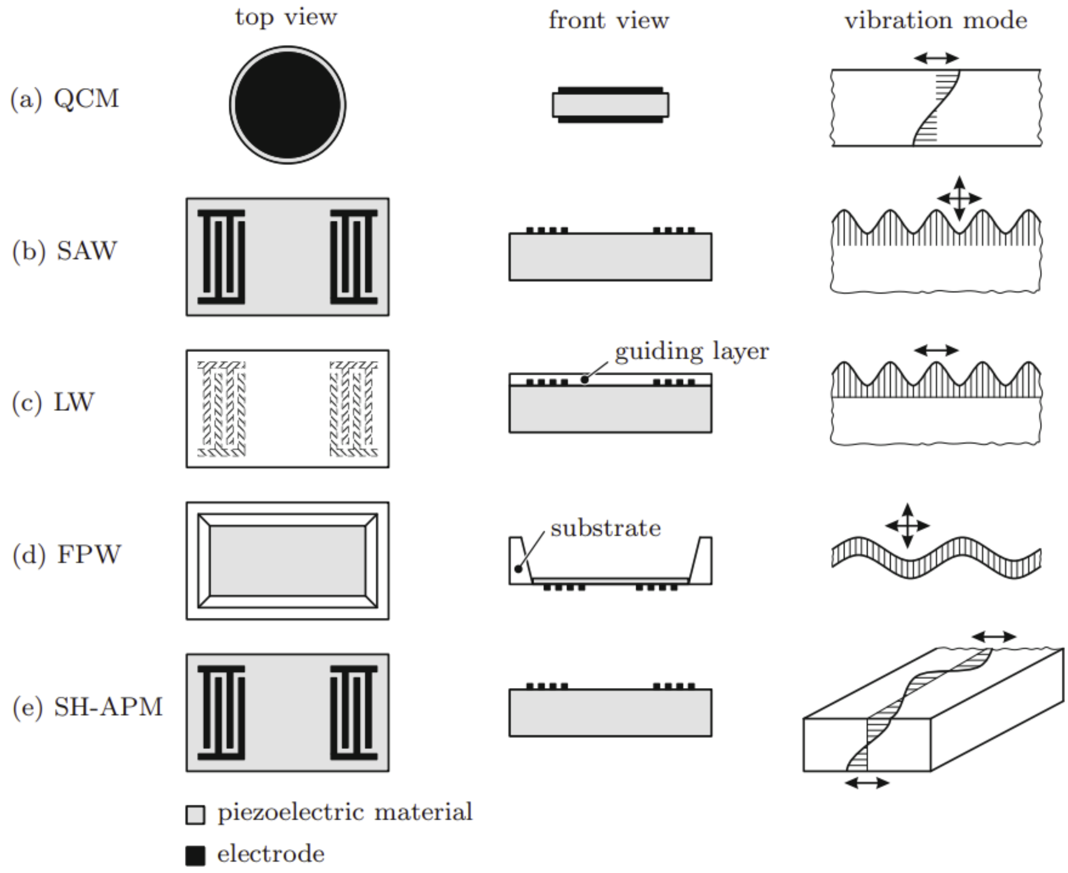

Figure 7 Principle setup of a quartz crystal microbalance (QCM) sensors, b surface acoustic wave (SAW) sensors, c love wave (LW) sensors, d flexural plate wave (FPW) sensors, and e shear-horizontal acoustic plate mode (SH-APM) sensors; schematic representation of propagating waves in right panels; arrows indicate dominating directions of particle motion [7, p. 408]

4 LATHE MACHINE

The metal working industry relies heavily on the lathe machine, which operates by rotating a work piece and applying a fixed cutting tool. As the tool is fed into the rotating work piece, it shapes the material into the desired form. This process has been used for centuries, with wood lathes dating back to at least 1569 in France. During the Industrial Revolution in England, the lathe machine was adapted for metal cutting, and became known as the "Engine Lathe" due to its early steam engine-driven design. The lathe machine is often considered the progenitor of all machine tools, earning it the nickname "the mother/father of the entire tool family" [9].

4.1 Construction of Lathe Machine

The manufacturing of a lathe machine is a challenging process therefore it should be started by producing individual parts of the machine and subsequently assembled. Most of these parts are made using cast iron, and it is manufactured one by one as each part is taken into consideration. The lathe machine comprises five key components as shown in Figure 8, which include the

- Headstock,
- Tailstock,
- Bed,
- Carriage and
- Gears [10, p. 1].

4.1.1 Headstock

The headstock is a crucial component of the lathe machine, situated on the machine's left side, and made from cast iron. This part of the machine houses all the mechanisms required for its operation, including the gears and motor used for starting and stopping the machine. Within the headstock, there are several important sub-components, such as the motor, gears, chuck, spindle, and clutch, which play a significant role in the overall performance of the lathe machine [10, p. 2].

4.1.2 Tailstock

The tailstock is a highly significant component of the lathe machine, located on the machine's right side and manufactured through casting with cast iron. This component comprises various sub-parts such as the tailstock spindle, tailstock lock lever, tailstock wheel, and tailstock lock spindle lock lever [10, p. 2].

4.1.3 Bed

The bed is the foundation of the lathe machine, with two- or four-feet providing support. The entire structure of the lathe machine is built upon the bed, which is cast from cast iron. The bed of the lathe machine also contains several racks beneath it, designed to hold various components such as tools, jaws, and other parts of the machine [10, p. 2].

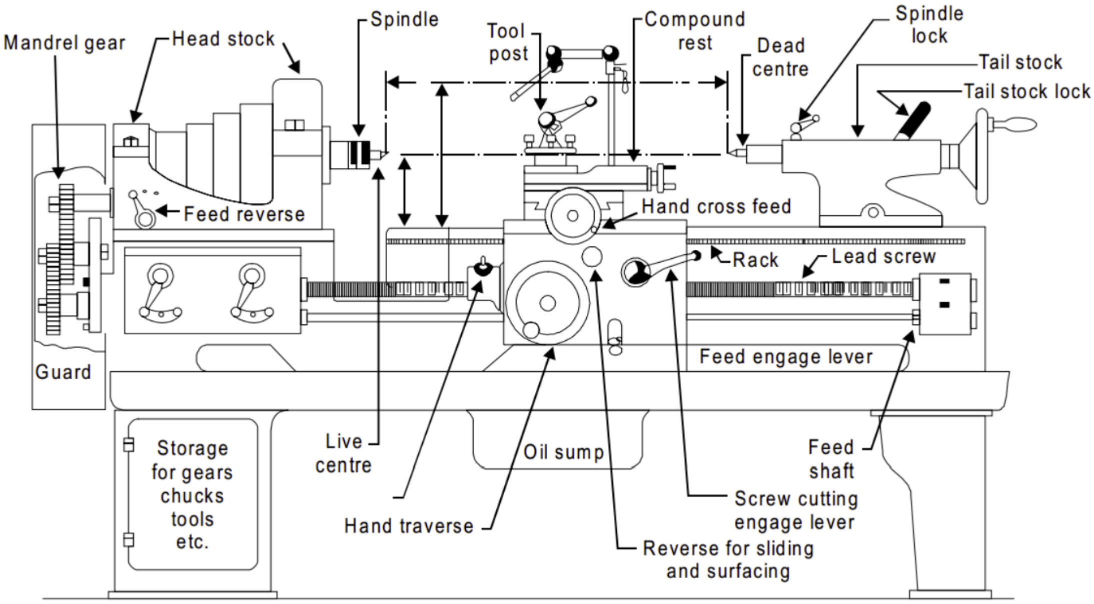

Figure 8 Lathe Machine [10, p. 2]

4.1.4 Carriage

The carriage is another critical component of the lathe machine, situated between the headstock and the tailstock, and cast from cast iron. It moves back and forth along the bed ways, which are situated on the lathe machine bed, and comprises several sub-components such as the carriage wheel, carriage auto feed lever, cross slide, compound slide, tool post, and tool post lock lever. The cross-slide moves along the cross-slide keyways on the carriage, in a vertical direction relative to the jab, allowing for depth of cut adjustments. The compound slide provides a means for turning tapers and cutting angles without having to rotate the headstock. The cutting tool can be mounted across the front or on either side of the head, and the tool post is used to clamp the tool on the lathe machine for various operations [10, p. 3].

4.1.5 Gears

The gears of the lathe machine are located within the headstock, providing the power required for its operation. They enable the machine to speed up or slow down, facilitating various processes performed on the lathe. It is essential to ensure that the gears are fully covered to prevent any potential damage to individuals or other equipment in the vicinity [10, p. 3].

4.2 Feed Mechanisms

For a smooth and steady machining process of a component, the feed mechanism is always governed by the spindle speed, as both need to be synchronized. In a conventional lathe machine, the spindle is driven by an induction motor, and the speed is regulated by different gear meshing ratios, resulting in coarse speed and feed. On the other hand, a CNC lathe machine's spindle speed and feed are optimized, as both systems are controlled with servo drives. Therefore, while describing the feed mechanism, it should be separately explained.

In a conventional machine, the drive is given to the feed box through a gear that has a combination of gear ratio meshing. This output feed shaft's rotation is transmitted to a pinion in the apron mechanism fitted on the saddle. The toothed rack, located under the longitudinal guide way throughout the bed's length, is meshed with this pinion, resulting in longitudinal feed. The feed rate can be selected using three selection control levers on the feed box. A lever fitted on the apron mechanism engages or disengages the feed pinion gear, causing the feed to engage or disengage.

In a CNC machine, the feed is achieved with a servo drive mechanism. This mechanism consists of a command feeder, a servo drive command controller, a servo motor, and a feedback mechanism. The command given through a computer is analyzed in the feed servo drive unit, which passes instructions to the drive motor to move in steps of 0.001 mm, as set in the system parameters. The movement is counted with an optical instrument called an encoder, which gives feedback to the controller about the speed. The controller then calculates how much further instruction to give to reach the commanded point. This system is a closed-loop system [10, p. 4].

4.3 Lathe Machine Accessories and Attachments

In lathe machining operations, accessories refer to the various tools and equipment utilized regularly. On the other hand, attachments are specific fixtures that can be affixed to the lathe to broaden its capabilities and allow for operations such as taper cutting, milling, and grinding [10, p. 5].

4.3.1 Accessories

The accessories listed below are widely employed in lathes. By combining these elements, a lathe can be set up for operation.

- Chuck
- Lathe faceplate
- Lathe centers
- Mandrels
- Tapper attachments [10, p. 5]

4.3.1.1 Chuck

To secure the workpieces to the headstock spindle of a lathe, chucks, faceplates, or lathe centers are used. A lathe chuck is a tool that applies pressure on the workpiece to hold it firmly onto the headstock spindle or tailstock spindle. Some of the most commonly used chucks include independent chuck, Universal scroll chuck, Combination chuck, Drill chuck, Collet chuck and Step chuck [10, p. 5].

4.3.1.2 Lathe faceplate

The lathe faceplate is a circular, flat plate that can be screwed onto the headstock spindle of the lathe. It is primarily used for securing and machining workpieces that have irregular shapes and cannot be effectively held by chucks or positioned between centers [10, p. 5].

4.3.1.3 Lathe centers

Workpiece support in a lathe is commonly achieved using lathe centers. These centers typically feature a tapered point with a 600 included angle that matches the angle of the workpiece holes. The workpiece is supported between two centers, with one center placed in the headstock spindle and the other in the tailstock spindle. Other accessories commonly used for workpiece support include lathe dogs, male centers, pipe center [10, p. 5].

4.3.1.4 Mandrels

When a workpiece cannot be held between centers or on a chuck or faceplate, it is often machined using a mandrel, which is a tapered axle that is pressed into the bore of the workpiece to support it between centers. It's important to note that a mandrel is not the same as an arbor, which is used for holding tools. There are two types of mandrels: solid machine mandrels and expansion mandrels [10, p. 6].

4.3.1.5 Tapper attachments

The taper attachment is a lathe accessory that is utilized for turning and boring tapers. It is fixed to the back of the carriage saddle of the lathe. The taper attachment is connected to the cross-slide of the lathe in such a way that it shifts the cross-slide in a lateral direction as the carriage is moved longitudinally. This movement results in the cutting tool being positioned at an angle to the axis of the workpiece, which then facilitates the creation of a taper. The use of a taper attachment ensures that the taper produced is accurate and consistent throughout the length of the workpiece [10, p. 6].

4.3.2 Attachments

There are five distinct types of attachments used in lathe machines, each with a different purpose. These attachments are listed below:

- Taper Turning Attachment for Lathe
- Milling Attachment for Lathe
- Grinding Attachment for Lathe
- Gear Cutting Attachment for Lathe
- Spherical Turning Attachment for Lathe [10, p. 6]

4.3.1.1 Taper Turning Attachment for Lathe

Modern lathes are commonly equipped with a taper bar located at the rear of the bed that can be adjusted to various angles relative to the spindle axis. A sliding block is mounted on the bar as shown in Figure 9, which is connected to the back of the cross-slide during taper turning. As a result, when the saddle is moved along the bed, the cross-slide moves in parallel with the taper bar. The lead screw controlling the depth of cut is released, allowing the cross-slide to move independently. By moving the tool parallel to the taper bar, a taper is produced. To adjust the depth of cut, the top slide is rotated 90 degrees to be perpendicular to the work [10, p. 7].

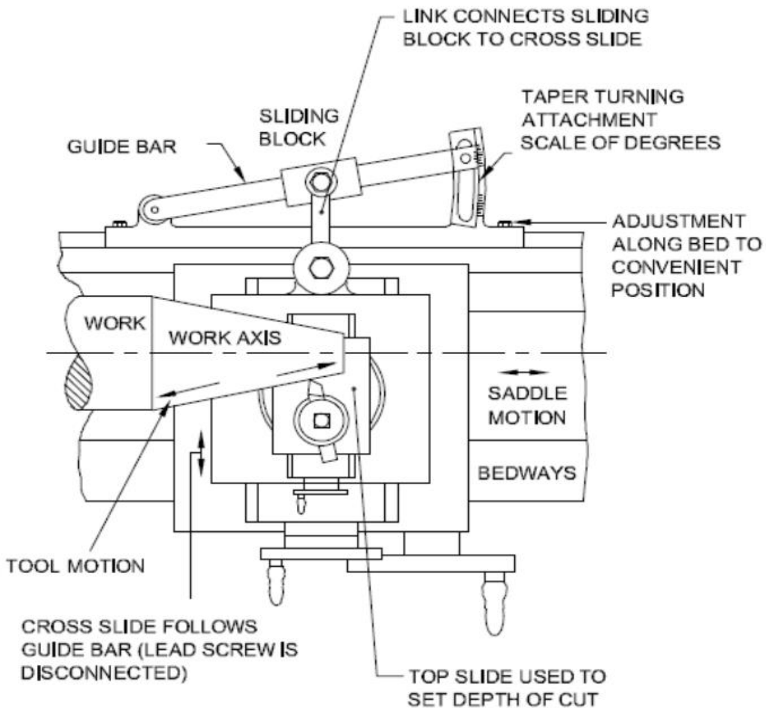

Figure 9 Taper Turning Attachment for Lathe [10, p. 7]

4.3.1.2 Milling Attachment for Lathe

The milling attachment is a lathe accessory that replaces the compound rest and is mounted on the cross-slide. It can hold the workpiece perpendicular to the milling cutter, which is either mounted in a collet or a chuck. The other type of attachment involves holding the workpiece between centers, and both the indexing head and milling cutter are mounted on the compound rest, which has a driving unit. These attachments allow for feeding in all three directions, making it possible to perform a variety of operations, including keyway cutting, angular milling, Tee slot cutting, and thread milling [10, p. 7].

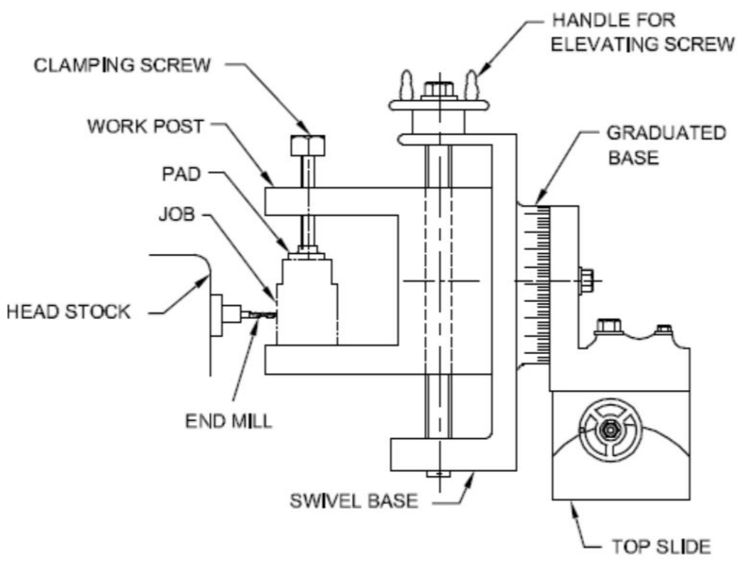

Figure 10 Milling Attachment for Lathe [10, p. 7]

4.3.1.3 Grinding Attachment for Lathe

By using a high-quality electric grinding attachment, the lathe becomes capable of various grinding operations, such as re-sharpening reamers and milling cutters, as well as grinding hardened bushings and shafts [10, p. 8].

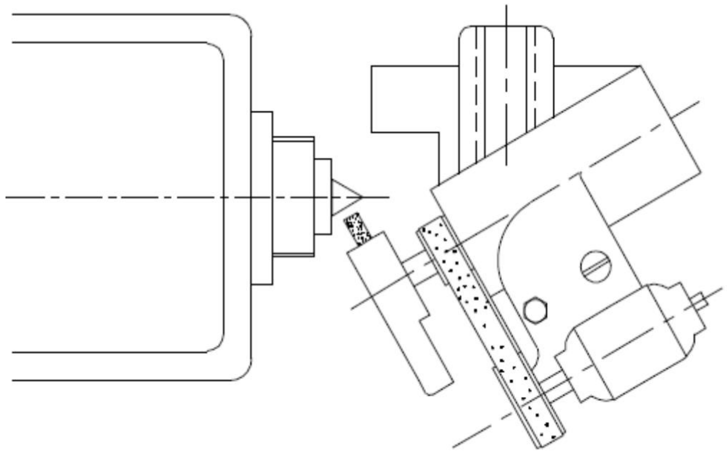

Figure 11 Grinding a center on a Lathe [10, p. 8]

4.3.2.4 Gear Cutting Attachment for Lathe

The gear cutting attachment enables the cutting of both bevel and spur gears, as well as performing external keyway cutting, linear indexing, slotting, and other standard lathe operations [11].

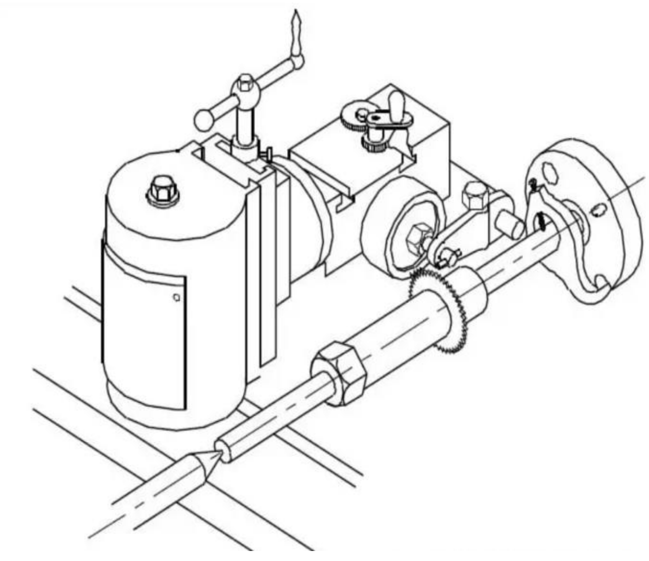

Figure 12 Gear Cutting Attachment for Lathe [11]

4.3.2.5 Spherical Turning Attachment for Lathe

The spherical turning attachment is typically installed on the cross slide of center lathes to shape concave, convex, and spherical surfaces. By positioning the tool in the tool post at a specific angle relative to the workpiece, this attachment can be used to produce various components [11].

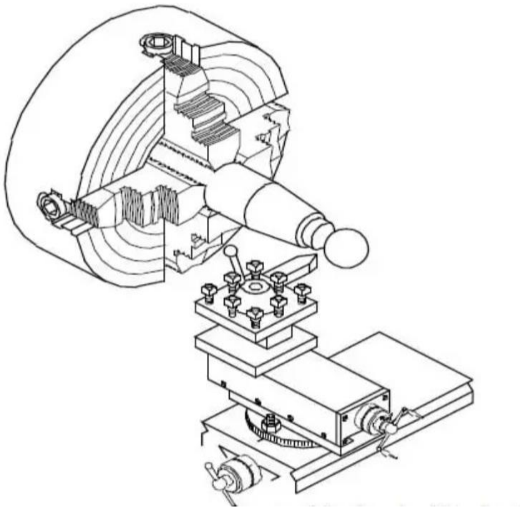

Figure 13 Spherical Turning Attachment for Lathe [10]

4.4 Lathe Operations

This chapter will discuss various types of lathe operations that can be performed using attachments.

4.4.1 Turning

Among all the operations performed on lathe machines, turning is the most used one. The objective of turning is to remove the excess material from the workpiece to obtain a cylindrical surface of the desired length. The workpiece is held either between centers or in a chuck, and it rotates at the required speed. The cutting tool is moved longitudinally with a proper depth of cut towards the headstock to give the desired feed. Turning produces a very good surface finish on the workpiece [10, p. 10].

4.4.2 Facing

This operation involves cutting the end of the workpiece perpendicular to the lathe axis, reducing its length. A regular turning tool or facing tool may be used for this operation. It is important to set the cutting edge of the tool at the same height as the center of the workpiece. Facing can be divided into two operations: roughing and finishing. During roughing, a depth of cut of 1.3mm is used, while during finishing, a depth of cut of 0.2-0.1mm is used [10, p. 10].

4.4.3 Chamfering operation

Chamfering is the process of creating a beveled surface at the edge of a cylindrical workpiece, such as bolt ends or shaft ends. This is done to prevent damage to the sharp edges and to protect the operator from getting hurt during other operations. Chamfering also makes it easier to screw a nut onto a bolt [10, p. 10].

4.4.4 Knurling Operation

Chamfering involves creating a beveled surface at the edge of a cylindrical workpiece, such as the ends of bolts or shafts. The purpose of chamfering is to prevent damage to the sharp edges and to protect operators from injury during subsequent operations. Additionally, chamfering makes it easier to thread a nut onto a bolt. On the other hand, knurling is typically performed at the lowest speed setting available on a lathe. It is used to create a patterned surface on handles and gauge ends. The feed rate for knurling ranges from 1 to 2 mm per revolution, and it may require two or three passes to produce the desired impression [10, p. 10].

4.4.5 Thread Cutting

Thread cutting is an important lathe operation used to create continuous helical grooves on a workpiece. External thread cutting produces threads on the outside surface, while internal thread cutting creates threads on the inside surface. The workpiece rotates between live and dead centers, with the tool moved longitudinally to produce the desired thread type. The motion of the carriage is driven by the lead screw, and depth of cut can be controlled by rotating the handle with a pair of change gears [10, p. 11].

4.4.6 Grooving

Grooving is the method of decreasing the diameter of a workpiece over a narrow surface using a grooving tool, which is like a parting-off tool. This operation is commonly performed at the end of a thread or near a shoulder to leave a small margin [10, p. 11].

4.4.7 Forming

Form-turning is the process of shaping a workpiece into a convex, concave, or irregular shape. This process can be achieved by using a forming tool, combining cross and longitudinal feed, or by tracing a template. The objective of using forming tools is to achieve a fine surface finish while minimizing the removal of material. There are two main types of forming tools: straight and circular. The straight type is used for wider surfaces, while the circular type is used for narrow surfaces [10, p. 11].

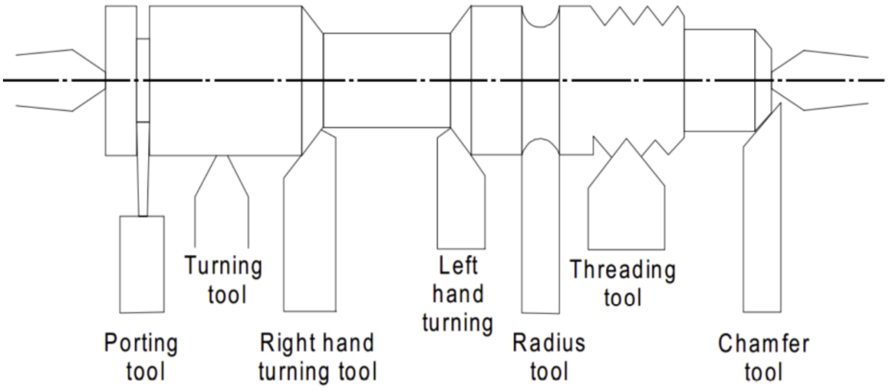

Figure 14 Lathe Machine Operations [10, p. 12]

4.5 Working Principle of Lathe Machine

The main function of a lathe machine is to remove material from the surface of a workpiece using cutting tools and providing the necessary amount of feed. This is achieved by placing the workpiece in a chuck which is rotated by a motor. Three-jaw chucks are used for circular workpieces while four-jaw chucks provide better stability for rectangular or square workpieces. The headstock of a lathe machine contains a power transmission system that is engaged using suitable levers. It also has a chuck to hold the workpiece securely. For smaller workpieces, a tailstock may not be necessary, but for larger ones, it is required to support the workpiece firmly without any vibrations during machining. A tool post holds the cutting tool perpendicular to the workpiece to remove material from its circumference, reducing its diameter. The workpiece rotates when power is supplied, and the tailstock is adjusted accordingly depending on the type of operation being performed. For turning operations, the workpiece and tool are perpendicular to each other, while for taper turning, they are inclined. By providing the necessary amount of feed, material removal takes place, and the speed can be increased by adjusting the levers in the headstock to suit the material removal. Lathe machines can be operated manually or automatically. In small-scale industries, manual operation may be sufficient, while large-scale industries use CNC machines, which can run automatically with the help of a program [11].

4.6 Requirement

When designing a lathe machine, several factors must be considered to ensure it meets the necessary requirements. The first consideration is the size of the machine, which should be appropriate for the intended use. The material being machined should also be considered, as different materials require different cutting speeds and feeds. The precision required in the finished product is another important factor, as some machines are designed for higher precision than others. The power and torque of the machine should also be considered, as this will determine the maximum size and hardness of the material that can be machined. The ease of use and accessibility of the machine controls are also important, as well as the safety features that are built into the machine. Finally, the cost of the machine should be considered to ensure that it is within budget while still meeting all necessary requirements. In order to produce or select the best possible Lathe machine, certain criteria should be taken into consideration [12].

4.7 Chip Formation in Lathe

During any machining process, chips are formed as material is removed from the workpiece, with the characteristics of the chips varying depending on the operation. The analysis of chip formation is crucial, as the size and shape of the chips can reveal important information about the nature and quality of the process. Chips are produced through either tearing or shearing. When chips are formed by tearing, the material adjacent to the tool face is compressed, causing a crack to propagate towards the body of the workpiece. The resulting chip is heavily deformed, while the workpiece material remains relatively unchanged. Cutting occurs intermittently, with no movement of the workpiece material over the tool face. Conversely, in chip formation by shearing, the chip moves more freely over the tool face. As the cutting tool advances into the workpiece, the metal ahead of the tool is subjected to severe stress. The tool creates an internal shearing action in the metal, causing the material below the cutting edge to yield and flow plastically, resulting in the formation of a chip. Initially, the metal beneath the tool edge is compressed, and then the metal separates when its compression limit is exceeded [13].

The chip formation process depends on various factors such as cutting speed, feed rate, depth of cut, and the material properties of both the workpiece and the cutting tool. The chip formation process can be broadly categorized into three types:

1. Continuous chip formation: In this type of chip formation, a continuous, long, and narrow chip is formed due to high cutting speeds, shallow depths of cut, and low feed rates. This type of chip formation is commonly observed in ductile materials.

2. Discontinuous chip formation: In this type of chip formation, the chips are broken into small, irregularly shaped pieces due to high feed rates, low cutting speeds, and deep depths of cut. This type of chip formation is common in brittle materials.

3. Built-up edge chip formation: In this type of chip formation, a small edge of material from the workpiece adheres to the cutting tool due to high temperature and pressure, forming a built-up edge. This built-up edge then breaks off, forming a chip. This type of chip formation is common in materials that have a tendency to adhere to the cutting tool.

Proper chip formation is crucial in achieving high-quality surface finish and dimensional accuracy in lathe operations. We must select appropriate cutting conditions and cutting tools to optimize chip formation and prevent tool wear and workpiece damage [14].

Improving chip formation in lathe can lead to better surface finish, longer tool life, and higher productivity. Here are some ways to improve chip formation in lathe:

1. Appropriate cutting conditions: The cutting speed, feed rate, and depth of cut are critical factors that affect chip formation. By adjusting these parameters, we can optimize chip formation and avoid issues such as chip clogging, built-up edge formation, and tool wear.

2. Suitable cutting tools: By choosing the right cutting tool can improve chip formation and prevent chip-related issues. For example, using a tool with a sharp cutting edge and a chip breaker design can help break chips into manageable sizes and prevent chip clogging.

3. Proper lubrication and cooling: Using appropriate lubrication and cooling can reduce friction and heat generation during cutting, which can improve chip formation and prevent tool wear. Proper lubrication and cooling can also help remove chips from the cutting zone and prevent chip recutting.

4. Ensure proper workpiece holding: Proper workpiece holding is crucial for stable cutting and consistent chip formation. Machinists should ensure that the workpiece is securely held in place and that the cutting forces are evenly distributed.

5. Maintain lathe machine: Proper maintenance of lathe machine, including cleaning and lubrication of the machine and its components, can help improve chip formation. A well-maintained machine can ensure stable cutting conditions, prevent machine vibration, and improve chip evacuation.

By implementing these techniques, we can optimize chip formation in lathe operations, leading to better surface finish, longer tool life, and higher productivity [15].

4.8 Piezoelectric sensors and actuators in Lathe Machine

Piezoelectric sensors and actuators are commonly used in lathe machines for precision positioning, active damping, tool vibration control, and monitoring various machining parameters. In this chapter it is described how these components are used in a lathe machine.

Piezoelectric sensors are used to measure different machining parameters such as cutting forces, vibration, and surface roughness. These sensors can be mounted on the tool holder, workpiece, or machine structure, depending on the application. The sensor generates a voltage when it experiences mechanical deformation, and this voltage is proportional to the deformation. By measuring this voltage, the sensor can provide information about the machining process.

Piezoelectric actuators are used for precision positioning, active damping, and tool vibration control. These actuators can be used to adjust the position of the tool holder or workpiece with high precision. They can also be used to control the vibration of the cutting tool and compensate for cutting forces in real-time, improving machining accuracy and surface quality. The actuator generates a mechanical deformation when a voltage is applied to it, and this deformation can be used to produce precise movements.

Piezoelectric sensors and actuators can be used simultaneously in a lathe machine. The sensor data can be used to adjust the actuator output and optimize machining parameters in real-time. For example, if the sensor detects high vibration or cutting forces, the actuator can adjust the tool position or compensate for the forces to improve the machining quality. By using both sensors and actuators, the machining process can be monitored and adjusted in real-time to achieve the desired surface finish and accuracy.

In summary, piezoelectric sensors and actuators are essential components in modern lathe machines. They can be used to monitor various machining parameters, control tool vibration, and improve machining accuracy and surface quality. By using both sensors and actuators, the machining process can be optimized in real-time to achieve the desired results.

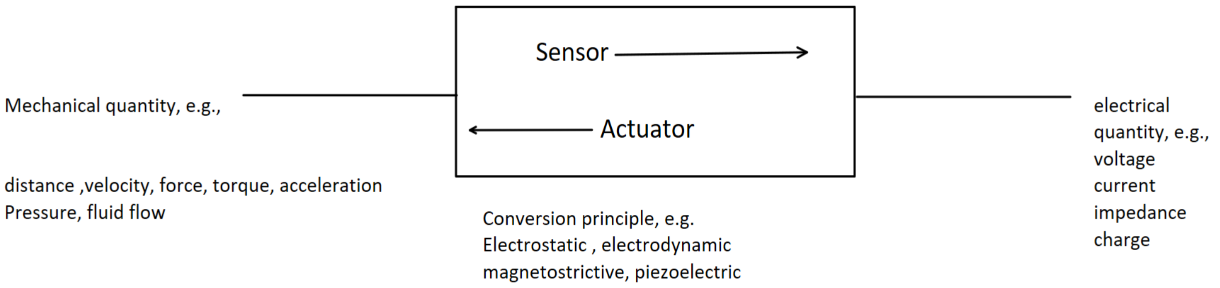

Figure 15 Typical conversion principles [7]

By combining the capabilities of piezo sensors and actuators, lathe operators can achieve more precise, efficient, and safe machining operations. The sensors provide real-time feedback on machining parameters, while the actuators can actively control and adjust the machining process to optimize performance and quality. The typical conversion principle is illustrated in Figure 15 [7, pp. 1-4].

In Table 4 the utility of piezo sensors and actuators in lathe machine mentioned in paragraph above is illustrated including more information:

Table 4 Utility of piezo sensors and actuators in lathe machine

Piezo Sensor in Lathe	**Piezo Actuator in Lathe**	**Combined**
1. Measuring cutting forces, vibrations, and tool wear during machining process	1. Active vibration control to suppress chatter and improve surface finish	1. Sensor gives feedback to optimize actuator control and improve machining performance
2. Detecting tool wear and providing an indication for replacement or re-sharpening	2. Actively adjusting cutting parameters for optimal machining performance	2. Uses sensor feedback to adjust actuator control and extend tool life
3. Monitoring the amplitude and frequency of vibrations to avoid chatter and improve the quality of the machined parts	3. Actively compensating for thermal expansion and deflection of the machine tool	3. Sensor feedback is used to adjust actuator control and improve surface finish
4. Measuring surface finish and dimensional accuracy to ensure quality standards are met	4. Providing rapid and precise actuation for various machining processes	4. Sensor feedback also used to optimize actuator control and ensure quality standards are met
5. Detecting and diagnosing tool breakage or collision	5. Actively controlling and adjusting the cutting tool path for complex geometries	5. Information from sensor is used to adjust actuator control and ensure safe operation

5 EXPERIMENTAL VERIFICATIONS

In this chapter experimental verification of two manufactured piezoelectric sensor and actuator in Lathe described.

5.1 Design of a Piezoelectric Actuator

The machining process of turning is crucial in manufacturing, particularly in high-precision applications where surface finish is critical. The surface finish is related to the vibrations and interactions between the part and cutting tool. Real-time variations in spindle speed, cut depth, feed rates, and material properties can result in undesirable effects on the vibrations and dynamic interactions. Therefore, a high-bandwidth actuator, such as a piezoelectric actuator, is necessary to enable a control system to react to changing vibration conditions and improve surface finish. This research project focuses on designing and evaluating a high-force, low-displacement, and high-bandwidth piezoelectric actuator for use in a conventional CNC lathe. The actuator's dynamic characteristics are predicted by creating a finite element model, and the baseline performance is evaluated experimentally using accelerometers and a non-contact laser displacement sensor. The actuator's self-sensing capability is measured, and its performance is evaluated in face cutting operations on aluminum rods to determine its effects on surface finish. The goal is to document the actuator's performance characteristics for future use in high-precision machining operations. The use of piezoelectric actuators can also help to reduce chatter and improve surface finish quality in other machining processes, such as boring and precision shaft cutting.

In this study from Albert, Luke and Matthew, the fast tool servo will be initially simulated through a finite element model to gain knowledge about the operating frequency ranges. Then, the actuator's performance will be evaluated in a laboratory setting to validate the FE model. Following this, the actuator will be affixed to a CNC lathe for testing purposes. During the lathe testing, the facing operations will be carried out in three different modes, i.e., with the actuator turned off, powered at a constant frequency, and subjected to a voltage sine sweep [16].

5.1.1 Apparatus

The experimental setup involves a lathe tool assembly consisting of various components such as a cutting tool piece, tool holder assembly, diaphragm, piezoelectric stack, preload piece and supporting shell structures as shown in Figure 16. Three diaphragms with different thicknesses like 1.5875 mm,3.1750 mm and 4.7625 mm were tested. Instruments like Photon DACTRON, Keyence LC -2400A laser displacement system, FLIR Thermacam, and a model 354C10 ICP tri-axial accelerometer were used to determine the dynamic characteristics of the assembly. The HPSt 500/10-5/15 model of piezoelectric stack was used. For cutting testing, a NI 6052E PCI data acquisition card and MATLAB Data Acquisition Toolbox were used for data collection [16].

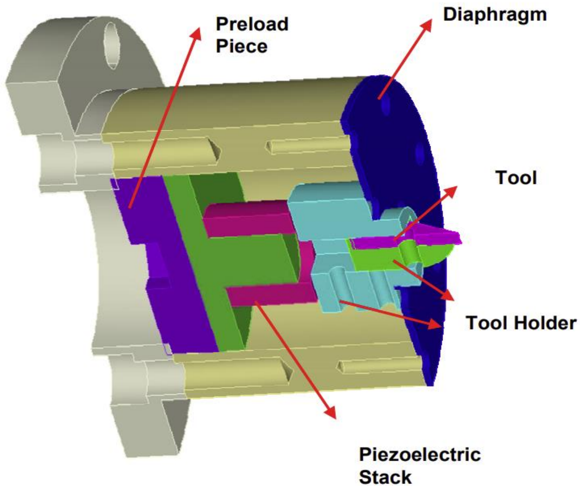

Figure 16 Lathe Tool Assembly [15]

5.1.2 Procedure

This study involves four distinct types of tests: modulus test, piezoelectric hysteresis test, thermal piezoelectric characteristics test, and facing cuts with a fast tool servo test. In modulus test, three diaphragms of different nominal thicknesses (1.5875 mm, 3.1750 mm and 4.7625 mm) were tested individually for each setup. The first step of the modal tests was to perform a free-free impact test of each diaphragm to validate the accuracy of the model. Once the model was properly modified, the dynamics of the metal casing and the bolted boundary condition were introduced to the FE model of the diaphragm assembly and compared to the corresponding experimental data. After testing all the components without the piezoelectric stack, the complete FTS was assembled and tested. After the complete assembly of the FST, the piezoelectric stack was inserted within it. The actuator comprises four wire leads, out of which the voltage input wires are identified by the red (+) and black (-) leads. These two wires were joined to the output terminals of a 200 V, 50 mA amplifier. The light blue terminals are designated as the PZT sensor output connections. The FTS frequency response was determined using a burst random signal excitation, and the experiment was repeated for each of the different diaphragm thicknesses.

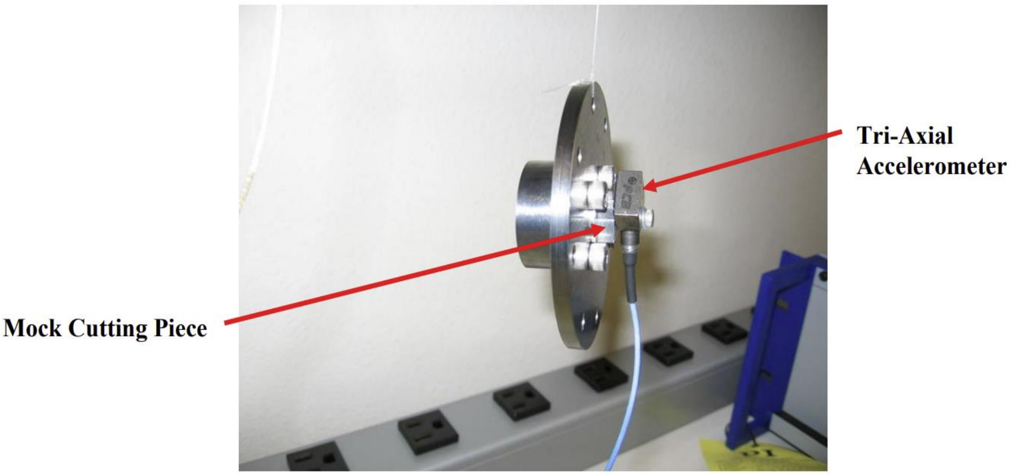

Figure 17 Diaphragm Assembly in Free-Free condition [16]

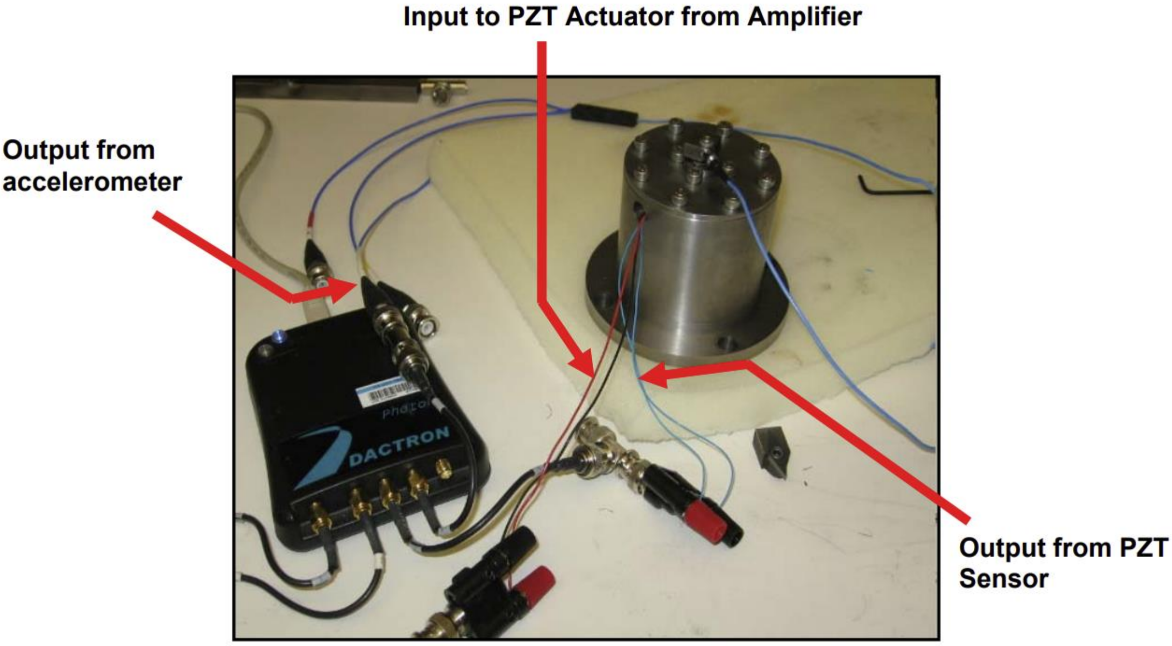

Figure 18 Powered FTS Frequency Response Analysis Setup [15]

Next step was piezoelectric hysteresis to get tested. To test the piezoelectric hysteresis of the fully assembled FTS as shown in Figure 18, a voltage was applied in incremental steps, starting from zero and increasing up to 1000 V, using a 1000 V DC amplifier. The displacement of the tool tip was measured by a Keyence LC-2400 A laser displacement sensor. The voltage was increased up to 1000 V then decreased back to zero, and this cycle was repeated three times for each diaphragm to ensure consistency. To test the thermal properties of the piezoelectric stack, a FLIR SC500 Thermacam and a 1000 V amplifier were used. The piezoelectric stack was secured under a C-clamp to replicate the fixed condition it experiences when fully assembled in the lathe assembly. The amplifier applied a voltage of 500 volts to the piezo stack at a frequency of 1000 Hz, while the Thermacam continuously captured images. The voltage was increased until the piezoelectric stack reached a temperature of 49°C (120°F). The laboratory setup for this process is illustrated in Figures 18 and 19 respectively.

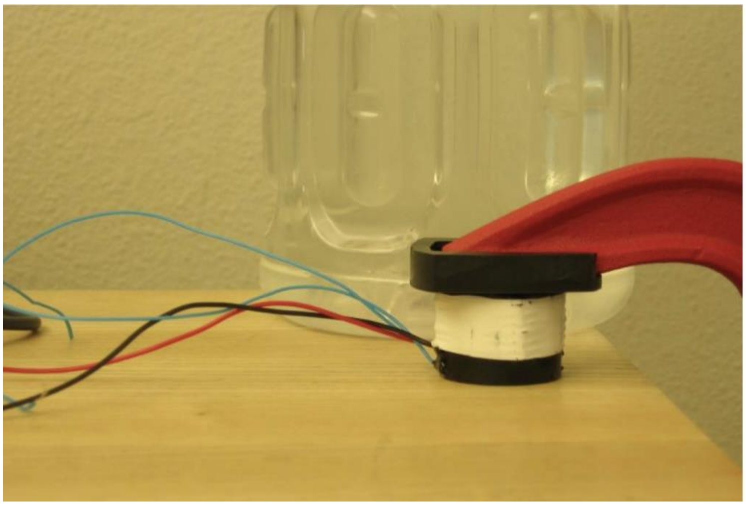

Figure 19 Piezoelectric Thermal testing Set up [16]

As a final step Facing Cuts with Fast Tool Servo was tested. This final testing involved executing facing cuts on aluminum rods to compare the surface finish of three different cuts. The first cut was made using an unmodified conventional CNC lathe. The second cut was made using the lathe with the FTS attached, but no voltage applied to the piezoelectric stack during the cut. The third cut was made using the system attached to the lathe with a constant 2 kHz signal or a sine swept voltage applied to the FTS. The surface of each cut was analyzed using white light profilometry. The next step is to observe the results and analyze the outcomes [16].

5.1.3 Result

In this section will be results analyzed beginning with the analyzing results of modulus tests. To verify the unconstrained FE model, free-free impact tests were conducted to characterize the responses of the main moving components of the actuator. The data sets were processed using ME Scope, and resonant peaks, damping values, resonant magnitudes, and resonant phases for each mode were obtained for the three diaphragms, as presented in Tables 5-7. In subsequent sections, the comparison between the experimental data and the finite element model results will be discussed. Tables 5-7 reveal that the natural frequencies of the FTS increase as the diaphragm thickness increases. For example, when comparing the fully assembled FTS tests, the frequency of the first mode more than doubles from 2.24e3 to 4.88e3 Hz when the thickness doubles from 1.5875 to 3.1750 mm. It is noteworthy, however, that the increase in the first natural frequency only slightly increased from 4.88e3 to 5.00e3 Hz when the thickness increased from 3.1750 to 4.7625 mm. Therefore, beyond a certain point, further increasing the thickness is not an effective way to raise the frequency of the first mode.

Table 5 Modal Experiment Data for 4.7625 mm Diaphragm [16]

4.7625 mm (3/16") Diaphragm				
Fixed Diaphragm Assembly - Unmounted				
Mode	Frequency (Hz)	Damping	Res. Mag.	Res. Phase
1	5.00E+03	0.0268	809	172
2	6.56E+03	0.68	3.67E+04	270
3	8.29E+03	0.196	1.22E+04	226
4	9.92E+03	0.954	1.78E+04	281
Free Diaphragm Assembly				
Mode	Frequency (Hz)	Damping		Res. Mag.
1	4.70E+03	0.0288	5.20	10.9
2	5.50E+03	0.303	2.94E+02	249
3	5.63E+03	0.224	8.68E+02	250
4	6.12E+03	0.503	1.31E+03	63.8
Diaphragm				
Mode	Frequency (Hz)	Damping	Res. Mag.	Res. Phase
1	3.83E+03	0.0131	661	321
2	6.21E+03	0.0163	1.11E+02	207
3	7.65E+03	0.00163	1.05E+00	23.8
4	9.31E+03	0.0169	5.26E+01	56.9

Table 6 Modal Experiment Data for 3.1750 mm Diaphragm [16]

3.1750 mm (1/8") Diaphragm				
Fixed Diaphragm Assembly - Unmounted				
Mode	Frequency (Hz)	Damping	Res. Mag.	Res. Phase
1	4.88E+03	0.0332	62.4	227
2	5.57E+03	0.0396	77.7	38.1
3	6.04E+03	0.494	1.97E+04	241
4	7.25E+03	0.996	4.11E+04	108
Free Diaphragm Assembly				
Mode	Frequency (Hz)	Damping	Res. Mag.	Res. Phase
1	4.12E+03	0.338	4.48E+04	328
2	4.22E+03	0.194	5.11E+04	330
3	4.44E+03	0.732	2.63E+04	286
4	5.53E+03	0.451	1.70E+05	339
Diaphragm				
Mode	Frequency (Hz)	Damping	Res. Mag.	Res. Phase
1	2.46E+03	0.0143	71.6	37.9
2	3.91E+03	0.0403	3.90E+06	170
3	5.93E+03	0.0468	3.39E+01	287
4	8.55E+03	0.122	1.48E+03	223

Table 7 Modal Experiment Data for 1.5875 mm Diaphragm [16]

1.5875 mm (1/16") Diaphragm				
Fixed Diaphragm Assembly - Unmounted				
Mode	Frequency (Hz)	Damping	Res. Mag.	Res. Phase
1	2.24E+03	1.17	1.47E+04	207
2	2.89E+03	1.21E+00	3.50E+04	191
3	5.66E+03	1.74E+00	1.29E+04	40.3
4	7.09E+03	7.88E-01	3.24E+04	100
Free Diaphragm Assembly				
Mode	Frequency (Hz)	Damping	Res. Mag.	Res. Phase
1	2.19E+03	0.350	4.71E+04	335
2	2.50E+03	0.129	1.36E+04	342
3	2.73E+03	1.04	9.90E+04	352
4	2.98E+03	0.426	6.57E+04	3.51
Diaphragm				
Mode	Frequency (Hz)	Damping	Res. Mag.	Res. Phase
1	1.28E+03	0.0276	249	185
2	2.04E+03	0.0466	7.25E+01	193
3	3.17E+03	0.00785	3.33E+02	96.6
4	4.58E+03	0.0957	1.77E+03	14.0

In this experiment FEM verification was conducted. This paragraph describes FEM where experimental results were compared to an analytical model to better understand the behavior of the fast tool servo. To improve the modeling of the fast tool servo's behavior, a series of experiments were conducted and compared to an analytical model. Modal tests were performed in increasing order of constraints to separate boundary conditions from system dynamics. The physical parameters of the system were measured and input into the free-free diaphragm model along with generic material properties to determine the elastic modulus (E) and Poisson's ratio (v) of the diaphragm. Eight simulations were conducted to determine the sensitivity of the model to these two parameters, and a cubic equation was fitted to map the inputs to the first four modal frequencies of the model. The optimal values for E and v were determined by evaluating a range of values in the vicinity of the generic values using an error metric (N). The experimental modal frequencies were used to form the M0 vector, and after fitting the equations, N was plotted against the two unknown parameters. The plot for the free-free diaphragm with a thickness of 4.7625 mm is shown in Figure 20. The optimal values for E and v were determined from the minimum error metric "N," denoted by the red dot in Figure 20, which corresponds to 222 GPa (3.22e7 psi) for the former and 0.28 for the latter. These values were then utilized as inputs for the free-free diaphragm model in ABAQUS. The simulation results are presented in Tables 8-10.

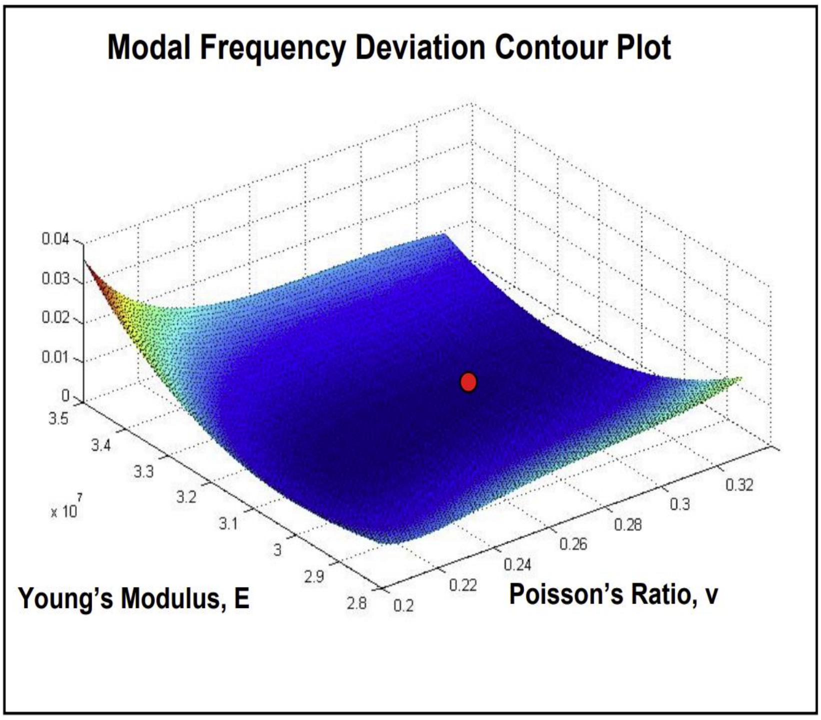

Figure 20 Modal Frequency Error Variation [16]

Table 8 Modal Frequencies for 4.7625 mm Diaphragm [16]

4.7625 mm (3/16") Diaphragm	
Mode	**Frequency (Hz)**
1	3.80E+03
2	3.83E+03
3	6.26E+03
4	9.26E+03

Table 9 Modal Frequencies for 3.1750 mm Diaphragm [16]

3.1750 mm (2/16") Diaphragm	
Mode	**Frequency (Hz)**
1	2.44E+03
2	2.46E+03
3	4.00E+03
4	6.02E+03

Table 10 Modal Frequencies for 1.5875 mm Diaphragm [16]

1.5875 mm (1/16") Diaphragm	
Mode	**Frequency (Hz)**
1	1.27E+03
2	1.28E+03
3	2.08E+03
4	3.15E+03

Tables 5-7 and Tables 8-10 demonstrate that the analytical modal frequencies are nearly 10% different from the experimental modal frequencies, except for the third experimental mode in the 4.7625 mm diaphragm which is absent in the FE model. In addition, the FE simulation predicts that the first two modes are very close, which explains why the third and fourth modes obtained from the model correspond to the second and third modes, respectively, obtained from the modal experiments. Since only one accelerometer was used for the modal tests, it is possible that the test data did not reveal the two close peaks, but rather a single peak resulting from the superposition of the first two modes. The two close modes are known to be a consequence of symmetry. In the next two configurations (free-free diaphragm and tool assembly, and fully constrained FTS), the only model parameter that could be optimized was the equivalent constrained surface. For the free-free diaphragm and tool assembly, the constrained surface that was altered was the front face of the tool holder assembly and its mating surface on the diaphragm. This surface is visible in Figure 21. The impact of changing the outer radius of the constrained surface was assessed by conducting simulations with five different radii for each diaphragm. The data obtained was then correlated with the first three experimental modal frequencies using the same approach as that used for the free-free diaphragm described earlier. The optimal radius was then determined, and the outcomes are presented in Tables 11-13.

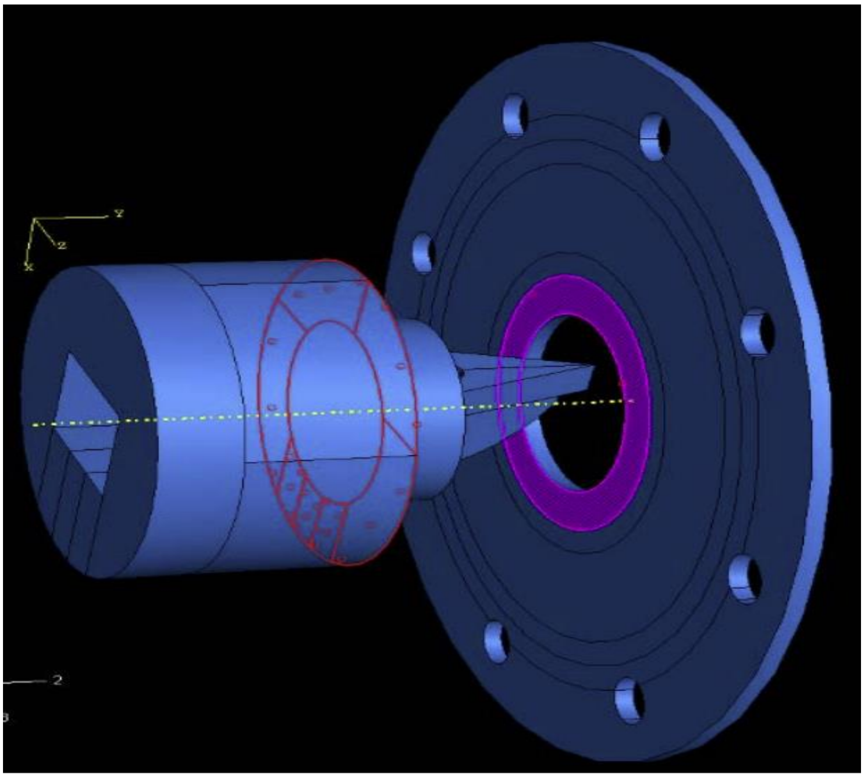

Figure 21 Constrained surface for free-free Diaphragm and Tool Assembly [16]

Table 11 Free-free thin diaphragm and tool model results [16]

1.5875 mm (1/16") Diaphragm and Tool	
Mode	**Frequency (Hz)**
1	**2167**
2	**2269**
3	**2735**

Table 12 Free-free medium diaphragm and tool model results [16]

3.1750 mm (1/8") Diaphragm and Tool	
Mode	**Frequency (Hz)**
1	4118
2	4124
3	4249

Table 13 Free-free thick diaphragm and tool model results [16]

4.7625 mm (3/16") Diaphragm and Tool	
Mode	**Frequency (Hz)**
1	5099
2	5111
3	5705

The fully constrained FTS model utilized the outer ring of the diaphragm that was bolted to the housing as the modified constrained surface. This specific surface can be observed in Figure 22. To evaluate the impact of different inner radii of the constrained surface, the models were run at four distinct radii for each diaphragm. Subsequently, this data was mapped to the first two experimental modal frequencies using the same procedure as the previous two configurations. The results of this analysis are presented in Tables 14-16.

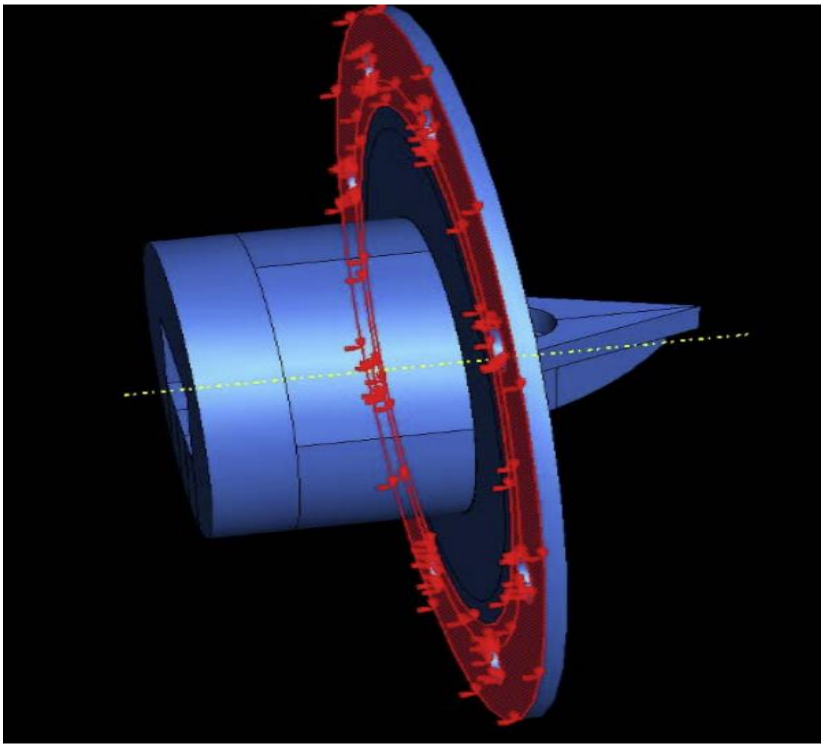

Figure 22 Constrained surface for constrained diaphragm assembly [16]

Table 14 Constrained thin diaphragm and tool model results [16]

1/16" (1.5875 mm) Assembly	
Mode	**Frequency (Hz)**
1	2241
2	2634

Table 15 Constrained medium diaphragm and tool model results [16]

1/8" (3.175 mm) Assembly	
Mode	**Frequency (Hz)**
1	5002
2	5822

Table 16 Constrained thick diaphragm and tool model results [16]

3/16" (4.7625 mm) Assembly	
Mode	**Frequency (Hz)**
1	4997
2	5179

For each diaphragm, the displacement resulting from an applied DC voltage to the assembled FTS was measured using an LC-2400A Keyence laser displacement sensor and recorded. The displacement, measured in micrometers, was plotted against the applied voltage for each diaphragm. The LC-2400A Keyence laser displacement sensor has a resolution of half a micron and a random value variance of approximately 1.5 microns, as observed from previous measurements. Based on the sample Figure 23 below, the maximum hysteresis values obtained from each cycle are approximately 2 µm. Consequently, it can be concluded that the accuracy of this displacement sensor is exceeded by the hysteresis analysis, and a more sensitive sensor would be necessary to further investigate the hysteresis effect. Despite its limitations, the piezoelectric hysteresis testing did yield useful results. Specifically, the displacement measurements at 1000 V provided diaphragm displacement values that exhibited a consistency of within 2 microns. The thin diaphragm exhibited a displacement of 17-18.5 µm, the middle diaphragm exhibited 12.5-13.5 µm, and the thick diaphragm exhibited 9-9.5 µm. These values offer insight into the maximum displacement that can be anticipated from each diaphragm. For additional hysteresis plots, please refer to Appendix A.

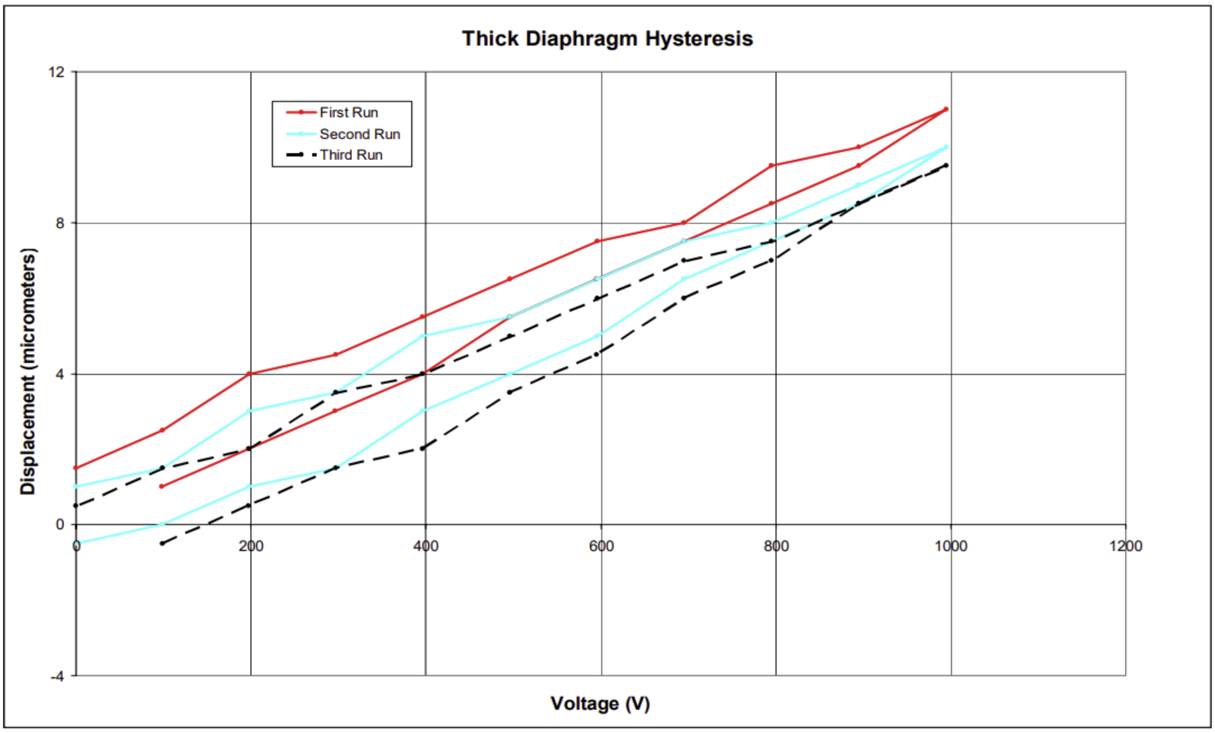

Figure 23 Thick Diaphragm Hysteresis [16]

Due to time constraints caused by a malfunctioning amplifier, thermal testing in this experiment was only conducted on the piezoelectric stack itself. Originally, thermal testing was intended to be performed on the fully assembled lathe tool to measure the amount of heat transferred from the piezo stack to the tool tip. The resulting data would then have been compared with the FE thermal model temperature spectrum of the diaphragm and tool assembly to assess the accuracy of the predictions. To conduct the testing, a 1000 V amplifier was used to provide 500 V to the piezoelectric stack at a frequency of 4000 Hz. The voltage was increased until the piezoelectric stack reached a temperature of 49°C (120°F), which took around 22 seconds. During the test, a continuous set of frames was captured, and three sample frames are depicted in Figure 24.

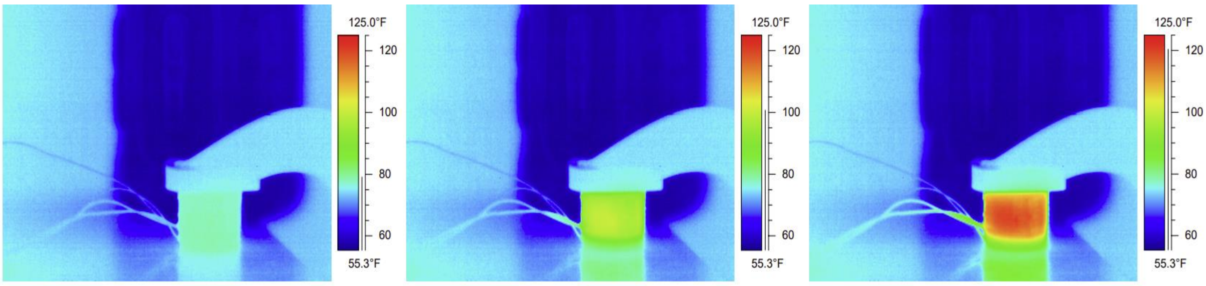

Figure 24 Infrared pictures of activated piezoelectric stack [15]

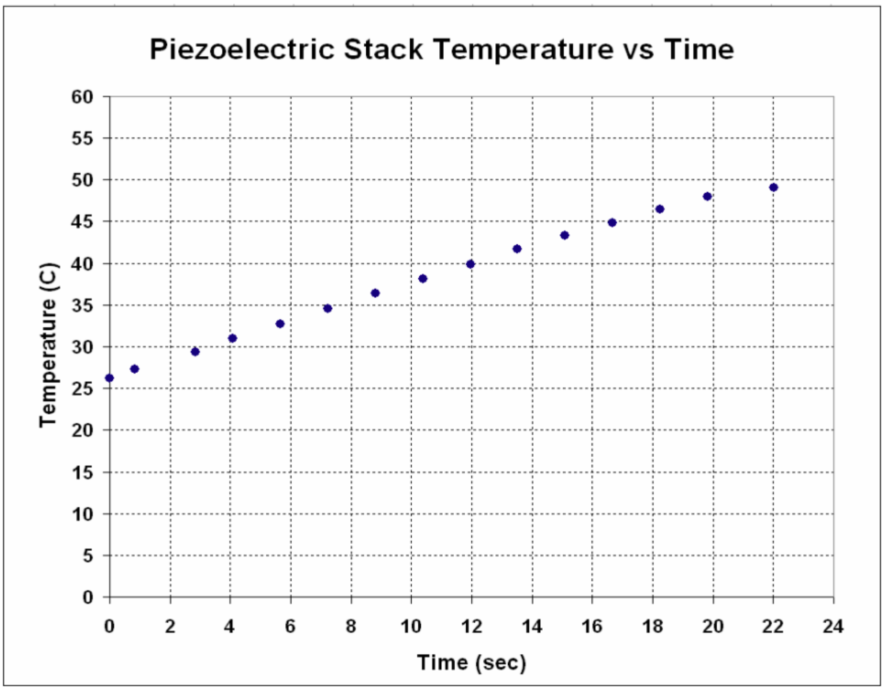

Figure 25 Piezoelectric Stack Temperature in Time [15]

The temperature change over time of the piezoelectric stack is the relevant thermal data for this project. To obtain this data, specific frames were chosen from the images captured by the FLIR camera and the corresponding time and temperature values were extracted and plotted in Figure 25. It shows that the temperature increase is linear with respect to time within the range of temperatures that were tested. This is a desirable outcome, as the temperature increase is expected to follow an exponential trend beyond this range.

Aluminum 6061 was chosen for the cutting tests due to its superior machinability. The unpowered facing cut using the thick diaphragm was replicated, and a spectrogram of the voltage output from these tests is provided in Appendix B. For the second series of tests, the thin diaphragm (1.5875 mm, 1/16" nominal) replaced the thick diaphragm. First, an unpowered facing cut was conducted, and then three sets of data were taken from the same aluminum sample at a decreasing radius from the axis of rotation with the FTS powered by a constant 2kHz sine wave. The final test consisted of three sets of data taken at a decreasing radius from the axis of rotation with a sine sweep from 100 Hz to 10 kHz applied to the FTS. All cutting test spectrograms can be seen in Appendix B. The spectrograms from the sine-swept tests indicate that the frequencies of the resonances appear to "bounce" off of 10 kHz. This is because the voltage measured from the piezo sensor was unfiltered, and the sampling rate of 20 kHz causes aliasing of any frequency above 10 kHz.

The surface roughness of each faced sample was evaluated using a white light profilometer, and the resulting data was processed in MATLAB to replace any bad data points with interpolated values from adjacent points. The objective was to analyze the shape of the cut depth and determine any effects caused by powering the FTS. To detect specific spatial frequencies, a fast Fourier transform (FFT) was applied to 600 vertical strips of surface data, since the tool path was oriented in a primarily vertical direction. These FFT graphs were then averaged to produce a final FFT. Surface profiles, vertical strip profiles, and surface FFT graphs are available in Appendix C. The spectrograms exhibit a notable characteristic of even-numbered resonances attenuation in the forcing function. The thin plate indicates two resonances and one anti-resonance near 5kHz. The lathe seems to have resonances at 6kHz and 8.5 kHz, as indicated by power at these frequencies in every test, regardless of the diaphragm used. Additionally, the tests conducted at the outer edge of the Al 6061 sample showed two response frequencies that start at one frequency, settle to a different frequency, and then fade out. These frequencies were not as prevalent in data taken closer to the axis of rotation. For the thick plate, these signals appeared at 6 and 7 kHz, and for the thin plate, they appeared at 4.5 and 7.5 kHz.

The surface profilometry data appears to be inconclusive as no data set stands out as unique. Each sample seems to have roughly equivalent surface quality in terms of surface roughness [16].

5.1.4 Conclusions

The results of this study from Albert, Luke and Matthew are inconclusive, but a visible effect on surface finish was observed in the sample faced with the FTS running at 2kHz. However, this effect could not be detected analytically, indicating that a higher power system may be necessary. The tests were originally intended to use a more powerful amplifier, but due to a malfunction, a less powerful one was used instead. Despite this, it is noted that the average surface roughness of each test is similar, suggesting that the addition of the FTS to the lathe did not negatively affect surface finish. Overall, the conclusion acknowledges the limitations of the study while also highlighting potential for further research [16].

Table 17 Surface roughness of all test samples [16]

Surface roughness of test samples (microns)	
Thick Diaphragm, Unpowered	6.3, 6.1
Thin Diaphragm, Unpowered	5.2, 5.1
Thin Diaphragm, 2kHz	5.4, 5.3
Thin Diaphragm, Sine Sweep	6.0, 6.4

5.2 Design and analysis of a piezoelectric film embedded smart cutting tool

The state of a cutting tool plays a significant role in the production process. When the tool wears out, it exerts more force on the material being cut, leading to a subpar surface finish and affecting the precision of the workpiece's dimensions. As a result, measuring cutting forces with a dynamometer while machining is a common technique, but it has drawbacks such as being expensive, unsuitable for harsh industrial machining environments, and interfering with cutting dynamics. In this study from Chao Wang and Kai Cheng, a new type of intelligent cutting tool is introduced, which employs a separate single-layer piezoelectric film as a sensor to detect the orthogonal cutting force. To verify the practicality of the suggested design, simulations were conducted, and the model successfully identified enhanced force measurement sensitivity. Additionally, experimental cutting trials were performed to validate the performance of the tool.

In modern manufacturing, monitoring cutting forces is crucial for achieving desired machining outcomes. Increases in cutting forces due to wear or breakage of cutting inserts can result in poor surface finish and dimensional tolerance loss of the workpiece. Special devices have been developed to measure cutting forces accurately, including dynamometers in laboratory settings. However, these sensors have limitations, such as reduced reliability in harsh environments and impractical size and weight for constrained layouts. Recent advancements in cutting tools have led to the development of integrated thin-film sensors to detect wear and micro-channels with internal coolant to reduce temperature at the cutting tool tip. This trend has spurred the creation of a smart cutting tool with a single-layer piezoelectric film to measure the orthogonal cutting force. The feasibility of the proposed design concept was proven through ANSYS coupled-field simulations, which also detected the force measurement sensitivity of various strategies. The smart cutting tool was calibrated using a Kistler dynamometer and tested for cross-sensitivity with an impact hammer. In preliminary cutting trials, the calibrated smart cutting tool displayed good agreement with Kistler force measurement readings [17].

5.2.1 Force Measurement Strategy

There are three general methods for measuring force: force shunt, direct, and indirect force measurement. Direct force measurement involves mounting a sensing unit directly in the load path to measure the entire force of the process. Indirect force measurement measures a strain proportional to the process force. Force shunt measurement measures a fraction of the process force passing through the sensing unit. Of the three force measurement strategies, force shunt measurement was selected for the development of the smart cutting tool for three reasons. Firstly, it is challenging to mount a sensor fully in line with the force path, and this force may cause the piezoelectric element to fracture. Secondly, the measured strain in the indirect method is only a small fraction of the force, and the measurement sensitivity may be limited. An ANSYS model will be used to analyze the measurement sensitivity between the indirect and force shunt methods. Finally, there are practical difficulties in mounting the piezoelectric film onto the surface of the cutting insert and establishing a reliable electrical contact with the indirect method [17].

5.2.2 Smart cutting tool configuration

The proposed prototype of a smart cutting tool from Chao Wang and Kai Cheng includes a cutting insert, a single-layer piezoelectric film, a metal shim, and two pieces of insulation tape, as shown in Figure 26(a). The piezoelectric film is a PIC181 sensor from PI, with dimensions of 3x3x0.26 mm and placed on the top surface of the metal shim. Two pieces of insulation tape are used to insulate and fix the sensor in position, and a wire is soldered onto the metal shim to function as the output electrode of the sensor. The sensing unit is located 6 mm away from the cutting tip, between the cutting insert and spacer, with the exposed wire and metal shim still distant from the cutting tip, as shown in Figure 26(b). A second piece of piezoelectric film is placed at the back to level up the insert and distribute the force over the sensor surface area, as shown in Figure 26(c). The study used the Kistler 5011 charge amplifier to convert a charge into an equivalent voltage for determining transducer sensitivity and scale. The proposed smart cutting tool configuration introduced pre-stress on the piezoelectric film to establish a firm contact between the elements and reduce unwanted hysteresis effect. Cross-sensitivity was minimized by choosing a piezoelectric film with the d_{33} sensing mode, which should only detect the orthogonal cutting force acting perpendicular to the cutting insert's top surface [17].

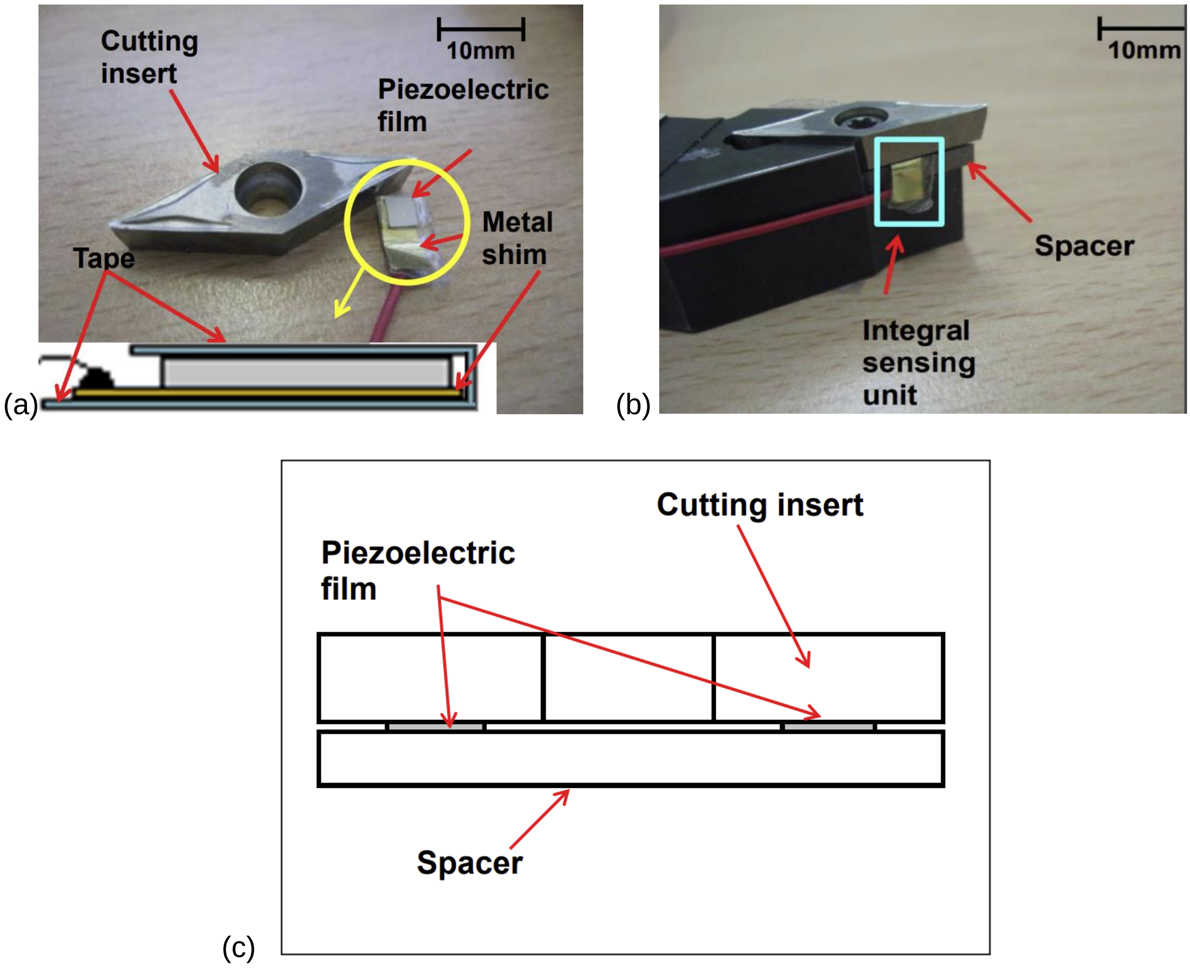

Figure 26 (a) Components of smart cutting tool; (b) integral configuration of smart cutting tool (c) Cross section drawing [17]

5.2.3 Modelling and simulation of the smart cutting tool

The piezoelectric effect, which converts force into electric voltage, can be simulated using ANSYS software by using a stiffness matrix, dielectric matrix, and piezoelectric constant matrix. These matrices can be created using data from the manufacturer and are used to calculate the voltage output. This process is described by equations (5.1) and (5.2).

$$\underline{\textit{Stiffness matrix}}\ [S^E] = [C^E]^{-1} = \begin{bmatrix} 11.8 & -3.42 & -4.12 & 0 & 0 & 0 \\ & 11.8 & -4.12 & 0 & 0 & 0 \\ & & 14.2 & 0 & 0 & 0 \\ & & & 30.4 & 0 & 0 \\ & & & & 53.5 & 0 \\ & & & & & 53.5 \end{bmatrix} \times 10^{-12}\ \ [\mathrm{N/m}]$$

$$\underline{\textit{Dielectric matrix}}\ [\varepsilon^S] = \varepsilon_0 \begin{bmatrix} K_{11}^S & 0 & 0 \\ & K_{11}^S & 0 \\ & & K_{33}^S \end{bmatrix} = (8.85 \times 10^{-12}) \begin{bmatrix} 1023.7 & 0 & 0 \\ & 1023.7 & 0 \\ & & 571.35 \end{bmatrix}\ \ [\mathrm{farad/m}]$$

$$\underline{\textit{Piezoelectric constant matrix}}\ \ [d]^t = \begin{bmatrix} 0 & 0 & 0 & 0 & 0 & 4.75 \\ 0 & 0 & 0 & 0 & 4.75 & 0 \\ -1.20 & -1.20 & 2.65 & 0 & 0 & 0 \end{bmatrix} \times 10^{-10}\ \ [\mathrm{C/N}]$$

$$\{T\} = [C^E]\,\{S\} + [e]\,\{E\} \tag{5.1}$$

$$\{D\} = [e]^t\,\{S\} + [\varepsilon^S]\,\{E\} \tag{5.2}$$

An ANSYS coupled-field model was created to simulate the performance of a smart cutting tool under a static force. The model used either the force shunt method or the indirect force method, both of which included a half-sized cutting insert and a piece of piezoelectric film. To properly simulate the performance, boundary conditions had to be defined for both the cutting insert and the piezoelectric film. In the force shunt method, the boundary conditions were defined based on the area number system, with certain areas constrained in specific degrees of freedom. The piezoelectric sensor was defined as grounded on the side in contact with the insert and constrained in the Z direction on the other side. In the indirect method, the only difference was that the bottom area of the cutting insert was constrained in the Z direction [17].

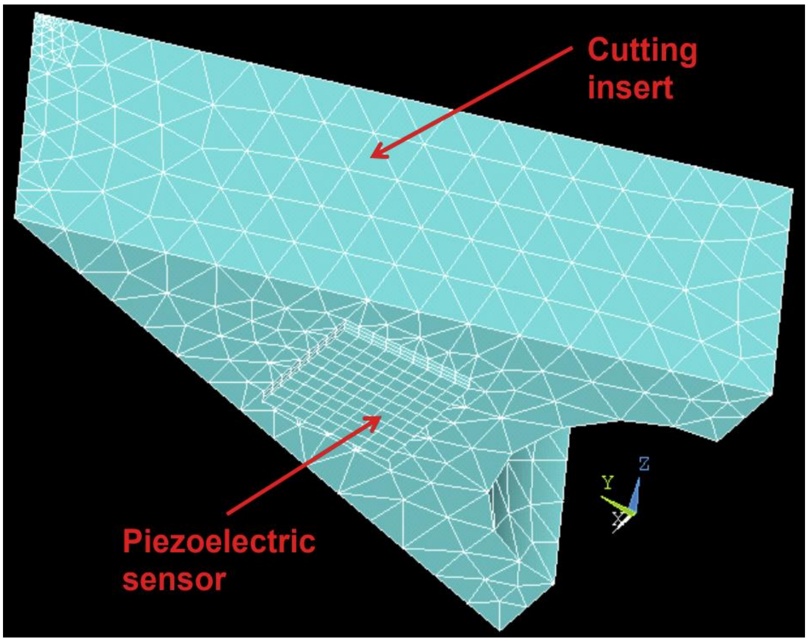

Figure 27 ANSYS coupled-field model of piezoelectric sensor and cutting insert [16]

5.2.3 Smart cutting tool used for machining trails

The CNC lathe (ALPHA 1350XS) was used to perform several cutting trials, during which both the proposed intelligent cutting tool and the Kistler dynamometer 9257B were utilized to measure the orthogonal cutting force. To measure the force, the smart cutting tool was installed onto the Kistler dynamometer through a tool holder, as shown in Figure 28. Prior to its use as a force measurement sensor, the dynamometer was used to calibrate the smart cutting tool. During cutting, a piezoelectric sensor generated a charge that was input into the Kistler 5011 charge amplifier. The transducer sensitivity and scale were set to 265 pc/N and 1.38 N/V, respectively, based on the manufacturer's specifications. The workpiece, composed of AL6082, was machined under dry cutting conditions with a constant feed rate of 0.15 mm/rev and a constant cutting speed of 330 m/min. The depth of cut was increased in increments of 0.1 mm for each pass, ranging from 0.1 to 0.8 mm [17].

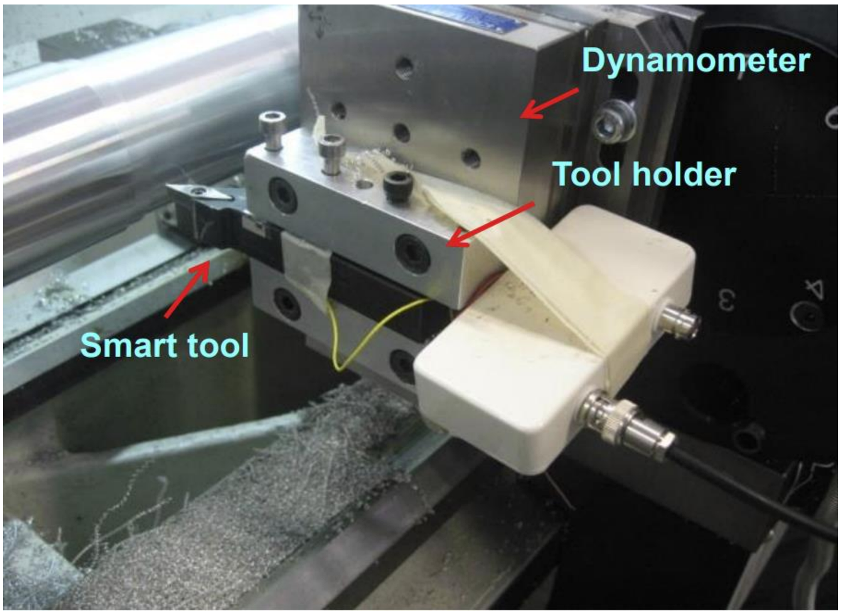

Figure 28 Smart cutting tool and Kistler dynamometer on the lathe [17]

5.2.4 Results

In section 5.2.1, it was noted that the force shunt and indirect force measurement methods are both capable of predicting cutting force, but they differ in their measurement principles and methodologies. The former measures a portion of the process force, while the latter measures strain that is proportional to the process force. Consequently, even with identical loading, the voltage output response may vary between the two methods due to their different measurement sensitivities. Figure 29 illustrates the voltage outputs resulting from a 10 N force applied to the tool tip. In Figure 29(a), the indirect method produces a voltage output of -0.147 V, represented in blue, whereas the force shunt method produces a voltage output of 9.142 V, represented in red, as shown in Figure 29(b). The voltage outputs from the dynamometer, smart tool, and tool holder are markedly dissimilar, indicating that the force shunt method provides significantly greater measurement sensitivity. Furthermore, it is not advisable to leave the piezoelectric sensor, which protrudes from the surface of the cutting insert, exposed to the long swarf produced during machining when using the indirect method in practical applications.

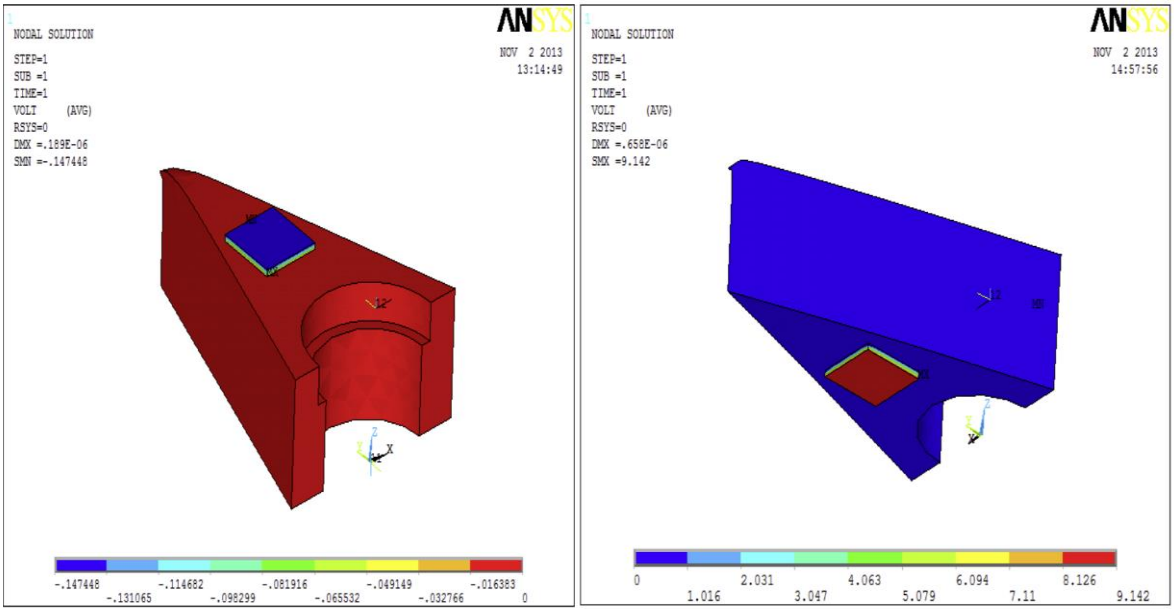

(a) (b)

Figure 29 Voltage output with a force of 10 N applied on the tool tip: (a) with indirect force measurement method; (b) with force shunt measurement method [16]

To determine the voltage output corresponding to a known static force, a FT 200 force gauge is employed to apply the force on the tool tip, which is then removed after a few seconds. This process results in a voltage output step due to the loading, as illustrated in Figure 30. The graph displays a linear correlation between the force and the voltage output, with a maximum deviation of 4.6% observed in the measured output signal curve from the ideal, over the full range of 0 to 90 N. This linear relationship may be attributed to the insert's deformation occurring within its elastic range and the piezoelectric film's voltage generation having a linear connection to force. Although ANSYS simulation predicts a maximum voltage output of 9.142 V when a 10 N force is applied to the tool tip, the experimental results show a significantly lower voltage output of only 0.09956 V. In order to explain the difference between the theoretical and experimental results, only the piezoelectric film subjected to a 10 N force on its top surface is considered. According to Equation 5.3 and ANSYS simulation, the voltage output is -7.22V. In the experimental setup, the piezoelectric sensor is placed on a flat surface, and a known force is applied using a FT 200 force gauge. Furthermore, a solid block is placed on top of the piezoelectric film to ensure that a constant vertical force of 10 N is uniformly applied to it. Consequently, only a voltage output of -0.072V is obtained. By dividing the V_{charge} amplifier by V_{PZT}, a constant gain of approximately 100 is calculated based on the two voltage outputs. In Equation 5.4, the voltage output is reduced by a factor of 100 due to the capacitance introduced by the charge amplifier, resulting in a close match between the experimental and theoretical values shown in Figure 31 when the experimental voltage output results are multiplied by the gain factor.

$V_{PZT} = -(g_{33}T\ h) = -\ 25\times10\text{-}3 \times (10/\ 9 \times10\text{-}6\ ) \times 0.26 \times10\text{-}3 = -\ 7.22\ V$ (5.3)

$V_{charge\ amplifier} = -\ 0.072\ V$

$gain = V_{charge\ amplifier} / V_{PZT} = 720\ /7.22 = 99.72\ 100$

$V_{charge\ amplifier} = -\ Q / C$ (5.4)

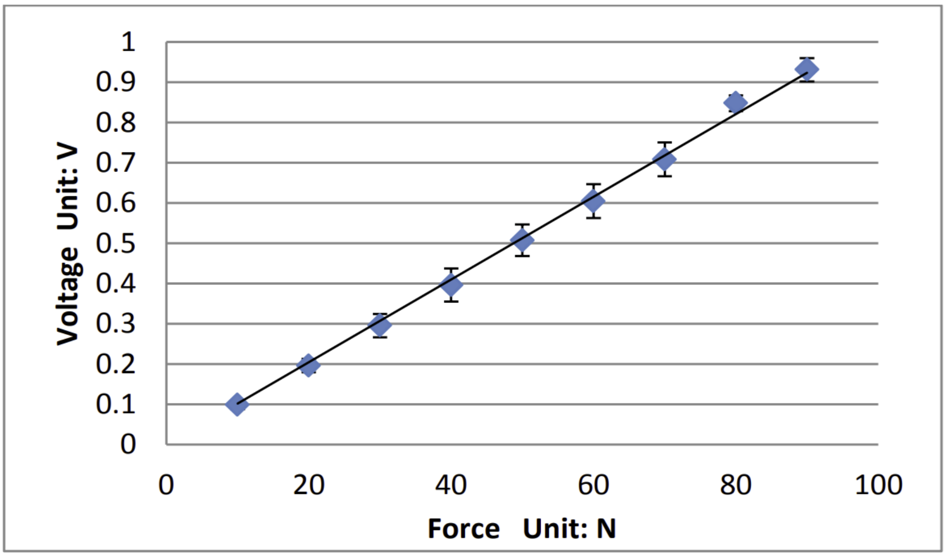

Figure 30 Linear relationship between static force and voltage output [17]

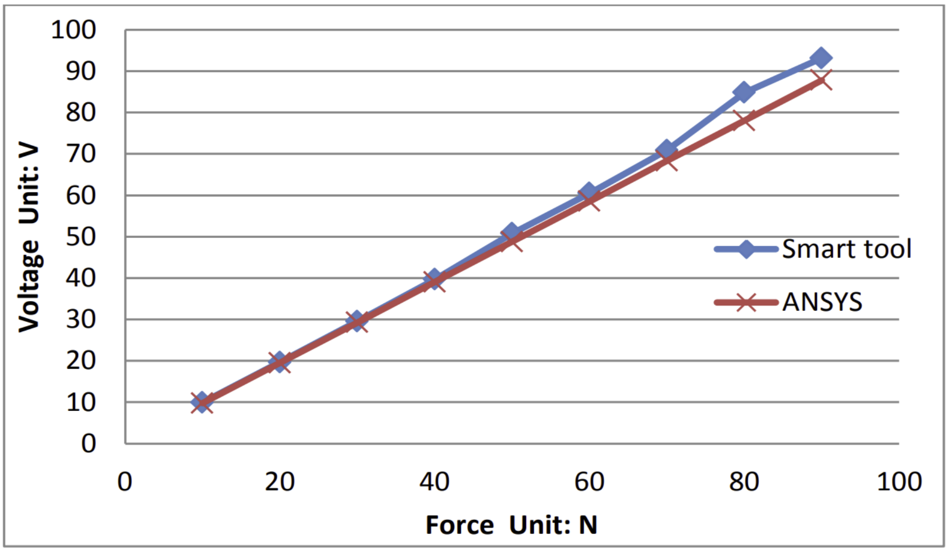

Figure 31 Comparison of voltage outputs in terms of applied forces between smart cutting tool and ANSYS simulation [16]

To identify the cross-sensitivity in the proposed piezoelectric sensor configuration, the impact hammer testing technique was employed. The Kistler impact force hammer (Type 9722A), capable of generating forces ranging from 0 to 500 N with a sensitivity of 10 mV/N, was used to impact the cutting tip of the insert both vertically and horizontally. A plastic tip head was attached to the impact hammer to generate a strong signal in the low frequency range. The signal outputs from both the impact force hammer and the piezoelectric sensor were converted from the time domain to the frequency domain. In the frequency domain, only low-frequency components between 0 and 50 Hz were considered. Table 18 presents the responses of the piezoelectric sensor and the impact hammer when vertical and horizontal impact forces were applied, as shown in columns two and three, and columns four and five, respectively. The next step involved normalizing the responses of the two impacts by dividing the dynamic response of the piezoelectric sensor with that of the impact hammer. This normalization procedure was repeated three times, and the averages of the normalized values were recorded for both vertical and horizontal impacts. These values were then divided to compute the cross-sensitivity, which was found to be 5.97% for this piezoelectric sensor configuration.

Table 18 Cross-sensitivity of the proposed piezoelectric sensor [17]

Impact Number	**Vertical Piezo-sensor**	**Vertical Impact hammer**	**Horizontal Piezo-sensor**	**Horizontal Impact hammer**
1	2.3E-4 V	1.2E-4 V	4.0E-5 V	2.5E-4 V
2	2.1E-4V	1.0E-4 V	5.0 E-5 V	4.5E-4V
3	2.0E-4 V	1.0E-4 V	5.0 E-5 V	4.5E-4 V
Averaged response	2.01 V		0.12 V	
Cross-sensitivity	5.97%			

The dry turning process was used with a smart cutting tool to measure cutting force as the depth of cut was increased from 0.1 to 0.8 mm, in increments of 0.1 mm for each pass. The feed rate was kept constant at 0.15 mm/rev and cutting speed was set at 330 m/min. Figure 31(a) illustrates the voltage output during cutting, with the circled steps indicating the cutting force. The slow-changing portion of the waveform seen in Figure 32(a) is unrelated to the cutting force but is likely due to the pyroelectric effect of the piezoelectric ceramic material. The cutting trials were repeated four times for each depth of cut. Figure 32(b) depicts the cutting forces obtained from both the Kistler dynamometer and the piezoelectric sensor, using the same cutting conditions as described previously. The average values of the orthogonal cutting forces were calculated based on four cutting trials, and the error bars were plotted using the standard error. The difference between the measured cutting forces from the two sensors is negligible, and the narrow range of the error bars indicates high precision and good repeatability in the measurements [17].

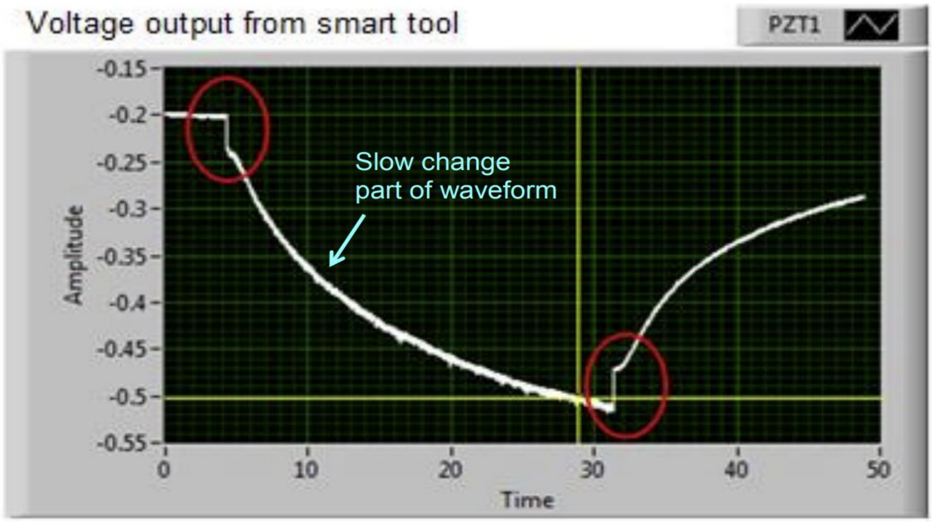

(a)

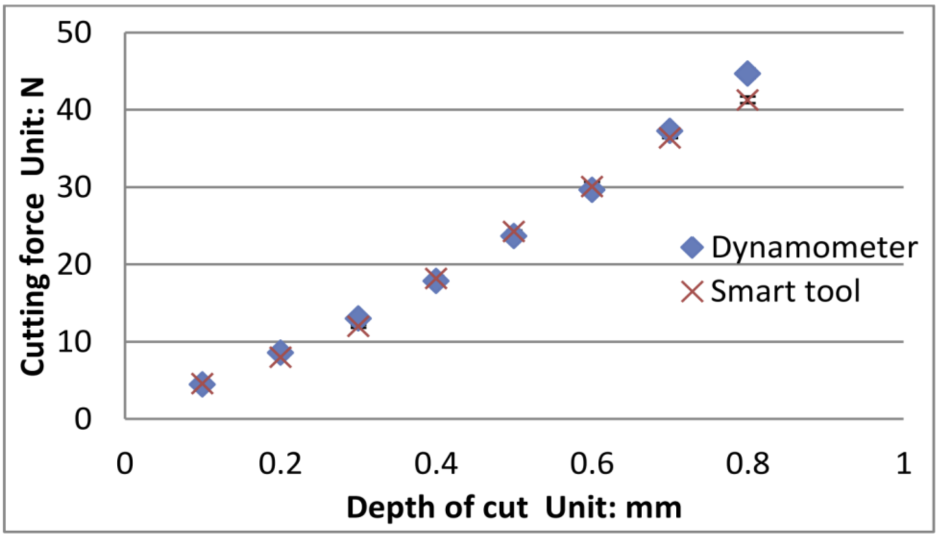

(b)

Figure 32 Voltage output waveform from the smart cutting tool sensor; (b) Cutting force prediction by smart cutting tool compared to that of a dynamometer for various depth of cut [16]

5.2.5 Conclusions

The result presented in the study from suggests Chao Wang and Kai Cheng that the proposed smart cutting tool using a piezoelectric film is a feasible solution for measuring orthogonal cutting force in dry machining processes. The tool demonstrated a linear relationship between applied force and voltage output, with low cross-sensitivity and reduced hysteresis effect due to pre-stress introduced in the setup procedure. The feasibility of the design was validated through ANSYS simulation, which showed better force measurement sensitivity compared to other methods. The simulation results also showed close agreement between the smart cutting tool and ANSYS simulation in terms of voltage output. Additionally, the results of cutting trials showed that the proposed smart cutting tool can predict the orthogonal cutting force with good repeatability and precision, as there was close agreement between the measurement results obtained from the Kistler dynamometer and the smart cutting tool. Overall, the result suggests that the proposed smart cutting tool can be an effective tool for measuring orthogonal cutting force in dry machining processes [17].

6 FINAL CONCLUSIONS

The main goal of the Thesis was the development of a new concept, implementation and analysis of the piezoelectric sensor/actuator that can improve cutting process in Lathe.

6.1 Research results and achievements

The study from Albert, Luke and Matthew which focused on the design of a piezoelectric actuator for turning, was aimed to develop a low-profile piezoelectric actuator that could generate high-frequency vibrations for precision machining applications. The experiment demonstrated that the designed actuator could be inconclusive, but a visible effect on surface finish was observed in the sample faced with the FTS running at 2 kHz. Despite this, it is noted that the average surface roughness of each test is similar, suggesting that the addition of the FTS to the lathe did not negatively affect surface finish. Overall, the conclusion acknowledges the limitations of the study while also highlighting potential for further research. This experiment mainly focused on developing a piezoelectric actuator that could be used in precision machining applications. On the other hand, second study which included in this thesis from Chao Wang and Kai Cheng, was aimed to design and analyze a piezoelectric film embedded smart cutting tool to measure orthogonal cutting forces during dry machining processes. The smart cutting tool demonstrated a linear relationship between the applied force and the voltage output, with a low cross-sensitivity effect. The experiment validated the feasibility of the proposed design by simulating the piezoelectric effect in an ANSYS coupled-field analysis. Furthermore, the smart cutting tool was able to predict the orthogonal cutting force during dry machining, with close agreement shown between the orthogonal cutting force measured by the Kistler dynamometer and the smart cutting tool. In conclusion, both experiments aimed to utilize piezoelectric elements for precision machining applications. However, study from Albert, Luke and Matthew focused on developing a piezoelectric actuator that could generate high-frequency vibrations, while second experiment from Chao Wang and Kai Cheng aimed to design a smart cutting tool that could measure orthogonal cutting forces during dry machining processes. The second study from Chao Wang and Kai Cheng, which had a more practical application, demonstrated the feasibility of using a piezoelectric film embedded smart cutting tool for force measurement during dry machining processes, with good measurement repeatability and high precision. Based on the results of these experiments and study, a possible experimental setup for IPT laboratory on a lathe at the UAS Hamburg (HAW) could involve testing the feasibility of integrating the piezoelectric actuator developed in experiment from Albert, Luke and Matthew into the lathe for precision machining applications. The high-frequency vibration generated by the actuator could potentially improve the surface finish and accuracy of the machined parts. Additionally, the smart cutting tool designed in experiment from Chao Wang and Kai Cheng could be used to measure the orthogonal cutting forces during the machining process to optimize the cutting parameters and improve the machining efficiency. The integration of these two technologies could lead to significant advancements in precision machining processes. Further research could also focus on optimizing the design and parameters of the piezoelectric actuator and the smart cutting tool for specific machining applications.

6.2 Future Research Work

The proposed smart cutting tool using a piezoelectric film has shown promising results in measuring the orthogonal cutting force during dry cutting machining processes. The tool demonstrated a linear relationship between the applied force and the voltage output, with low cross-sensitivity and reduced hysteresis effect due to pre-stress introduced during setup. The ANSYS simulation validated the feasibility of the design and confirmed the better force measurement sensitivity of the proposed tool compared to shunt and indirect force measurement methods. The simulation also showed good agreement with the experimental results, with a close agreement on voltage output obtained between the smart cutting tool and the simulation. In addition, the smart cutting tool was able to accurately predict the orthogonal cutting force during dry machining, with a close agreement between the Kistler dynamometer and the proposed tool. This suggests that the tool can be a useful alternative to traditional force measurement methods in manufacturing processes. Overall, the results presented in this study suggest that the proposed smart cutting tool using a piezoelectric film has the potential to improve machining processes by providing accurate and real-time measurements of cutting forces. Future work may involve exploring the use of the tool in different machining conditions and applications to further validate its effectiveness.

REFERENCES

[1] A. P. V. S. Shivam Shukla, INNOVATION AND APPLICATION OF PIEZOELECTRIC MATERIALS:A THEORETICAL, J.N.U. New Delhi, India: International Journal of Advanced Technology in Engineering and Science, March 2015.

[2] „Autodesk,“ 2023 02 12. [Online]. Available: https://www.autodesk.com/products/fusion-360/blog/piezoelectricity/. [Zugriff am 29 03 2023].

[3] L. M. B. Albert A. Espinoza, Design and Evaluation of a Piezoelectric Actuator for Turning, Research Gate, January 2006.

[4] A. S. Rolf H. Kuratle, The Basic of Piezoelectric Measurement Technology, Winterthur, Switzerland: Kistler Instrumente AG .

[5] M. L. K. SIENKIEWICZ, CONCEPT, IMPLEMENTATION AND ANALYSIS OF THE PIEZOELECTRIC RESONANT SENSOR/ACTUATOR FOR MEASURING THE AGING PROCESS OF HUMAN SKIN, Toulouse (France): Institut National Polytechnique de Toulouse (INP Toulouse), 7 Juni 2016.

[6] J. N. T. Bein, APPLICATION OF PIEZOELECTRIC MATERIALS IN TRANSPORTATION INDUSTRY, Darmstadt Germany : Global Symposium on Innovative Solutions for the Advancement of the Transport Industry, 4.-6. October 2006, San Sebastian, Spain, 6. October 2006.

[7] S. J. Rupits, Piezoelectric Sensors and Actuators Fundamentals and Applications, Erlangen, Germany: Springer, June 2018.

[8] IEEE Standard on Piezoelectricity, Institute of Electrical and Electronics Engineers (IEEE), 1988.

[9] „Introduction and History of Lathe,“ Jawaharlal Nehru Agricultural University India, [Online]. Available: http://www.jnkvv.org/PDF/11062020160615106201037.pdf. [Zugriff am 18 03 2023].

[10] Z. Salvi, „LATHE MACHINE AND IT'S MECHANISM 1.1. INTRODUNCTION,“ Nr. Research Gate, p. 12, 2020.

[11] M. SHAFI, „Lathe Machine Accessories and Attachments,“ [Online]. Available: https://mechanicalenotes.com/lathe-machine-accessories-and-attachments/. [Zugriff am 18 03 2023].

[12] P. Jacobs, 06 02 2023. [Online]. Available: https://www.cncmasters.com/lathe-machine-buyers-guide/#What_is_a_Lathe_Machine. [Zugriff am 18 03 2023].

[13] S. S, „Chip Formation: Meaning and Geometry | Metal Cutting | Metallurgy“.

[14] „Types of Chip Formation -Continuous, Built-Up Edge , Discontinuous and Serrated chips,“ [Online]. Available: https://www.mecholic.com/2016/02/types-of-chip-formation.html#:~:text=and%20Serrated%20Chips-,Types%20of%20Chip%20Formation%20%E2%80%93%20Continuous%2C%20Built-Up,Edge%2C%20Discontinuous%20and%20Serrated%20Chips&text=A%20machining%20environment%20such%20a. [Zugriff am 19 03 2023].

[15] C. FELIX, „Strategies for Managing Chip Control,“ 20 07 2018. [Online]. Available: https://www.productionmachining.com/articles/tips-for-troubleshooting-and-repairing-chip-conveyors. [Zugriff am 19 03 2023].

[16] L. M. B. Albert A. Espionaza, „Design and Evaluation of a Piezoelectric Actuator for Turning,“ *Research Gate,* January 2006.

[17] R. R. a. K. C. C Wang*, „Design and analysis of a piezoelectric film embedded,“ Nr. Brunel University, UK .

APPENDIXES

APPENDIX A Piezoelectric Stack Hysteresis Charts [16]

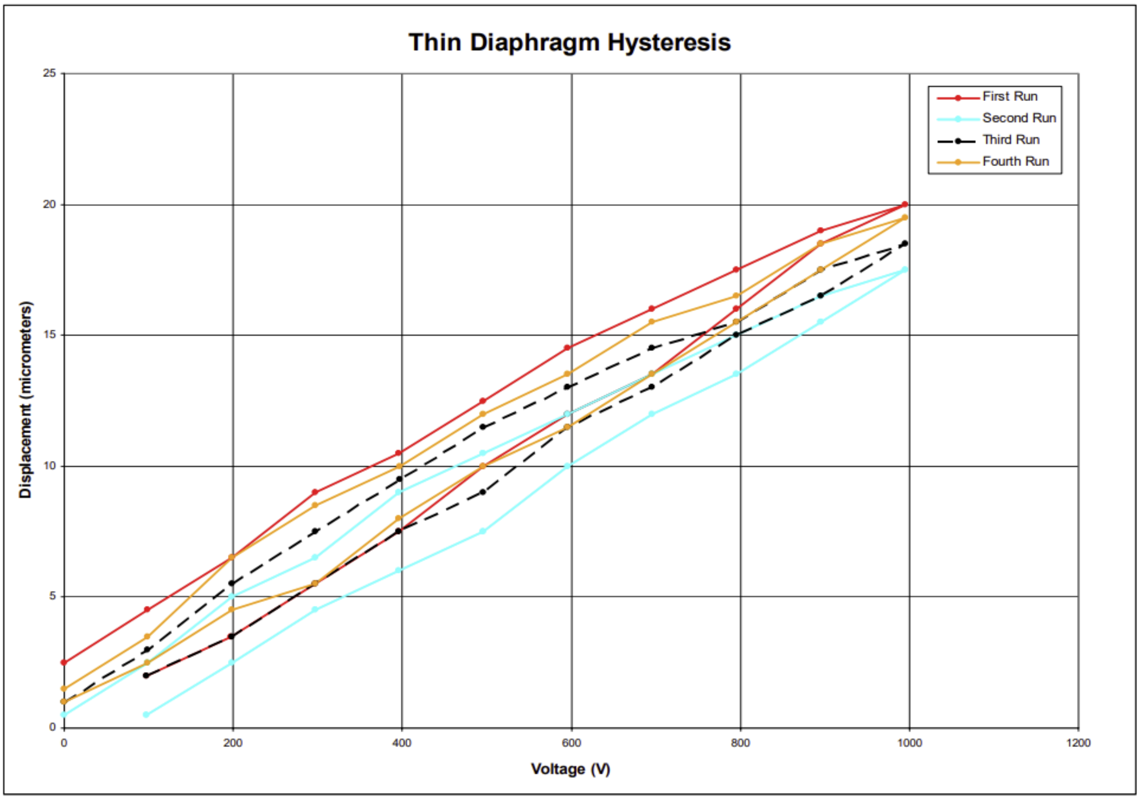

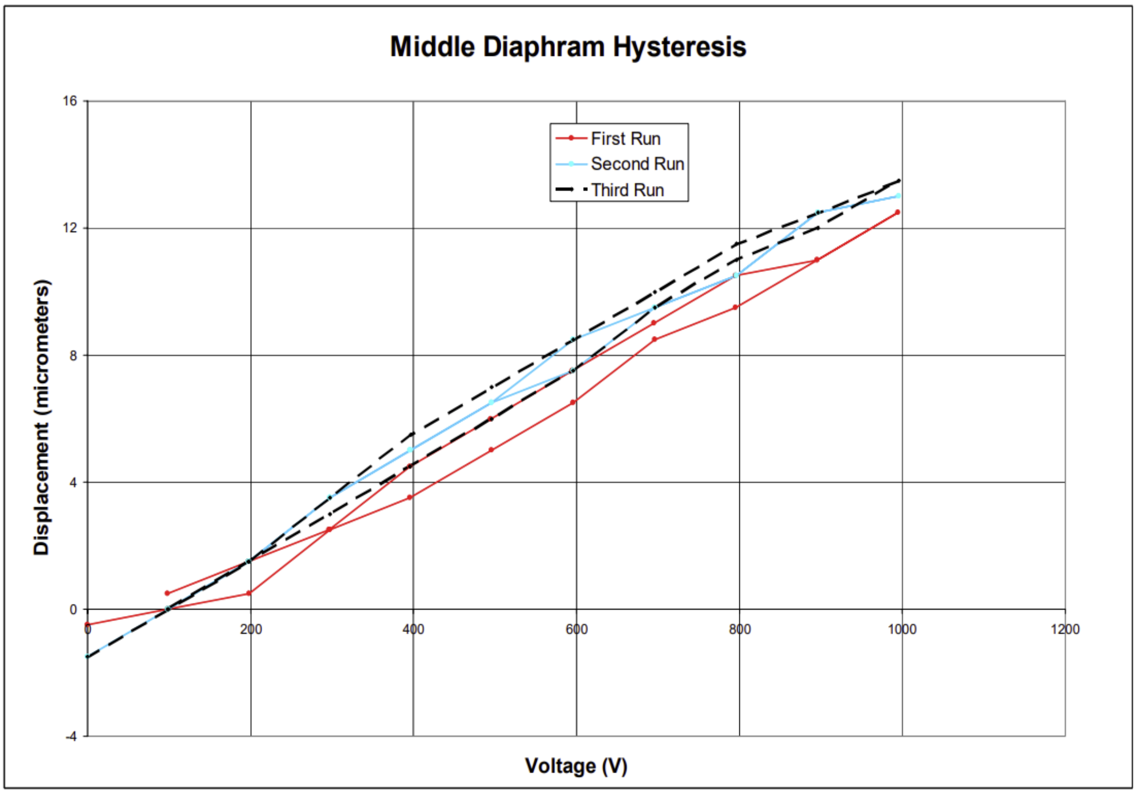

APPENDIX B Cutting Test [16]

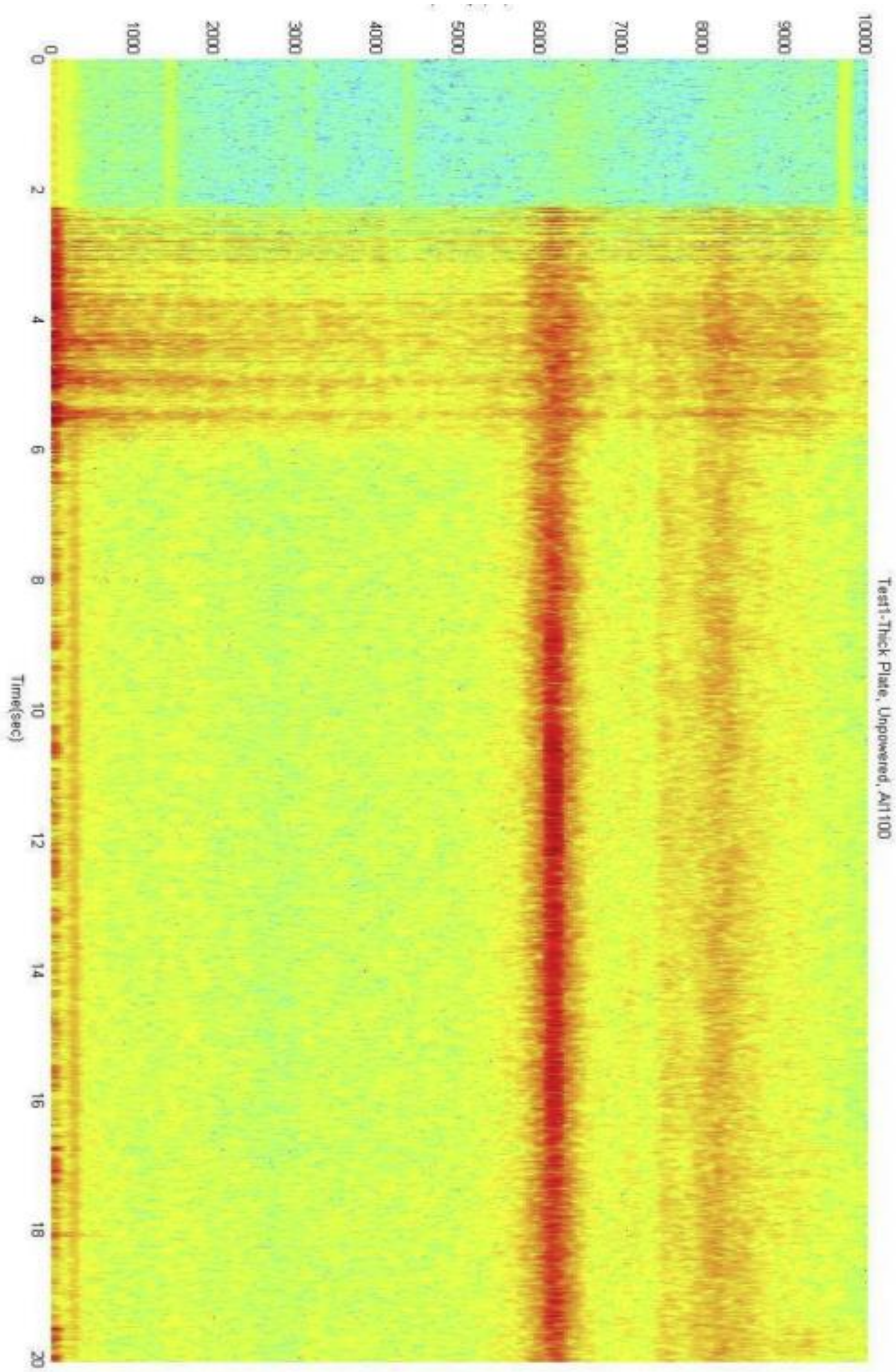

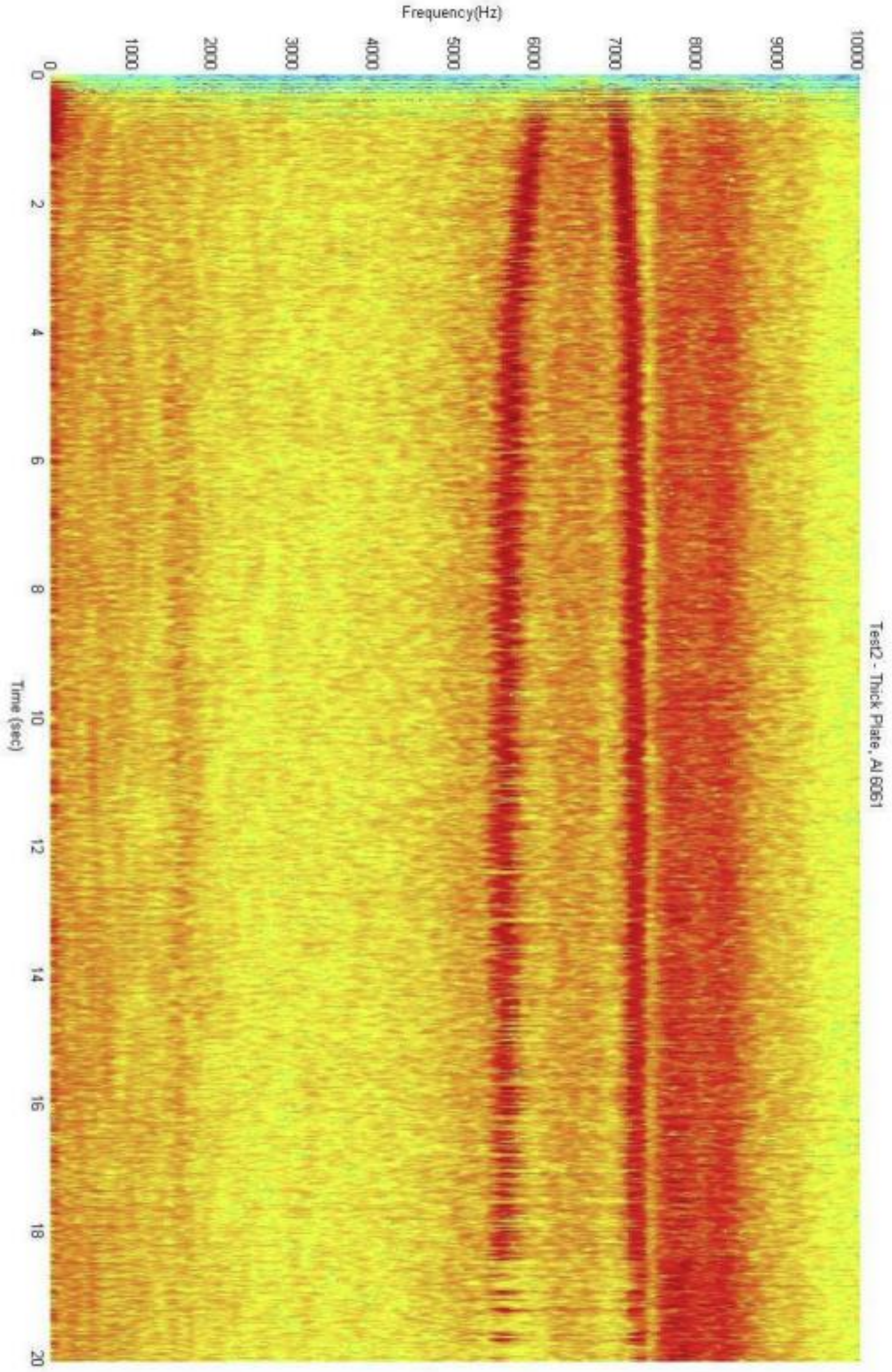
Test2 - Thick Plate, Al 6061
Frequency(Hz)
Time (sec)

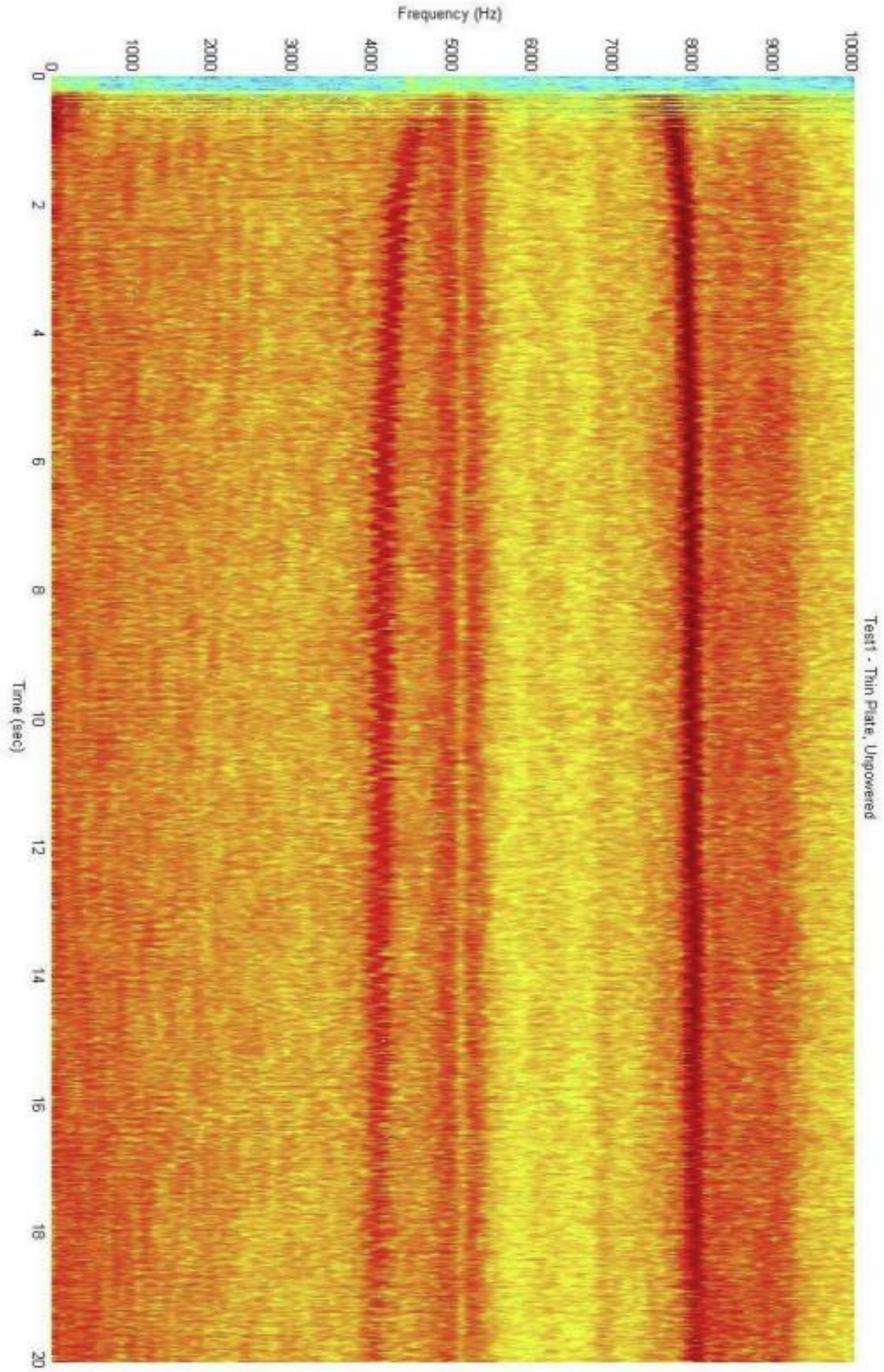

Frequency (Hz)
0
1000
2000
3000
4000
5000
6000
7000
8000
9000
10000
Time (sec)
0
2
4
6
8
10
12
14
16
18
20
Test1 - Thin Plate, Unpowered

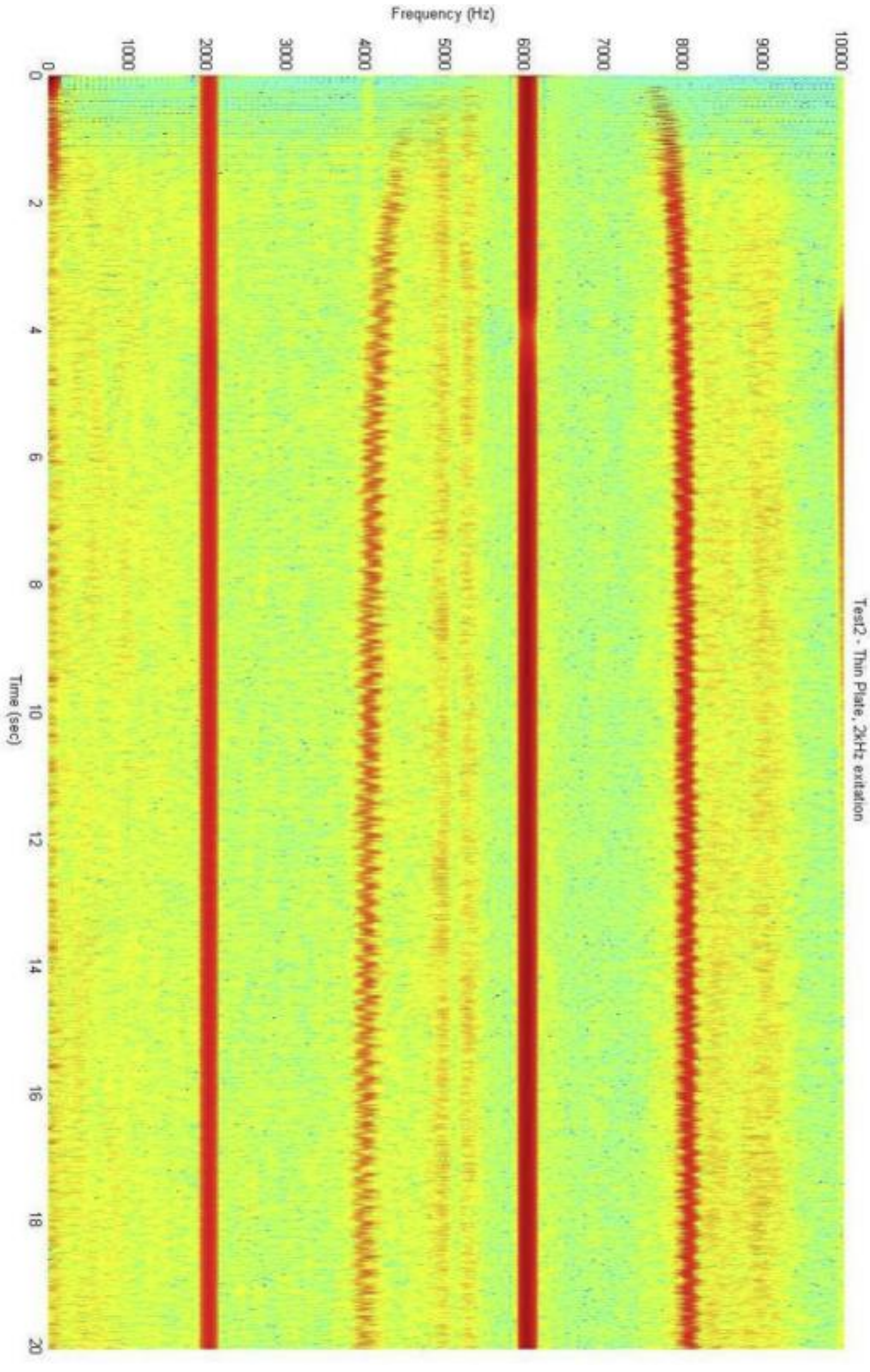
Frequency (Hz)
0
1000
2000
3000
4000
5000
6000
7000
8000
9000
10000
Time (sec)
0
2
4
6
8
10
12
14
16
18
20
Test2 - Thin Plate, 2kHz exitation

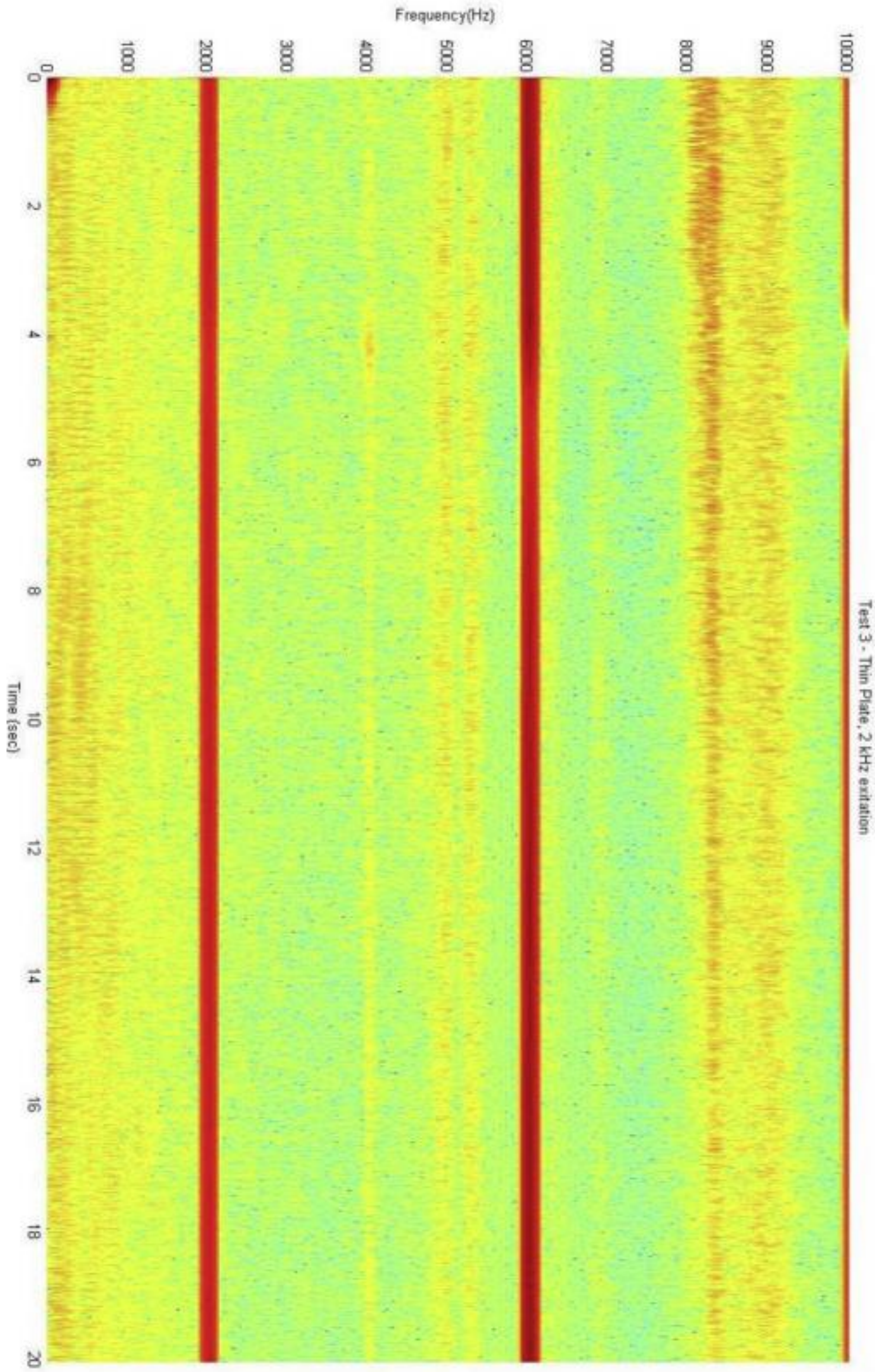
Test 3 - Thin Plate, 2 kHz exitation
Frequency(Hz)
0
1000
2000
3000
4000
5000
6000
7000
8000
9000
10000
Time (sec)
0
2
4
6
8
10
12
14
16
18
20

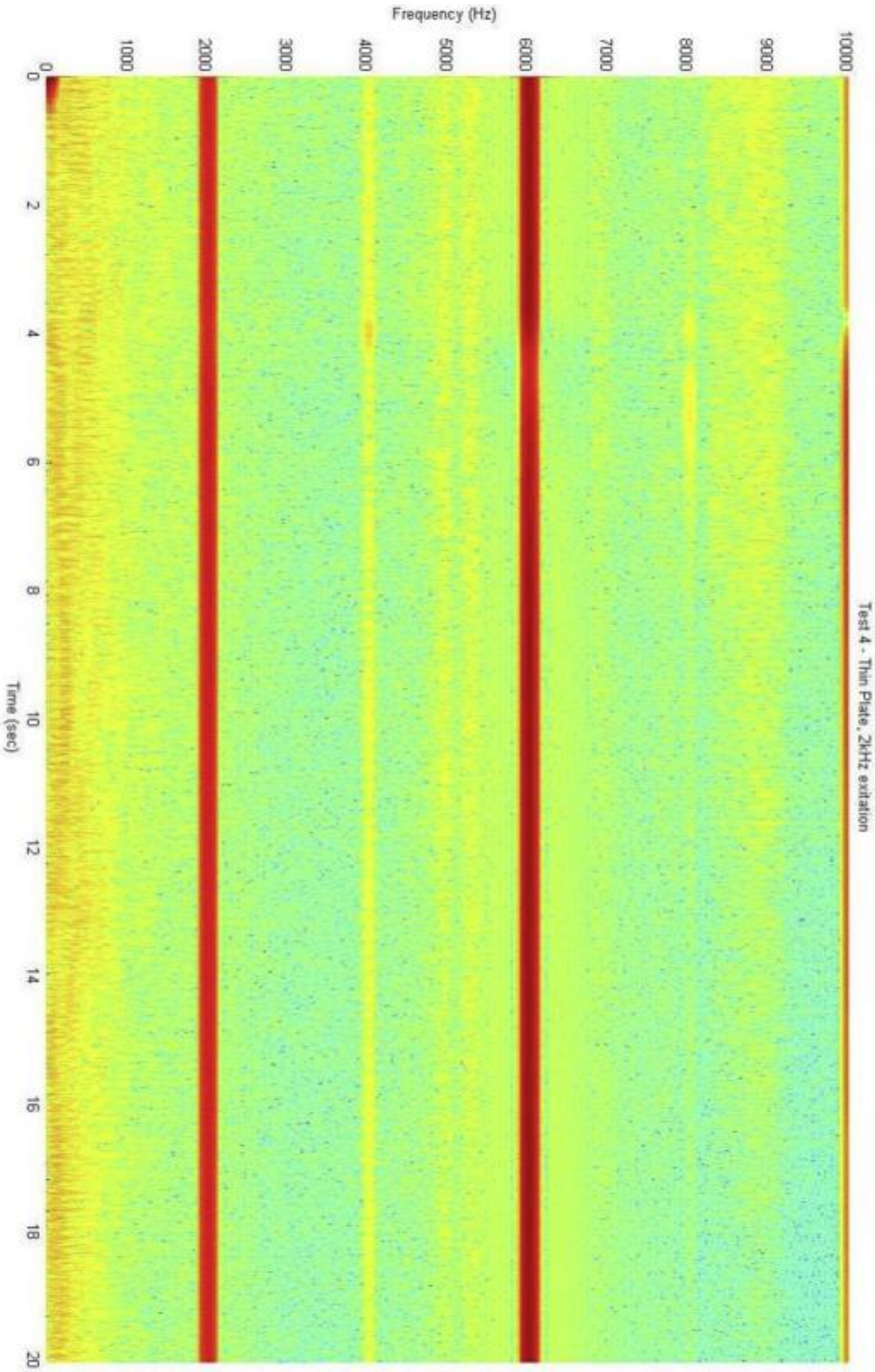
Test 4 - Thin Plate, 2kHz exitation
Frequency (Hz)
0
1000
2000
3000
4000
5000
6000
7000
8000
9000
10000
Time (sec)
0
2
4
6
8
10
12
14
16
18
20

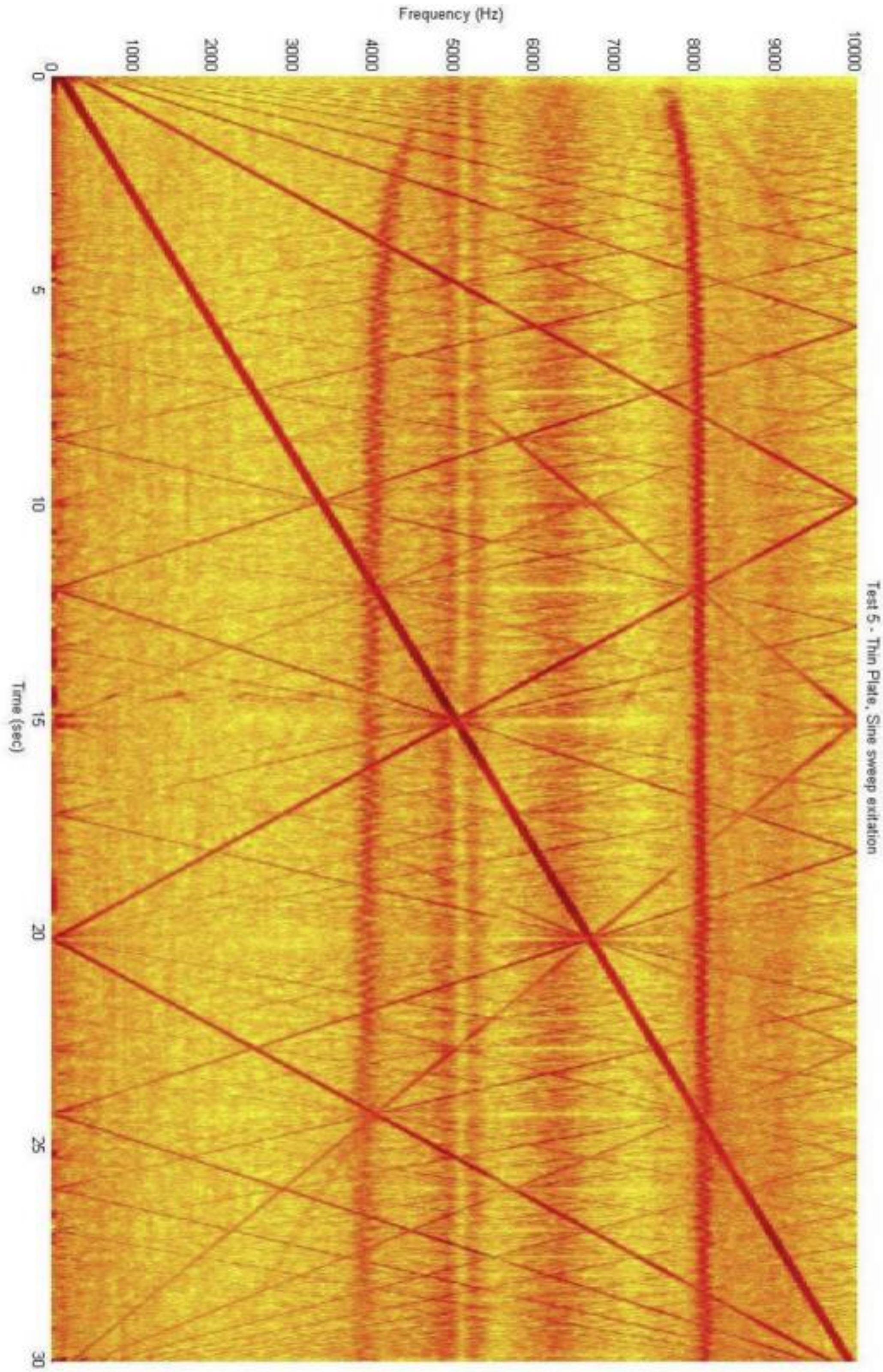
Test 5 - Thin Plate, Sine sweep exitation
Frequency (Hz)
0
1000
2000
3000
4000
5000
6000
7000
8000
9000
10000
Time (sec)
0
5
10
15
20
25
30

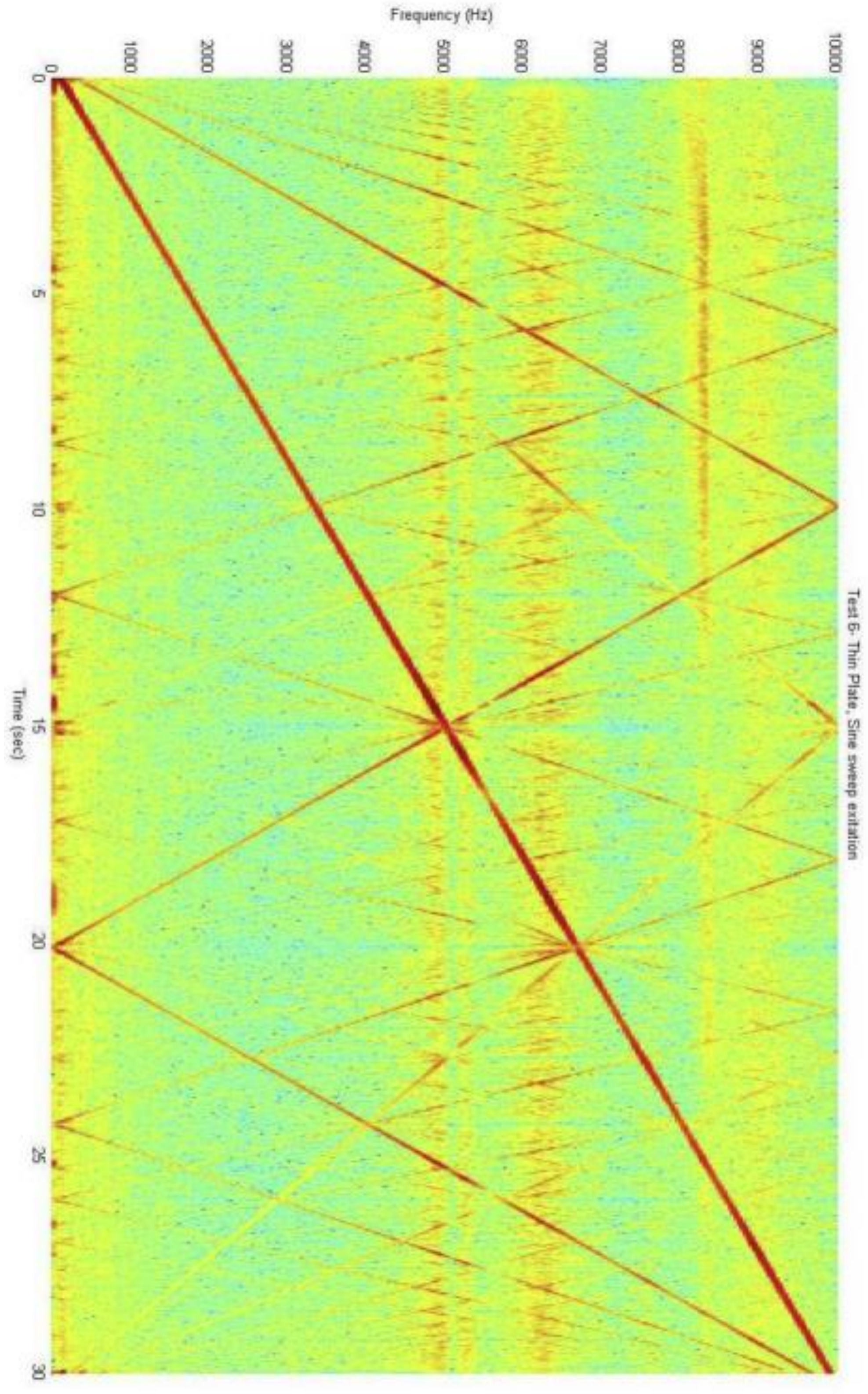
Test 6- Thin Plate, Sine sweep exitation
Frequency (Hz)
Time (sec)
0
1000
2000
3000
4000
5000
6000
7000
8000
9000
10000
0
5
10
15
20
25
30

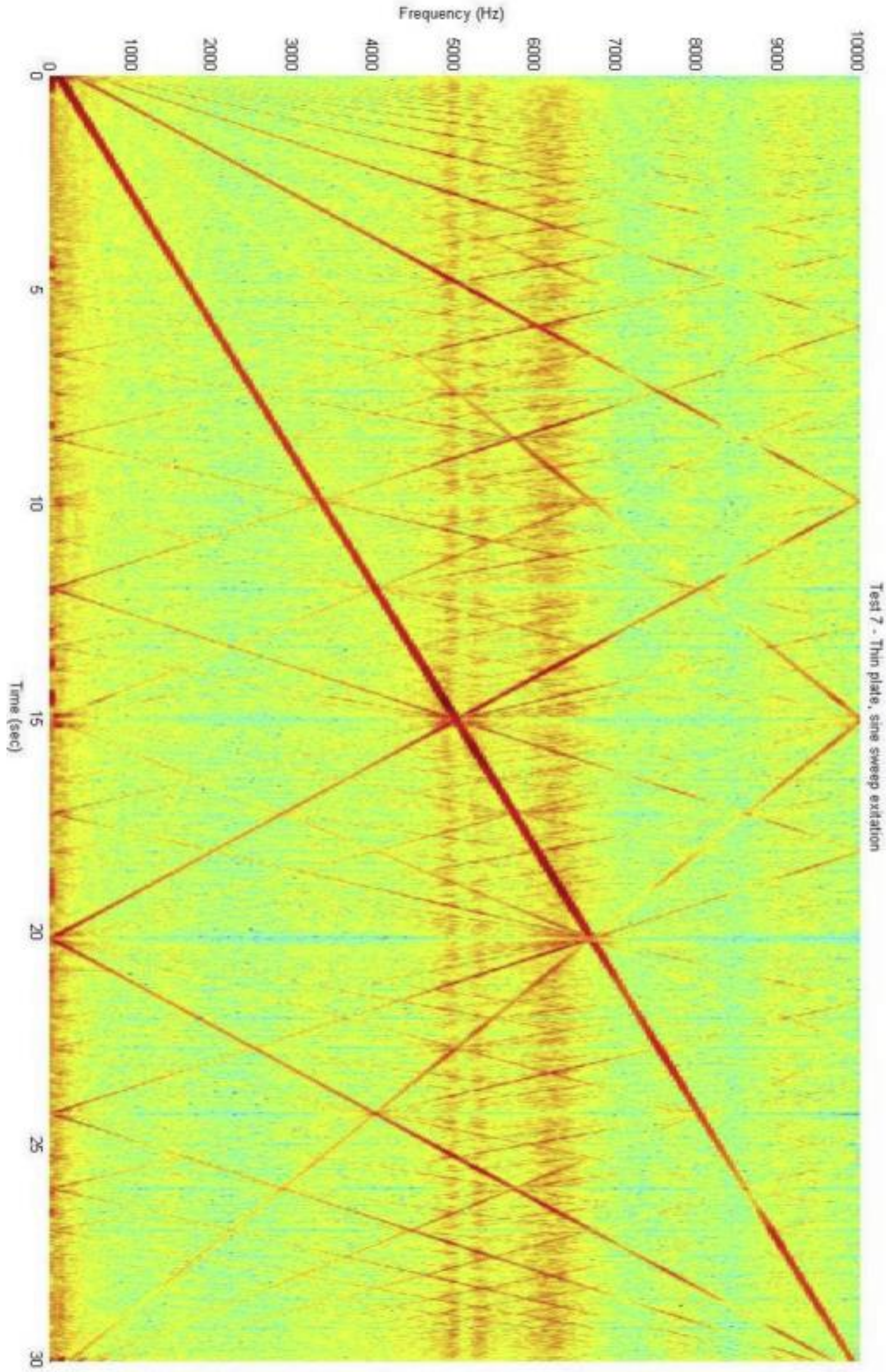
Test 7 - Thin plate, sine sweep exitation
Frequency (Hz)
0
1000
2000
3000
4000
5000
6000
7000
8000
9000
10000
Time (sec)
0
5
10
15
20
25
30

APPENDIX C Surface Profilometry [16]

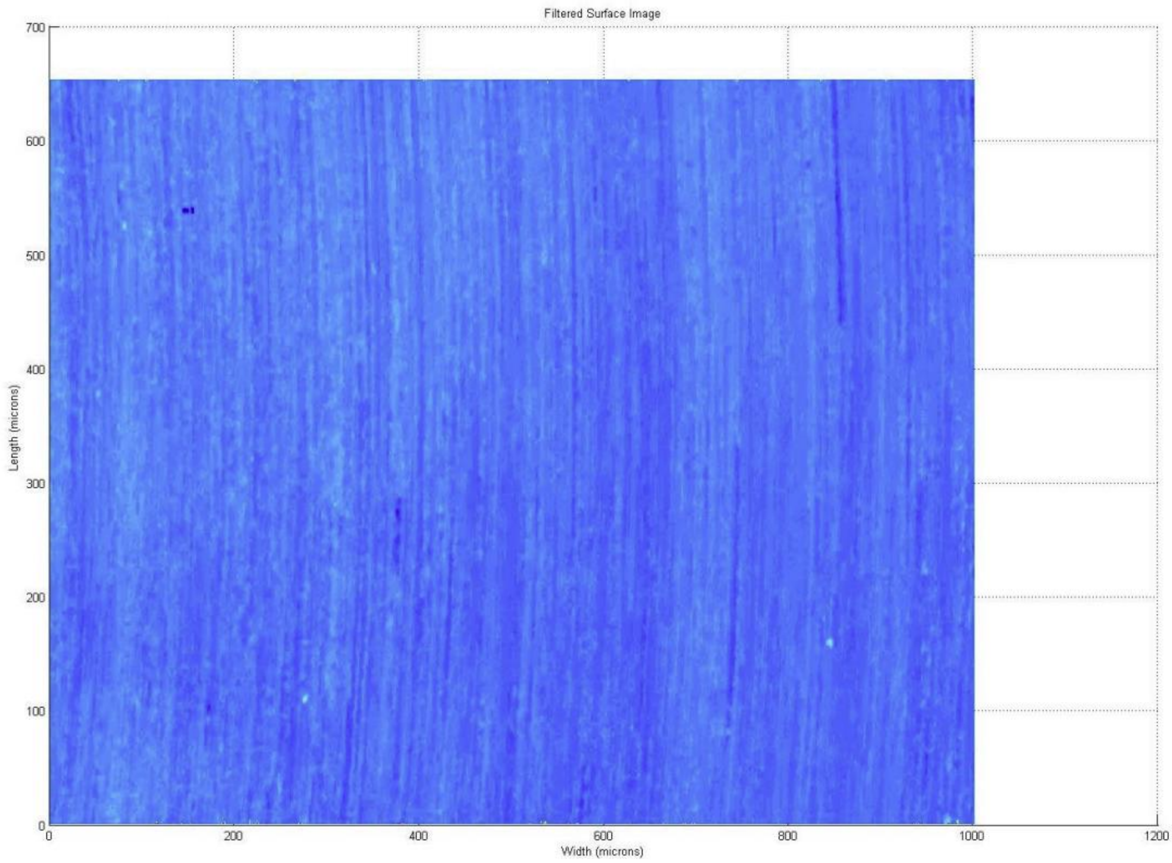

Test 1. Thick Diaphragm, Unpowered

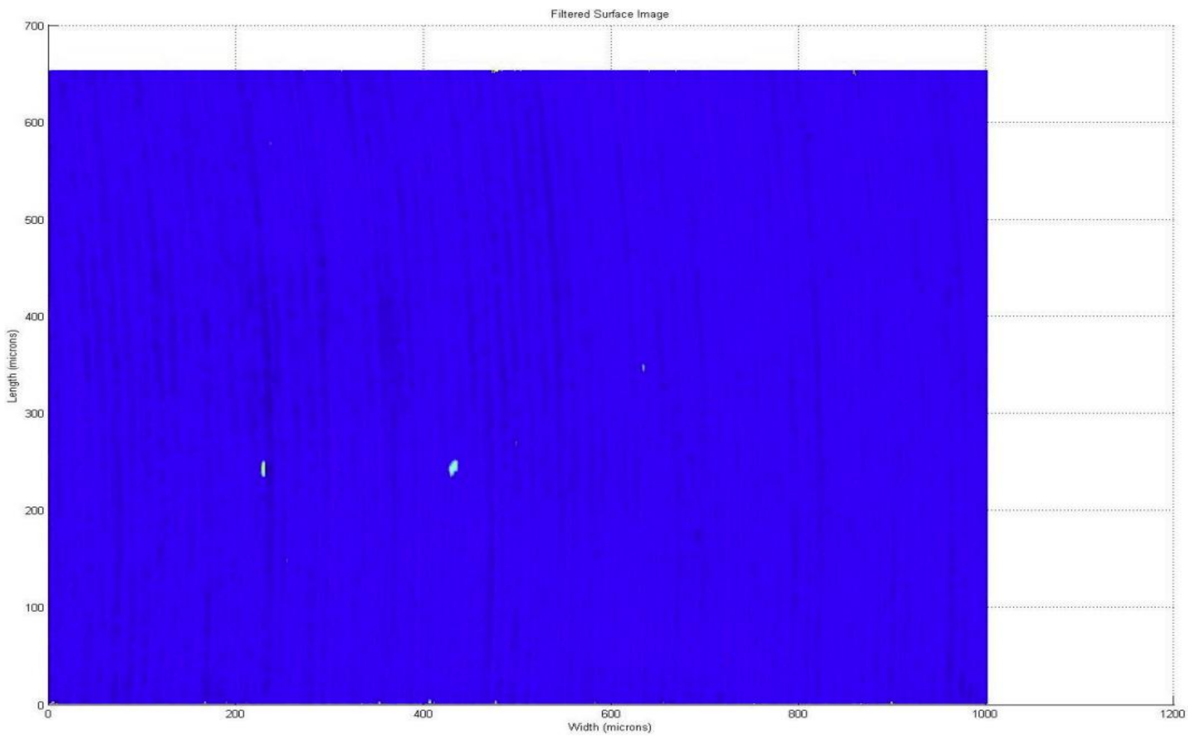

Test 2. Thin Diaphragm, Unpowered

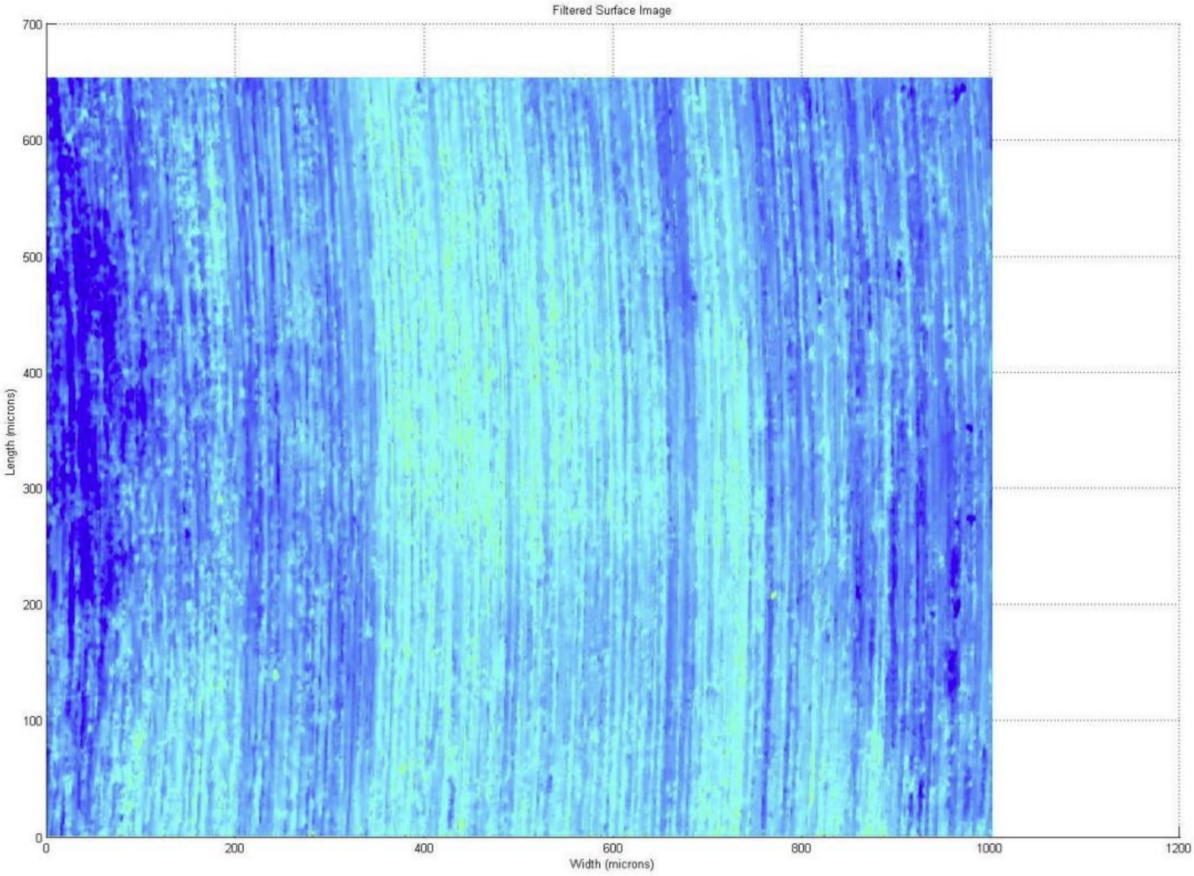

Test 3. Thin Diaphragm, 2 kHz excitation

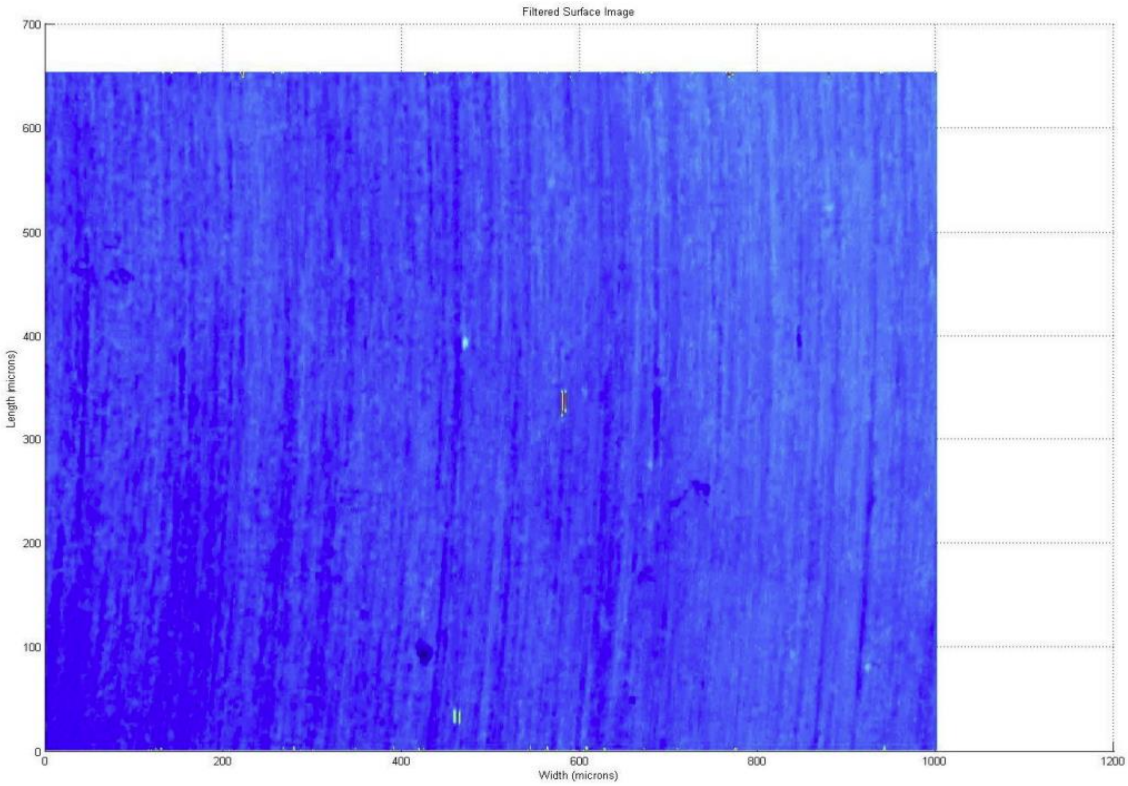

Test 4. Thin Diaphragm, 100 Hz – 10 kHz sine sweep excitation

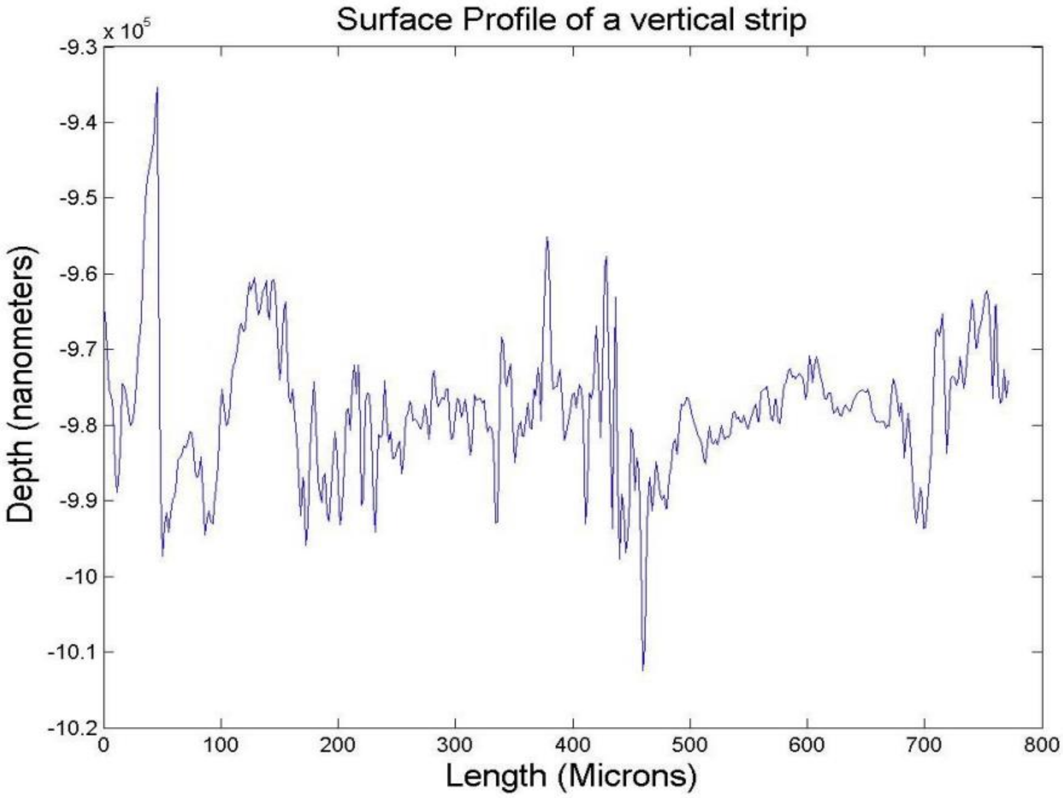

Test 1. Thick Diaphragm, Unpowered

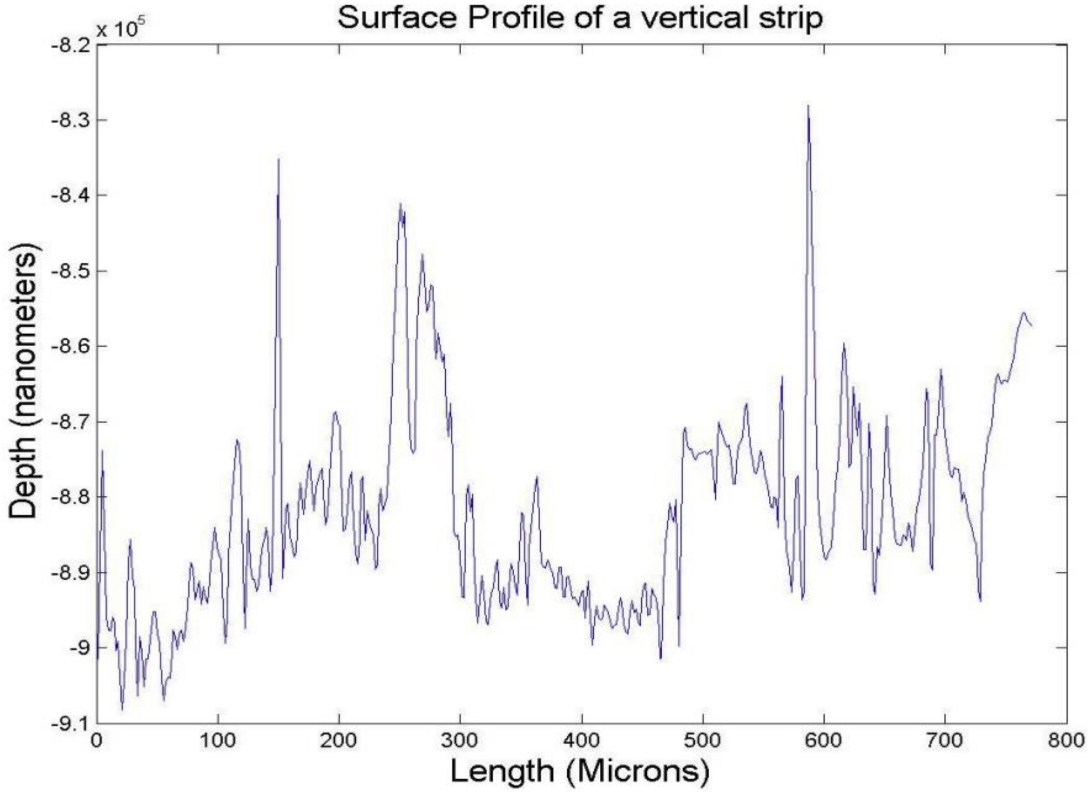

Test 2. Thin Diaphragm, Unpowered

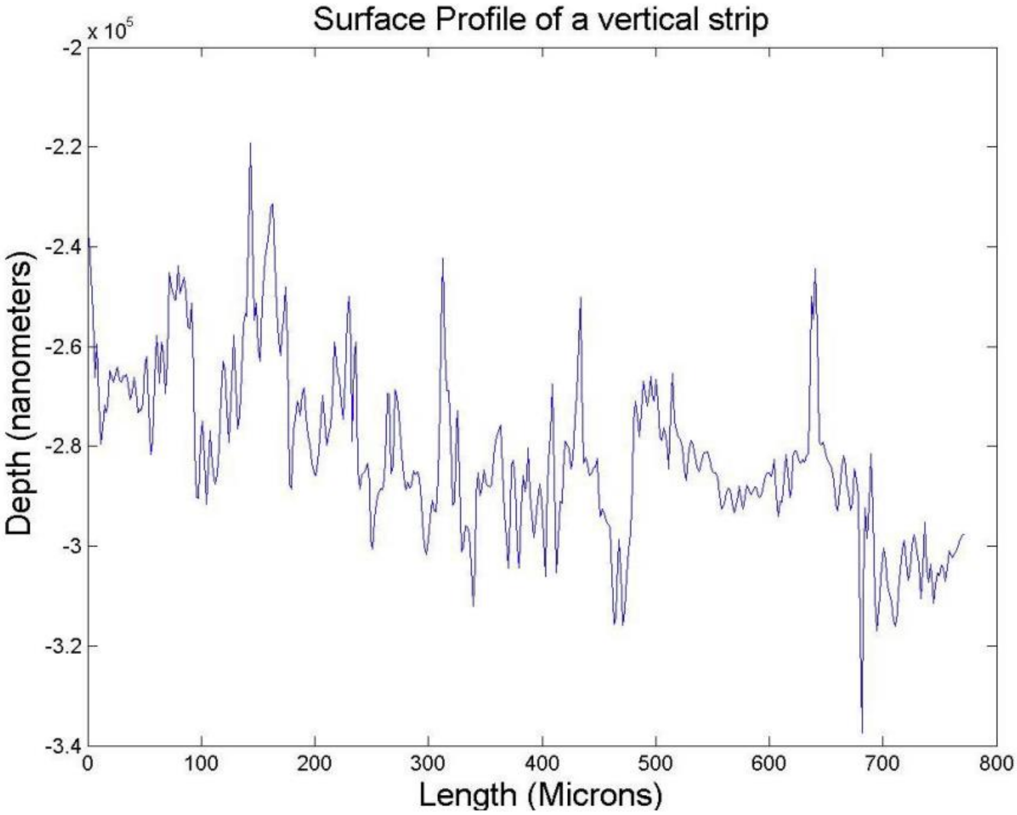

Test 3. Thin Diaphragm, 2 kHz excitation

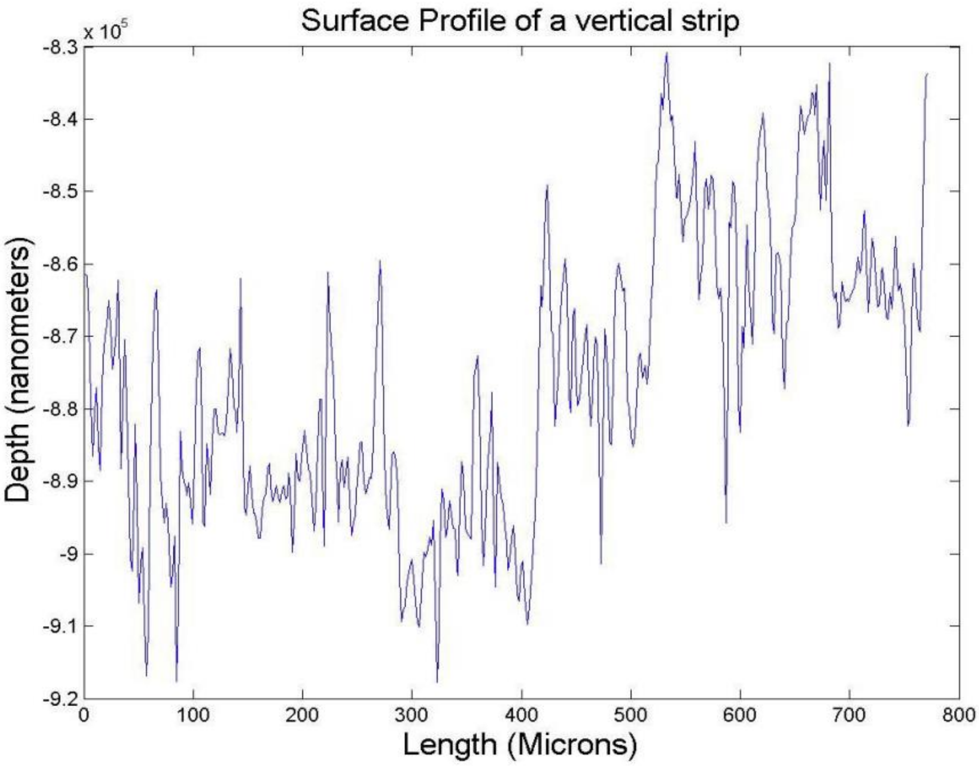

Test 4. Thin Diaphragm, 100 Hz – 10 kHz sine sweep excitation

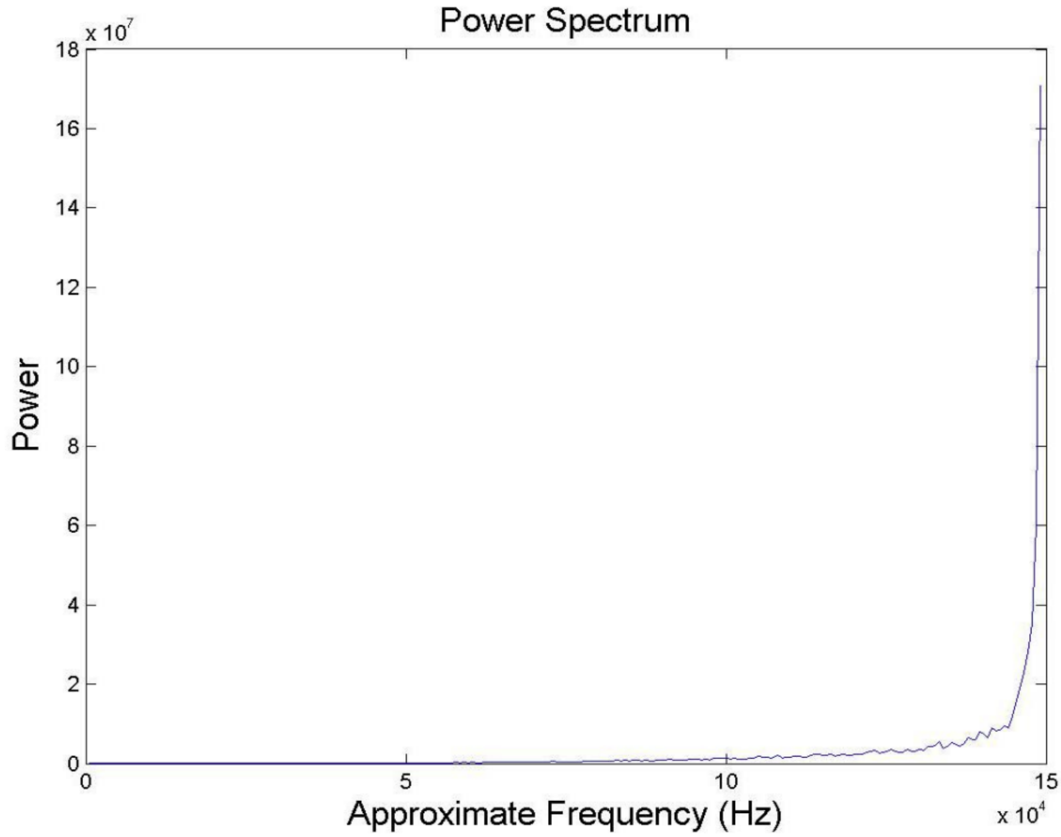

Test 1. Thick Diaphragm, Unpowered

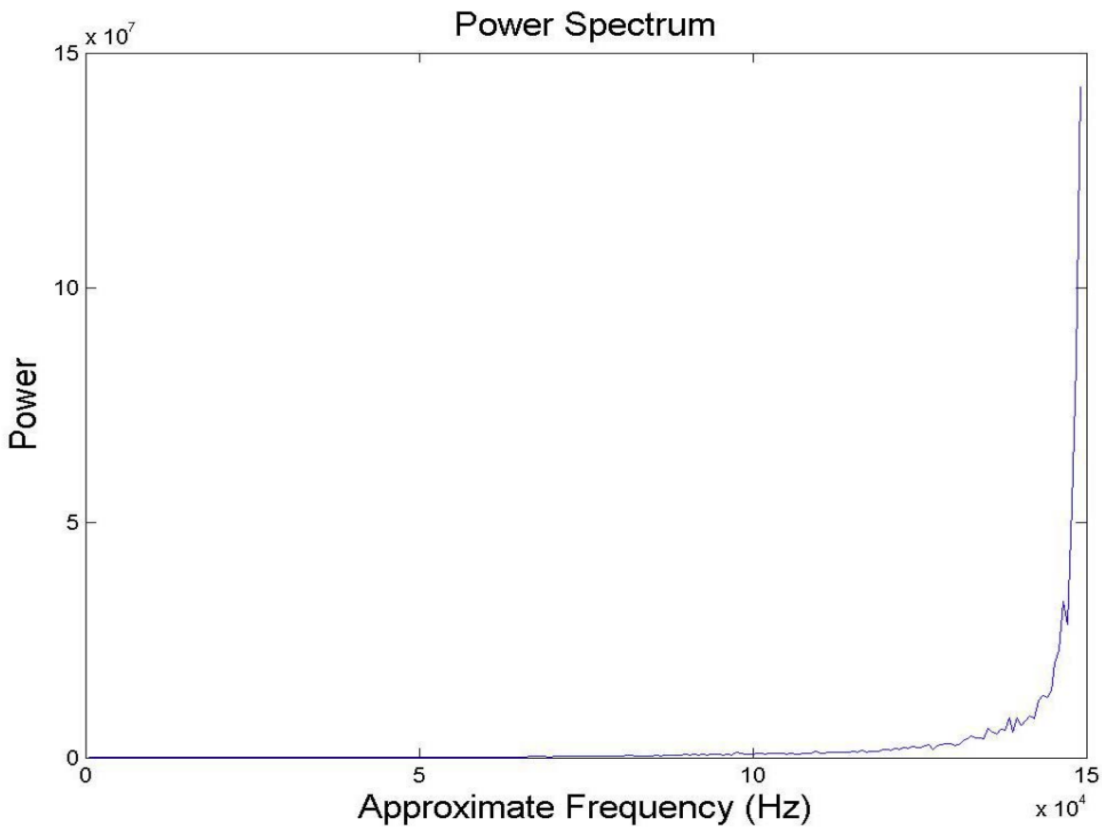

Test 2. Thin Diaphragm, Unpowered

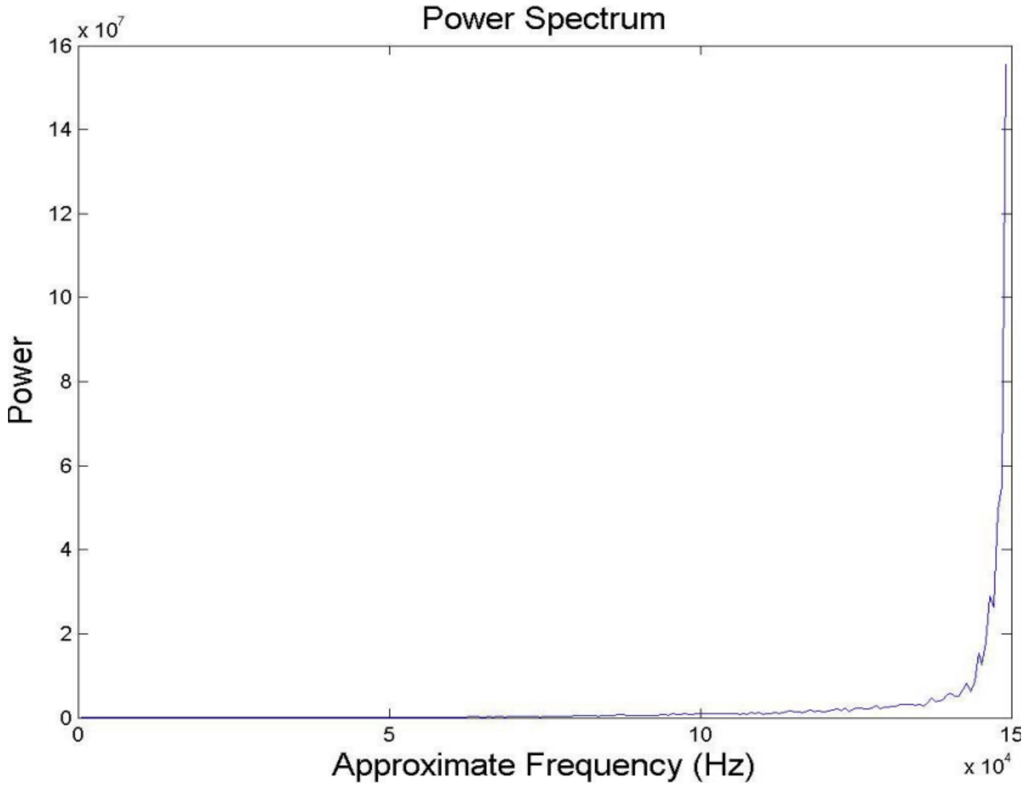

Test 3. Thin Diaphragm, 2 kHz excitation

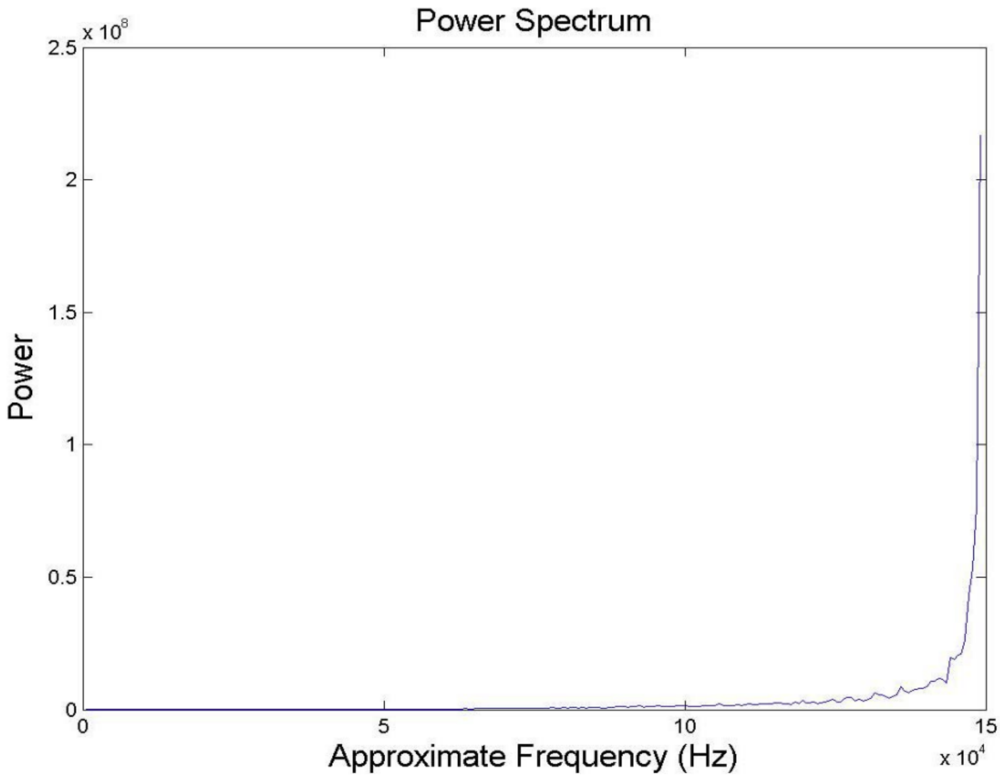

Test 4. Thin Diaphragm, 100 Hz – 10 kHz sine sweep excitation

Hochschule für Angewandte Wissenschaften Hamburg
Hamburg University of Applied Sciences

Erklärung zur selbstständigen Bearbeitung einer Abschlussarbeit

Gemäß der Allgemeinen Prüfungs- und Studienordnung ist zusammen mit der Abschlussarbeit eine schriftliche Erklärung abzugeben, in der der Studierende bestätigt, dass die Abschlussarbeit „– bei einer Gruppenarbeit die entsprechend gekennzeichneten Teile der Arbeit [(§ 18 Abs. 1 APSO-TI-BM bzw. § 21 Abs. 1 APSO-INGI)] – ohne fremde Hilfe selbstständig verfasst und nur die angegebenen Quellen und Hilfsmittel benutzt wurden. Wörtlich oder dem Sinn nach aus anderen Werken entnommene Stellen sind unter Angabe der Quellen kenntlich zu machen."

Quelle: § 16 Abs. 5 APSO-TI-BM bzw. § 15 Abs. 6 APSO-INGI

Dieses Blatt, mit der folgenden Erklärung, ist nach Fertigstellung der Abschlussarbeit durch den Studierenden auszufüllen und jeweils mit Originalunterschrift als letztes Blatt in das Prüfungsexemplar der Abschlussarbeit einzubinden.

Eine unrichtig abgegebene Erklärung kann -auch nachträglich- zur Ungültigkeit des Studienabschlusses führen.

Erklärung zur selbstständigen Bearbeitung der Arbeit

Hiermit versichere ich,

Name: Bhat

Vorname: Janak Singh

dass ich die vorliegende Bachelorarbeit - bzw. bei einer Gruppenarbeit die entsprechend gekennzeichneten Teile der Arbeit - mit dem Thema:

„Development and Implementation of a Concept for Optimizing a Piezoelectric System on a Machine Tool Lathe"

ohne fremde Hilfe selbstständig verfasst und nur die angegebenen Quellen und Hilfsmittel benutzt habe. Wörtlich oder dem Sinn nach aus anderen Werken entnommene Stellen sind unter Angabe der Quellen kenntlich gemacht.

- die folgende Aussage ist bei Gruppenarbeiten auszufüllen und entfällt bei Einzelarbeiten -

Die Kennzeichnung der von mir erstellten und verantworteten Teile der Bachelorarbeit ist erfolgt durch:

Hamburg	06.04.2023	
Ort	Datum	Unterschrift im Original